

# Exploring subsurface flowpaths at the Low Pass field site, Oregon, USA

Matthias Retter

Diploma thesis supervised by

Prof. Dr. Ch. Leibundgut<sup>1</sup>, Dr. S. Uhlenbrook<sup>1</sup>, Prof. Dr. J. McDonnell<sup>2</sup>, Dr. M. Weiler<sup>3</sup>

<sup>1</sup> Institute of Hydrology, University of Freiburg

<sup>2</sup> Dep. of Forest Engineering, Oregon State University

<sup>3</sup> Dep. of Forest Science, University of British Columbia

**Institut für Hydrologie**  
der Albert-Ludwigs-Universität Freiburg i.Br.

**Matthias Retter\***

**Exploring subsurface flowpaths  
at the Low Pass field site, Oregon, USA**

Referent: Prof. Dr. Ch. Leibundgut  
Koreferent: Dr. S. Uhlenbrook

Diplomarbeit unter der Leitung von Prof. Dr. Ch. Leibundgut  
Freiburg i.Br., November 2003

---

\* corresponding address: [retterm@gmx.ch](mailto:retterm@gmx.ch)

# Table of contents

<b>Preface .....</b>	<b>1</b>
<b>1 Introduction.....</b>	<b>1</b>
<b>2 Literature review.....</b>	<b>3</b>
2.1 Runoff generation processes at hill slope scale.....	3
2.2 Plot scale: Subsurface Flow processes .....	4
2.4 Conclusions.....	8
<b>3 Site description.....</b>	<b>9</b>
3.1 General .....	9
3.2 Climate .....	10
3.3 Geology and geomorphology .....	11
3.4 Soils .....	12
3.5 Vegetation .....	15
3.6 Overview of the hillslope site.....	16
3.7 Conclusions.....	16
<b>4 Methods.....</b>	<b>17</b>
4.1 Field methods.....	17
4.1.1 Determination of precipitation.....	19
4.1.2 Tipping buckets .....	20
4.1.3 Electrical conductivity .....	20
4.1.4 Automatic sampling setup .....	21
4.1.5 Bromide probe.....	21
4.1.6 Piezometer .....	22
4.1.7 Suction cup lysimeter .....	23
4.1.8 Mini v-notch weir .....	24
4.1.9 Soil moisture probes.....	25
4.2 Experimental hillslope table .....	26
4.2.1 Table itself .....	26
4.2.2 Soil filling .....	27

---

4.2.3 Rain simulator .....	28
4.2.4 Tipping buckets at table .....	30
4.2.5 Mini-wells for water sampling .....	31
4.2.6 Piezometers at table.....	31
4.2.7 Soil moisture probes.....	32
4.3 General information on the applied tracer.....	33
4.4 Characteristics of the tracer experiments.....	36
4.5 Data analysis.....	38
4.6 Conclusions.....	41
<b>5 Results and discussion: Field investigations.....</b>	<b>42</b>
5.1 Description of soil pipes .....	42
5.2 Precipitation .....	43
5.3 Soil pipe flow .....	47
5.3.1 Timing of soil pipe flow and flux .....	49
5.3.2 Discussion of soil pipe flow .....	50
5.4 Dynamic contributing area of soil pipes .....	51
5.5 Piezometer results .....	52
5.5.1 Water table levels.....	52
5.5.2 Timing of water table establishment.....	55
5.5.3 Spatial presentation of water table.....	56
5.5.4 Discussion of water table and flow mechanisms.....	59
5.6 Discharge at weir .....	61
5.7 Results tracer experiments .....	63
5.7.1 Amio G Acid .....	63
5.7.2 Bromide application.....	65
5.7.3 Discussion of tracer results .....	67
5.8 Conclusions of field investigations .....	68
<b>6 Results and discussion: Hillslope table.....</b>	<b>71</b>
6.1 Short overall description of the experimental run.....	71
6.2 Sprinkling .....	71
6.3 Runoff.....	72
6.4 Water balance .....	74
6.5 Soil moisture .....	74
6.6 Water table and water volume .....	75
6.7 Tracer.....	80

---

6.7.1 Amino G Acid line source .....	80
6.7.2 Discussion of Amino G Acid line source.....	83
6.7.3 Bromide .....	83
6.7.4 Discussion of bromide .....	84
6.7.5 Dye tracing with Brilliant Blue.....	85
6.7.6 Discussion of dye tracing with Brilliant Blue .....	87
6.8 Conclusions of hillslope table .....	87
6.9 Prospects for further experiments .....	87
<b>7 Concluding remarks and outlook .....</b>	<b>88</b>
<b>8 References .....</b>	<b>90</b>
<b>Appendix A</b>	
<b>Appendix B</b>	
<b>Appendix C</b>	

## List of figures

Fig. 2.2:	Hydraulic conductivity versus pressure head for sand and sandy loam; hydraulic conductivity versus water content; relative hydraulic conductivity versus pressure head; and relative hydraulic conductivity versus saturation.	5
Fig. 2.2.1:	Hydrological processes at infiltration.	7
Fig. 2.2.2:	Macropores and live-root (white) in the soil behind a trench face in a forest floor.	7
Fig. 2.3:	Conceptual model of runoff generation at the Maimai hillslope, New Zealand.	8
Fig. 3.1:	Location of field site and near climate stations.	9
Fig. 3.2:	Monthly climate summary for Noti.	11
Fig. 3.4a:	Soil characterisation. Beside forest road is the trench excavation with visible soil face (cutslope) of hillslope investigated.	13
Fig. 3.4b:	Cutslope along the forest road about 200 m further away of the hillslope.	13
Fig. 3.4c:	Soil profile of P_B4 up to a depth of 120 cm.	14
Fig. 3.4d:	View of trench below hillslope with location of the three soil pipes.	15
Fig. 4.1a:	Overview of instrumentation around data logging unit at Low Pass field side.	17
Fig. 4.1b:	Overview on investigated hillslope with instrumentation and extended catchment of a first order stream.	18
Fig. 4.1.1:	Throughfall gauging below canopy layer of mixed forest.	20
Fig. 4.1.8:	Flume with WT-HR water height recorder.	25
Fig. 4.2.1:	Artificial hillslope table and rainfall simulator.	27
Fig. 4.2.3a:	Shape of table, dividing for collection chambers of tipping buckets piezometers, soil moisture sensors and location of sampling wells.	29
Fig. 4.2.3b:	Distribution of sprinkling intensities (mm/hr) along different transects of table.	30
Fig. 4.2.6:	Three water table loggers at the side of the experimental table.	32
Fig. 4.3.1a:	Structure of Amino G Acid.	34
Fig. 4.3.1b:	Adsorption of Amino G Acid on humus sediment.	35
Fig. 5.2a:	Open land precipitation at the climate station Eugene, for overall investigation period and long-term mean.	44
Fig. 5.2b:	Daily rainfall at field site Low Pass and pipe flow for study period.	45
Fig. 5.2c:	Rainfall intensities per 10 min for selected interval, additionally hydrograph.	45
Fig. 5.3a:	Pipe flow shown in logarithmic scale and branches used for recession analysis.	47

---

Fig. 5.3b: Recession of mean discharge over recession branch and mean turnover time for selected events.	49
Fig. 5.5.1a: Water table at various piezometers, pipe flow and throughfall.	53
Fig. 5.5.1b: Water table levels at piezometers in row A ahead, while and after ID 4.	54
Fig. 5.5.1c: Water table levels at piezometers in row C ahead, while and after ID 4.	54
Fig. 5.5.3: Spatial distribution of water table at lower part of hillslope ahead, while and after ID 4.	57-58
Fig. 5.6a: Discharge of weir, soil pipes, and standardized weir flow.	61
Fig. 5.6b: Time shift of pipe flow and weir hydrograph for event related to tracer injection.	62
Fig. 5.7.1: Concentration of Amino G Acid at suction lysimeter below the line source tracer application.	64
Fig. 5.7.2a: Electrical conductivity after the tracer application, discharge soil pipes and precipitation.	65
Fig. 5.7.2b: Bromide concentration at bottom suction lysimeter.	66
Fig. 5.8: Assumed processes and conditions along transect of the hillslope.	69
Fig. 6.2: Overview on sprinkling and runoff for the whole experiment at the hillslope table.	72
Fig. 6.3: Variability of accumulated discharge at different tipping buckets and sprinkling intervals.	73
Fig. 6.5: Soil moisture at three different locations at the table for the period of experiment.	74
Fig. 6.6a: Height of water table at different time steps.	76-78
Fig. 6.6b: Sprinkling, runoff and water volume for the first interval of the experiments.	79
Fig. 6.7.1a: Amino G concentration and discharge at TB 8.	81
Fig. 6.7.1b: Amino G concentration, accumulated discharge and sprinkling for TB 8.	82
Fig. 6.7.1c: Accumulated discharge and Amino G concentration at TB 8.	82
Fig. 6.7.3a: Bromide concentrations, electrical conductivity, sprinkling intervals and accumulated discharge at TB 1.	84
Fig. 6.7.5a: Line source of Magic blue at y=290 cm and dye movement down slope.	86
Fig. 6.7.5b: Documentation of Brilliant Blue pathways at y=265 cm.	86
Fig. 6.7.5c: Documentation of Brilliant Blue pathways directly at the line application (y= 290 cm).	86

## List of tables

Tab. 3.2:	Documentation of climate stations and amount of total annual precipitation.	10
Tab. 4.3.1:	Amino G Acid adsorption on mineral and organic materials.	34
Tab. 5.1:	Features of soil pipes.	42
Tab. 5.2:	Selected characteristic of rainfall and runoff attributes for the hillslope and pipeflow.	46
Tab. 5.3:	Recession analysis of selected events and storage coefficient of the system.	48
Tab. 5.4:	Pipe flow records, DCA and runoff coefficients.	51
Tab. 5.5.2:	Data of selected piezometer on selected events, including time shift.	55

## List of figures in appendix

- Fig. A2a: Sabre growth indicating the soil creeping at the Low Pass field site.
- Fig. A2b: Sabre growth indicating the soil creeping.
- Fig. A3: Discharge soil pipes and rain events for the period of hydrograph separation.
- Fig. A4: Slug test at P\_D3 on March, 25 2003.
- Fig. A5: Water table at P\_A3 and runoff soil pipes.
- Fig. A6: Correlation between water table and pipe flow for selected piezometers.
- Fig. B1: Amino G breakthrough, accumulated discharge and sprinkling intervals at TB 1.
- Fig. B2: Amino G breakthrough, accumulated discharge and sprinkling intervals at TB 2.
- Fig. B3: Amino G breakthrough, accumulated discharge and sprinkling intervals at TB 3.
- Fig. B4: Amino G breakthrough, accumulated discharge and sprinkling intervals at TB 4.
- Fig. B5: Amino G breakthrough, accumulated discharge and sprinkling intervals at TB 5.
- Fig. B6: Amino G breakthrough, accumulated discharge and sprinkling intervals at TB 6.
- Fig. B7: Amino G breakthrough, accumulated discharge and sprinkling intervals at TB 7.
- Fig. B8: Correlation between electrical conductivity and bromide concentration of flow proportional hand samples at TB 1.
- Fig. B9: Correlation between electrical conductivity and bromide concentration of flow proportional hand samples at TB 1, for the times < 19.5.
- Fig. B10: Correlation between electrical conductivity and bromide concentration of flow proportional hand samples at TB 8.
- Fig. B11: Bromide concentrations, electrical conductivity, sprinkling intervals and accumulated discharge at TB 8.
- Fig. C1: Sketch of tipping buckets to provide a visual impression for information purposes.
- Fig. C2a: Water height recorder WT-HR.
- Fig. C2b: Sketch of PVC-pipe which encased the water table recorder, to be placed in a drill hole.
- Fig. C3a: Construction plan for triangular-notch weir.
- Fig. C3b: Details of notch.
- Fig. C3c: Rating curve of "v"-notched weir.
- Fig. C4: Sketch of soil water sampler.
- Fig. C5: Sketch and circuit diagram of electrical conductivity probe.
- Fig. C6: Structure of a mini-well for water sampling.

## List of tables in appendix

Tab. A1.1:	Field sheets, soil profile at P_A1.
Tab. A1.2:	Field sheets, soil profile at P_A3.
Tab. A1.3:	Field sheets, soil profile at P_A5.
Tab. A1.4:	Field sheets, soil profile at P_A7.
Tab. A1.5:	Field sheets, soil profile at P_A9.
Tab. A1.6:	Field sheets, soil profile at P_B1.
Tab. A1.7:	Field sheets, soil profile at P_B2.
Tab. A1.8:	Field sheets, soil profile at P_B4.
Tab. A1.9:	Field sheets, soil profile at P_C1.
Tab. A1.10:	Field sheets, soil profile at P_C3.
Tab. A1.11:	Field sheets, soil profile at P_C5.
Tab. A1.12:	Field sheets, soil profile at P_C7.
Tab. A1.13:	Field sheets, soil profile at P_C9.
Tab. A1.14:	Field sheets, soil profile at P_D1.
Tab. A1.15:	Field sheets, soil profile at P_D3.
Tab. A1.16:	Field sheets, soil profile at P_D5.
Tab. A3:	Exact data on hydrograph separation for selected runoff events.
Tab. A4:	Determination of input mass for Low Pass experiment.
Tab. A5:	Calculation on assumed drainage geometry of soil pipes.
Tab. B1:	Information on irrigation intervals during experiments at hillslope table.

## Abbreviations and synonyms

API <sub>7</sub>	-	Antecedent 7-days precipitation index	[mm]
DCA	-	Dynamic contributing area	[m <sup>2</sup> ]
DOC	-	Dissolved organic carbon	
EC	-	Electrical conductivity	[μS/cm]
ID	-	Assigned identification number for runoff peaks	
L_B	-	Bottom lysimeter	
L_U	-	Upper lysimeter	
P_ <i>[row]</i> <i>[number]</i>	-	Piezometer, includes alpha-numerical identification code	
Q	-	Discharge, runoff	[l/10 min]
R <sup>2</sup>	-	Coefficient of determination	[-]
r <sup>2</sup>	-	Correlation coefficient	[-]
TB	-	Tipping buckets	
W	-	Weir, flume	
ψ	-	Runoff coefficient	[-]

## Summary

Intense field studies and tracer studies illuminate the characteristics of subsurface flow at an unchanneled hillslope in the Oregon Coast Range, USA. The investigations presented, are based on the period March - May 2003. The soil order of the site is classified as an Inceptisols, series Bohannon sandy loam. The focus of investigation were three soil pipes (diameter up to 12 mm), which occurred at a soil depth of 1.8 m. An excavated trench at the bottom of the hillslope provided the opportunity to study pipe flow and interflow out of the hillslope. Supplementary, the initial first order stream at the convergence of hillslope, 50 m below the trench, was kept under surveillance.

Outflow of the hillslope was restricted to the pipes and no other interflow occurred. While the face of the cutslope in the south showed high moisture content, no major water table oscillation was found behind in the hillslope. Contrary, in the north part, with less hillslope convergence, trench faces remained completely dry and water tables behind showed significant changes, with a magnitude up to 60 cm below surface topography. Further, temporal data of water tables in the hillslope yielded information to identify its quick response to rainfall events. Peaks of water tables occurred about 11 hr before pipeflow peaks, although there was some variation due to individual piezometer response.

Pipe flow (sum of the three pipes) responded quickly to rainfall input during the first months. Observations that pipe flow became more important when rainfall intensities were extraordinary high could not be confirmed in this study. A recession analyses of the hydrograph showed the pattern of quick turnover times for high mean discharge conditions. Later in the year, when soil moisture was strongly diverse from field capacity, no response was observed. Pipe flow ran dry in June, effected by the seasonal rainfall characteristics in Western Central Oregon.

The calculation of the dynamic contributing area of the soil pipes (DCA) helped to classify the soil pipes. The result (max DCA) amounted to at least 9500 m<sup>2</sup>, although there is some uncertainty included. A further attempt on the characterisation of the soil pipe's drainage network is presented by a land drainage approach based on the HOOGHOUTD-equation. A rough estimation on the distance between draining pipes (original idea of parallel pipes) varied around 1 m. Further, data of the weir below the trench, are presented with a hydrograph time shift of 7 hr compared to the pipe flow peak.

An Amino G Acid line injection into the upper soil did not reveal any tracer breakthrough at the soil pipes as well as at the initial first order stream. Bromide sprayed over a wide range of the hillslope was not detected in pipe flow, either. Observations of suction cup lysimeter (depth 30, 50 and 70 cm) showed both tracers remaining in the unsaturated zone. Thus, dye

residence times in the unsaturated zone are controlled by quantity of injected tracer and amount of rainfall.

To extent the possibilities of investigation, an experimental model of the hillslope – an artificial hillslope table – was used in a parallel approach. This physical modelling allowed the same tracer experiments as in the field under triggered conditions. Sprinkling intervals were adjusted to rainfall characteristics of the Oregon Coast Range. Bromide added to the sprinkler water moved through the soil as plug flow controlled by rainfall rate and water content. The Amino G Acid line source experiments at the table verified that unsaturated conditions limit tracer movement in the upper part of the slope. A final excavation of Brilliant Blue, although an adsorptive tracer, corroborated the restricted movement in the sandy loam. Moreover, this suggests the high influence of soil pipe structures in this soil. By these findings the outlook of this work does encourage a next generation of physical modelling at the table with implemented artificial soil pipe structures in the soil. This would help to address the question of how runoff concentration and response time change in case of soil pipes acting.

**Keywords:** Oregon Coast Range, field study, preferential pathway, soil pipe, trench based investigation, physical model, sprinkling experiments

## Zusammenfassung

Zielsetzung der Arbeit war es, Kenngrößen und Prozesse von unterirdischen Fließwegen in einem gerinneten Hang der Oregon Coast Range, USA, zu untersuchen, wozu eine Feldkampagne mit Datenerhebung und Markierversuche durchgeführt wurden. Die vorliegenden Resultate stammen hauptsächlich aus dem Untersuchungszeitraum März bis Mai 2003. Eine Bodenklassifizierung am Untersuchngshang wies einen sandigen Lehm der Bahannon Serie aus. Kern der Untersuchung waren drei erweiterte Makroporen, im folgenden als *soil pipes* bezeichnet, die in einer Bodentiefe von 1,8 m auftraten und Durchmesser bis 12 mm aufwiesen. Mit Hilfe eines quer angelegten Untersuchungsgrabens am unteren Ende des Hangs konnte das Abflußverhalten der *soil pipes* und der Zwischenabfluss aus der Hangfläche untersucht werden. Zusätzlich wurde der 50 Meter unterhalb des Grabens auftretende Gewässerlauf erster Ordnung zur Analyse herangezogen.

Ausfluß aus der Hangfläche fand lediglich über die *soil pipes* statt, da kein Zwischenabfluß im Querschnitt auftrat. Die Abbruchkante des Grabens zum Hang hin zeigte in der südlichen Hälfte hohe Oberflächenfeuchtigkeit, doch traten Wasserspiegel im Hang selbst nur restriktiv auf. Dem gegenüber stehend, fanden sich in der nördlichen Hälfte, die jedoch weniger topographische Konvergenz zeigt, permanent ausgetrocknete Oberflächen und ein bedeutender Wasserspiegel mit Schwankungen bis 60 cm unter Geländeoberkante. Weiterhin ergab die zeitliche Auswertung der Wasserstandsdaten wichtige Informationen zur Erkennung der schnellen Systemantwort auf Niederschlagsereignisse. Obwohl die Daten der individuellen Piezometern eine hohe Variation zeigte, zeigte sich ein Nacheilen des *soil pipe*-Spitzenabflusses um 11 Stunden zu den Spitzen des Wasserstandes im Hang.

Der Abfluß aus den *soil pipes* (Aufsummierung der drei einzelnen *soil pipes*) zeigte eine schnelle Antwort auf Niederschlag während den ersten Monaten. Beobachtungen, dass *soil pipe*-Abfluß bei hohen Niederschlagsintensitäten eine dominanter Ausprägung erfährt, konnten durch diese Studie nicht belegt werden. Eine Rezessionsanalyse der Ganglinien zeigte den Zusammenhang von schnellen *turnover times* bei hohen mittleren Abflüssen. Zu späteren Zeitpunkten, bei einer Bodenfeuchte, die von der Feldkapazität weit entfernt lag, konnte keine Abflussreaktion aus Niederschlagsereignisse festgestellt werden. Das Versiegen der *soil pipes* im Juni ist durch die starke Saisonalität des Niederschlags mit verbundener Trockenheit im zentralen, westlichen Oregon zu begründen.

Um die *soil pipes* genauer beschreiben zu können, half die Berechnung einer dynamischen Beitragsfläche (dynamic contributing area, DCA), also einer Art Einzugsgebiet der *soil pipes*. Eine Fläche (max. DCA) von mindestens 9500 m<sup>2</sup> wurde abgeschätzt und die Unsicherheiten diskutiert. Ein weitere Ansatz zur Charakterisierung des Einzugsgebietes der *soil pipes*

erfolgt mit einem Drainierungsansatz der Entwässerungstechnik, welcher auf der Formel von HOOGHOUTD basiert. Eine grobe Abschätzung zu dem Abstand zwischen einzelnen *soil pipes* (ursprüngliche Idee von parallelen Rohren) variiert um 1 m für verschiedene Ereignisse und Annahmeparameter. Weiterhin ergab sich für den Abfluß am Gerinne erster Ordnung (Überfallwehr), verglichen mit dem Spitzenabfluss der *soil pipes*, eine Zeitverschiebung in der Ganglinie von 7 Stunden.

Ein Markierversuch (Injektion einer Linie aus Amino G Acid) in 5 cm Bodentiefe ergab keinen Markierstoffnachweis am Auslass der *soil pipes* sowie auch nicht am Überfallwehr. Ein weiterer flächenhafter Eintrag vom Lithiumbromid auf den Hang konnte ebenfalls nicht im Abfluß der *soil pipes* nachgewiesen werden. Die aus Saugkerzen entnommenen Proben in Tiefen von 30, 50 and 70 cm zeigten ein Verbleib des Markierstoffes in der ungesättigten Zone. Die Aufenthaltszeiten und die Mobilisierung von Markierstoff ist somit abhängig von der Einspeisemenge und von der gefallenen Niederschlagsmenge.

Um in einem weiteren Schritt die Untersuchungsmöglichkeiten zur Bedeutung von unterirdischen Fliesswegen zu erweitern, wurde ein experimentelles Modell des Untersuchungshanges – ein künstlicher Hangtisch – in die Studie integriert. Diese physikalische Modellierung erlaubte ähnliche hydrometrische Erfassung und die gleichen Markierversuche wie im Feld unter steuerbaren Bedingungen. Die künstlichen Beregungsintervalle wurden dabei abgestimmt auf die Charakteristika der Küstenkette von Oregon.

Das mit Bromide versetzte Beregungswasser bewegte sich durch den Boden in einer Front, welche durch Beregungsintervalle und Bodenwassergehalt maßgeblich gesteuert wurde. Die Ergebnisse des linienhaften Markierexperiments mit Amino G Acid bestätigten, dass die ungesättigten Bedingungen den Stofftransport im oberen Teil des Hanges begrenzen. Die schlussendliche Ausgrabung eines weiteren, jedoch absorbierenden Markierstoffes, Brilliant Blue, erhärtete die Erkenntnis von eingeschränkter Fortbewegung im sandigen Lehm. Ferner verdeutlichte dies die tatsächliche Bedeutung von *soil pipe* Strukturen in diesem Boden. Basierend auf diesen Erkenntnissen ermutigt der Ausblick dieser Arbeit eine nächste Generation von physikalischen Modellen am Hangtisch mit künstlich eingebauten *soil pipe* Strukturen. Dies wäre hilfreich für die Fragestellung inwieweit Abflußkonzentration und Systemantwort sich unter den Bedingungen von fungierenden *soil pipes* verändern.

## Preface

This research was conducted at the Watershed Laboratory of the Dept. of Forest Engineering, Oregon State University, USA and the Institute of Hydrology, University of Freiburg, Germany. It was supported by the Förderverein Hydrologie and financial assistance was received through "Eliteförderprogramm der Landesstiftung Baden-Württemberg GmbH" (research grant: "Einsatz geophysikalischer Methoden in Verbindung mit Tracermethoden in der Abflussbildungsforschung"). The project also received comprehensive support from the chair of Prof. Dr. J. McDonnell.

## 1 Introduction

In one of the earliest investigations of runoff generation, HURSH (1936) detected that subsurface flow, and not overland flow, was the source of storm runoff in forested catchments. Since then the mechanisms of subsurface flow paths have been the focus of much discussion and debate. Studies have shown that so called preferential pathways play an important role in runoff generation of forested hillslopes (e.g. BEVEN & GERMANN, 1982; BRONSTERT, 1999; MCGLYNN et al., 2002). The term preferential pathways includes macropores and other open structures, where water can move through the soil rapidly. Macropores occur in various soil types and are frequently found in slopes, often in a well connected network. Larger macropores are commonly referred as 'soil pipes' (e.g. JONES, 1971). Numerous hydrologists have performed tracer experiments to gain knowledge on the subsurface flow processes (MCDONNELL et al., 1998; SKLASH et al., 1996). Tracer information at the catchment outlet is treated as convergent or integrated data respectively as integration of individual hillslope processes (LEIBUNDGUT, 1984). Results have shown the high velocity of pipe flow (MOSLEY, 1982) and its relationship to soil water content and groundwater levels (MCDONNELL, 1990; CROZIER et al., 2003). UCHIDA et al. (1999) have noted the lack of discharge rates of pipe flow and stream flow in mountainous watersheds. Despite many years of study, subsurface flow pathways are still poorly understood. It may occur in highly permeable soil layers overlying low permeable layers, or in preferential flow pathways and more permeable (weathered) areas in the soil or at the soil bedrock interface.

Studies have shown that often “threshold mechanisms” of either rainfall intensities or antecedent moisture conditions (flow levels prior to storms) may trigger subsurface flow (UCHIDA et al., 1999; JONES, 1997; MCDONNELL, 1990; ZIEMER & ALBRIGHT, 1987; JONES & CRANE, 1984; WILSON & SMART, 1984). Nevertheless, the conversion of flow from vertical pathways in the soil into lateral matrix or preferential flow pathways is poorly understood. In general, the development of reliable methods to quantify the continuity and hydraulic conductivity of macropores *in situ* for a range of field moisture conditions, at a scale and depth sufficiently large to be useful for applying predictive models, is one of the greatest challenges for researchers in vadose zone hydrology (STEPHENS, 1996).

### **Problem and Objective**

This diploma thesis examines preferential flow processes, and explores the connection of vertical and lateral flow pathways at the hillslope scale. The study includes two main approaches focusing on this detection of flow mechanisms: (1) investigation of a natural forested hillslope in Western Oregon, USA, and (2) investigation of an artificial hillslope, filled with material from the Oregon field site. Questions posed for both study components included: How do soil pipes control hillslope response to storm rainfall? How does topographic convergence affect subsurface flow? How do matrix and pipe flows couple at the plot and hillslope scale?

To explore these topics, an intensive field campaign was conducted with various installed hydrometric measurements. Subsurface flow volumes, flow timing rates, water table levels and soil moisture conditions were determined over a period of March - May 2003. Further, tracer experiments were performed during selected rainfall events and tracer transport through the system with associated pipeflow was investigated. The physical hillslope extended the field work with controlled rainfall experiments where runs were performed for soils without and later with soil pipes. These experiments helped address the question of how does runoff concentration and response time change, when artificially implemented soil pipes are included in to matrix material (guided by the philosophy that hydrological science is in greater need of more and better experimentation HORNBERGER & BOYER, 1995).

The final objective strives for the combination of knowledge gained by both approaches.

## 2 Literature review

A short outline on the important runoff generation processes related to the hill slope scale is presented in the following. Thereafter a principle overview includes the hydrological processes at the plot scale, where the focus highlights the characteristics of macropores.

### 2.1 Runoff generation processes at hillslope scale

Within recent decades, understanding of the processes in rainfall-runoff systems has significantly improved. The classical dynamic-oriented division into surface flow, interflow, and base flow can not keep up with the complexity of hill slope processes, which are being described more and more precisely (GUTKNECHT, 1996). Nevertheless, a hill slope's response to rainfall will still be an interweaving of different components. Controlling factors like rainfall characteristic, topography and antecedent soil moisture conditions regulate the interaction of single processes in runoff generation.

#### **Hortonian Overland Flow**

Component is overland flow that results from impermeable surfaces. The saturation from above occurs where water-input rate exceeds the saturated hydraulic conductivity of the surface layer. The process is not postulated for entire hill slopes, it rather fits to the partial-area concept (DINGMAN, 2002; UHLENBROOK & LEIBUNDGUT, 1997).

#### **Saturation Overland Flow**

Overland flow occurs as the result of saturation from below. Saturation Overland Flow is performed by direct water input to the saturated area as well as by the return flow. This is of importance near streams, where the water table is already close to the surface. Further, it occurs at hill slope hollows (concavities), at concave slope breaks, where thin soil layers conduct subsurface flow, and at perched conditions. This mechanism is linked to the variable source area concept (DINGMAN, 2002; UHLENBROOK & LEIBUNDGUT, 1997).

#### **Subsurface Flow**

Subsurface flow mechanisms describe the non visible transmission or movement of water within the soil. Subsurface flow processes in soil may be separated in two domains: The homogeneous matrix flow, and the flow through structural pores, referred to as preferential flow. In the latter, water is primarily driven by gravity and is less obstructed by capillary forces. In the domain of matrix flow, water is subjected to capillarity, where potential flow approaches apply. The soil matrix here is quite often not completely saturated with water, because the time required for its complete saturation may exceed the time needed to

establish flow in macropores (ANDERSON & BURT, 1990). Section 2.2 provides a more detailed exposition on that topic. Second, processes may also be classified in temporal categories. E.g. infiltrated event water is by this means able to mobilize stored pre-event water in the near-stream zone. In particular because of its strong contribution to flood events, subsurface flow has been investigated well (e.g. BERGMANN et al., 1996).

## **2.2 Plot scale: Subsurface Flow processes**

Flow processes through field soils are in most cases highly irregular. There are vertical flow, lateral flow, and solute transport all occurring. However, often these processes are mixed up. For a start we focus on the vertically dominated processes.

### **a.) Matrix Flow**

Flow through the soil matrix is induced by, among other things, gravity and capillary forces in the little micropores. These are defined as having an average diameter or thickness smaller than 1/16 mm (CHOQUETTE & PRAY, 1970). Here, flow can occur in either saturated or unsaturated conditions. The speed of flow depends on the hydrological conductivity of the soil matrix, which itself is a function of the soil texture and the soil water content (BEVEN & GERMANN, 1982). The dependence of hydraulic conductivity on water content is shown in Fig. 2.2. Especially in the vadose zone, where a range of water contents is likely to be encountered, the hydraulic conductivity has great variability.

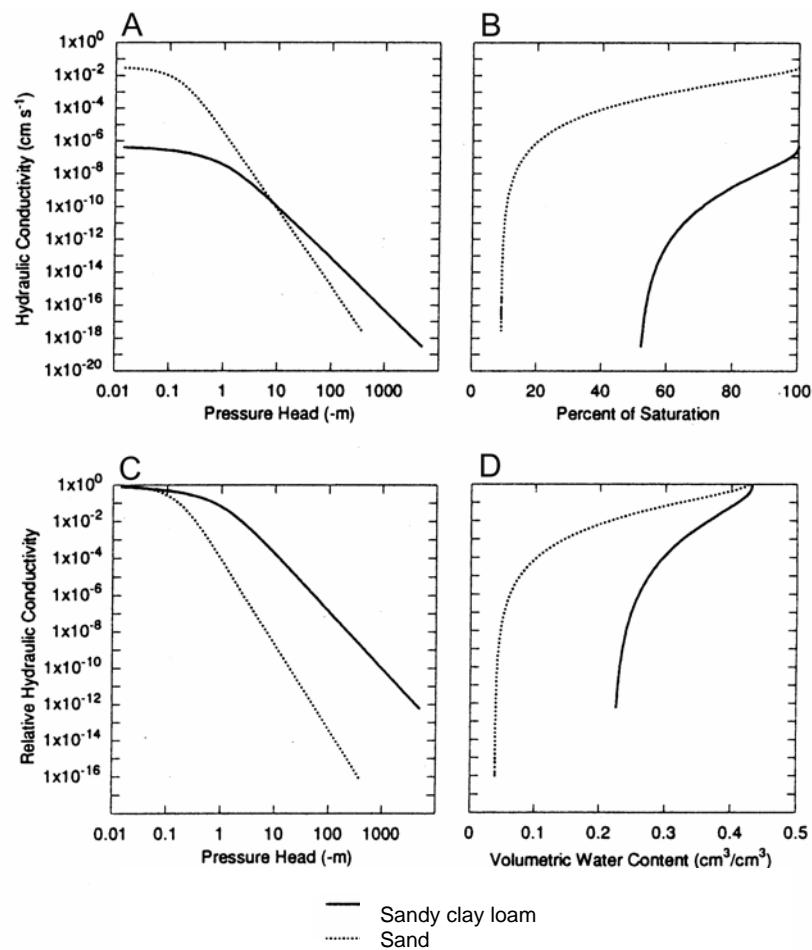


**Fig. 2.2:** Hydraulic conductivity versus pressure head for sand and sandy loam (A); hydraulic conductivity versus water content (B); relative hydraulic conductivity versus pressure head (C); and relative hydraulic conductivity versus percent saturation (D). Corresponding water retention curves and specific moisture capacity for these soils are not shown. From: STEPHENS (1996).

## b.) Preferential Flow

This includes all processes where infiltrating water is able to move better through the bulk soil (ANDERSON & BURT, 1990; LUXMOORE, 1981). Here, by-passing is not necessary but often achieved. Factors affecting preferential flow include: (1) soil structure; (2) soil hydraulic properties and profiles; and (3) rainfall intensity (MCINTOSH et al., 1999). Preferential flow is used as an umbrella term for the following presented:

### Finger Flow

Fingered flow occurs in a perfect homogeneous, sandy, porous medium. The wetting front becomes unstable, breaks up like a flame front and splits into "fingers" (HILLEL, 1987; GLASS & NICHOL, 1996). Fingers may occupy only a portion of the horizontal cross sectional area of the porous medium, an observation which led THOMAS & PHILLIPS (1979) to conclude that recharge of groundwater can occur long before the soil is thoroughly wetted. It is important to point out that there has been more experimental laboratory work than field work to verify the importance of unstable flow.

**Funnel Flow**

Funnel flow occurs when the downward water flow gets funneled or diverted towards one side because of the barrier concept. For further details on this very special process see WALTER et al. (2000).

**Macropore Flow**

Out of the presented types of preferential flow, macropore flow is predominant and very common. Macropores are structural pore spaces in the soil with a diameter of 3 to 100 mm according to DINGMAN (2002), although other authors set the lower boundary higher (overview in: LUXMOORE et al., 1990). Another definition is presented by LUXMOORE (1981) for soil pores with matric potentials greater than -0.3 KPa and corresponding diameters greater than one millimetre. BEVEN & GERMANN (1982) point out that size is not an absolute criterion as long the structure of the pore allows episodic, turbulent flow. A review of different definitions of macropores is provided by LUXMOORE (1981) and CHEN & WAGNER (1992). The origins of macropores are root holes, earthworm channels, and other kinds of bioturbation like vole tunnels as well as shrinking cracks or fissures (BEVEN & GERMANN, 1982). The resulting types of macropores therefore differ (Fig. 2.2.1) and often establish a wide, continuous, and diverse network (WANG et al., 1994). Fig. 2.2.2 gives an idea of the interconnecting, three dimensional network. Water conductivity is more strongly related to the continuity of a network than to pore size and shape (BOUMA et al., 1977).

Generally water can flow into macropores from the soil surface, or from the saturated or partially saturated soil layer. Flow initiation is controlled by initial water content, rainfall intensity, rainfall amount, hydraulic conductivity and surface contributing area (STEPHENS, 1996; PHILIP, 1993).

MOSLEY (1979) first found ample evidence that macropores can conduct water in considerable distances through otherwise unsaturated soils at velocities of several millimetres per second. Macropores allow the water to bypass the soil matrix, which is why the term "bypass flow" is commonly used (ONODERA & KOBAYASHI, 1995). This is possible under two main circumstances: Macropore flow with little or no interaction, and macropore flow with high interaction with the surrounding soil matrix (MCLAREN & CAMERON, 1994). Here, the potential gradient causing the macropore bypass flow, is not in equilibrium with the gradient in the soil matrix. The water transfer between macropores and the surrounding soil matrix depends on the properties of the surfacine of the macropore (BEVEN & GERMANN, 1982). There is also a general relation between the minimum pore diameter that will cause bypassing and the pore size of the soil matrix (DINGMAN, 2002).

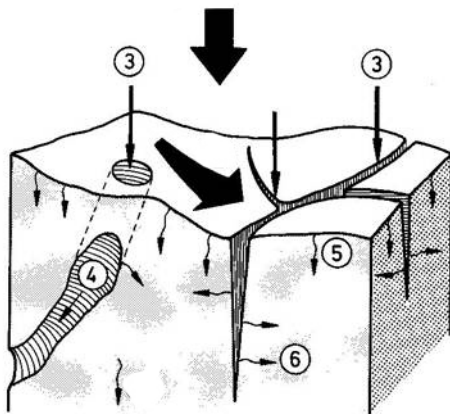


**Fig. 2.2.1:** Hydrological processes at infiltration. Note: Different shapes of macropores (3), macropore flow (4), infiltration in soil matrix (5), and interaction (6).  
From: BEVEN & GERMANN (1982).

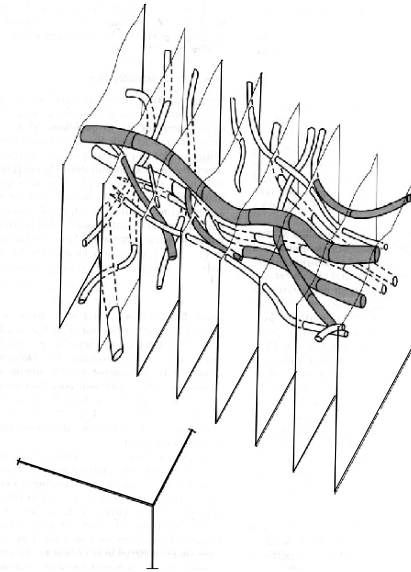


**Fig. 2.2.2:** Macropores and live-root (white) in the soil behind a trench face in a forest floor.  
From: STRESKY (1991) in DINGMAN (2002).

### Soil Pipe Flow:

Soil pipes are described as “a chain of connected macropores, developed nearly parallel to the soil surface” (T. UCHIDA, personnel communication). They are developed out of macropores as flow becomes turbulent and erosion is primarily affected by corrosion and undermining of pipe walls. This is promoted by chemical erosion, where the soil becomes more porous, a process called suffusion. Hydrologic function of soil pipes is strongly influenced by differences in morphology and connectivity of soil pipes. JONES & CRANE (1984) noted two groups of pipes, those that demonstrate a flash response and those that respond in a more subdued manner during storm events.

Generally they are most often rounded by the hydraulic enlargement, which means that cross sections are often approximately circular (TERAJIMA et al., 2000). The diameter of soil pipes is adjusted up to 2 m (KIRKBY in: BONELL, 1993). Velocities average 0.1 m/s and range as high as 0.8 m/s (JONES, 1971) in relation that the main pores of the soil pipes mostly ran parallel with the slope gradient (TERAJIMA et al., 2000). Soil pipes occur at greater soil depth particularly at less compacted, well draining soils with higher hydraulic gradients (BEVEN & GERMANN, 1982). Soil pipes are highly discontinuous (Tsuboyama et al., 1994). A length mapping of soil pipes by KITAHARA (1994) showed maximum lengths of usually a couple of meters. The occurrence of soil pipes does not depend on the soil texture. Ziemer (1992) pointed out that clear cut logging increased subsurface peak pipeflow by factor 3.7 in relation to natural conditions of a forested hill slope.

## 2.3 Conclusions

The alignment of macropores does provide flow possibilities in vertical and also transverse directions. Major characteristics are the rapid bypass of the soil matrix and the extended network of macropores, which is able to drain a great area.

An overall summary of already detected mechanisms at a singled out, well studied hillslope is shown in Fig. 2.3. The literature review shows that to date, not much is known about the connection of lateral and transverse flow paths. Many studies show these mechanisms only roughly and without details (e.g. Fig. 2.3).

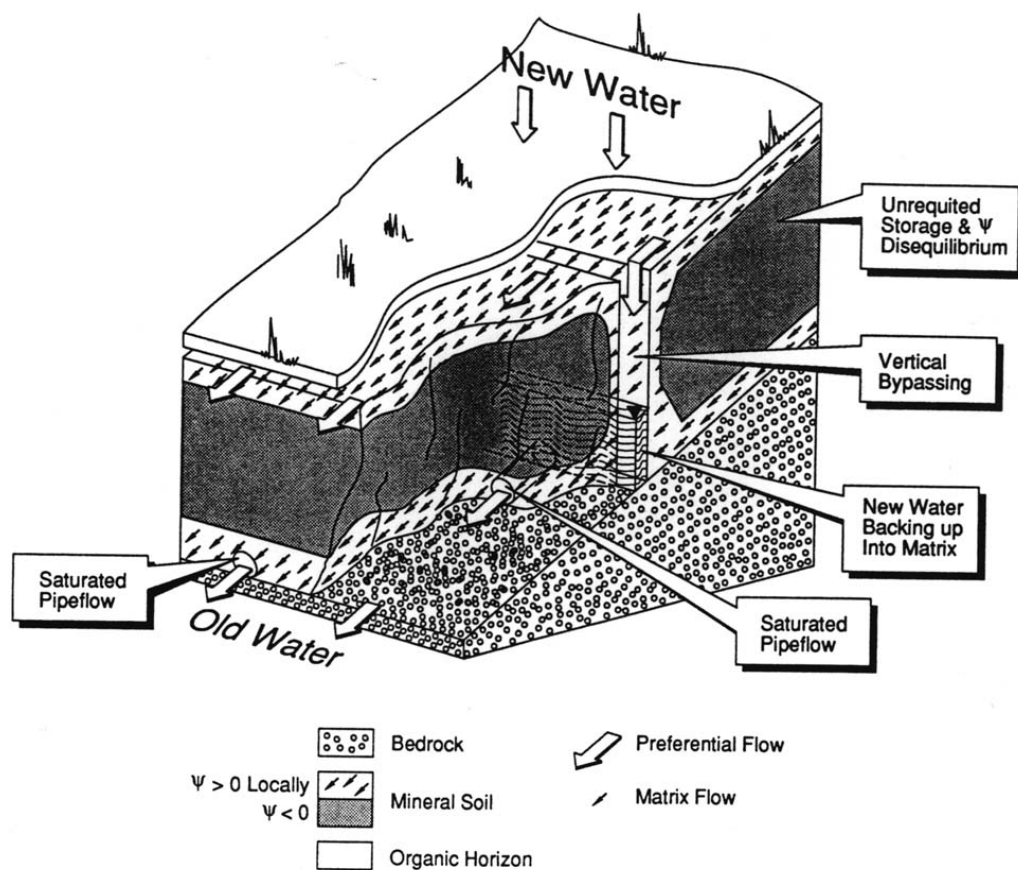


**Fig. 2.3:** Conceptual model of runoff generation at the Maimai hillslope, New Zealand. From: MCDONNELL (1990).

## 3 Site description

### 3.1 General

The fieldwork was carried out at a forested hillslope in the Coast Range, Western Central Oregon, United States of America. This site is called Low Pass with reference to its nearest geographically important feature and is situated approximately 34 km west of Eugene (Fig. 3.1). The United States Department's Interior Bureau of Land Management is in charge of the site and contracts Oregon State University, Corvallis, Oregon and the USDA Rocky Mountain Research Station, Boise, Idaho for the research project. The hydrological experimental setup in this catchment was established in autumn 2002 and in spring 2003. This new phase of research is related to an earlier study, although with a different focus, undertaken by the U.S. Forest Service. The features of this intensively studied single hillslope are described later in Fig. 4.1b.

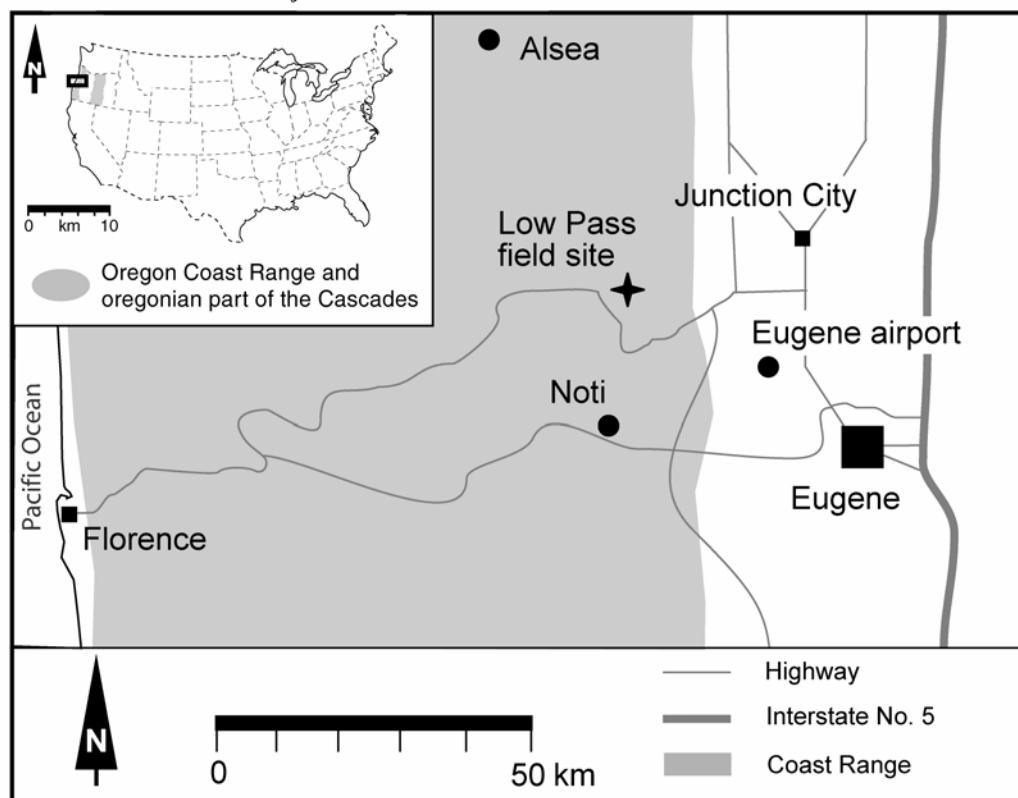


Fig. 3.1: Location of field site (indicated by star) and near climate stations.

### 3.2 Climate

The climate pattern of Central Oregon is dominated by the marine environment of the Pacific Ocean associated with fronts and large moisture supply. Air containing moisture must rise to pass over the mountain ranges and the vast majority of the precipitation falls on the western side of the mountains, leaving the eastern side much drier. Therefore two major precipitation gradients occur inland; first, at the Coastal Range and second, at the Cascades. In between the two ranges is the interior, drier region Willamette Valley.

The study site is located east of the Coastal Range divide and due to its remoteness, is distantly surrounded by three climate stations, listed in Tab. 3.2. Note that the distribution of precipitation is uneven due to drastic changes in physical geography, mainly related to changes in elevation. The climatic conditions of the hillslope is probably between those of the Noti and Alsea fish hatchery stations, with a little stronger similarity to Noti, as they are located on the same longitude and are closest to each other. We therefore assumed a total annual precipitation of ~1600 mm for our hillslope, which is based on open land precipitation. As later presented the throughfall value in this forested area is less.

**Tab. 3.2:** Documentation of climate stations and amount of total annual precipitation  
(From: WESTERN REGIONAL CLIMATE CENTRE (2003))

	Years	Total annual precipitation [mm]	Distance to study side [km]	Direction; location attributes	Elevation [m a.s.l.]
Noti	1964 - 1991	1557	8.3	S	137
Alsea, fish hatchery	1954 - 2002	2338	28.75	NNW	70
Eugene, airport	1939 - 2002	1093	18.25	ESE; lee valley plain	120

A high seasonality of rainfall is detectable for the site (Fig. 3.2). Most of the average annual precipitation falls between November and March. Note that the intense phase of field experiments for this study ran from March, 02, 2003 until May, 28, 2003. During very dry summer conditions the area is endangered because of bush fires.

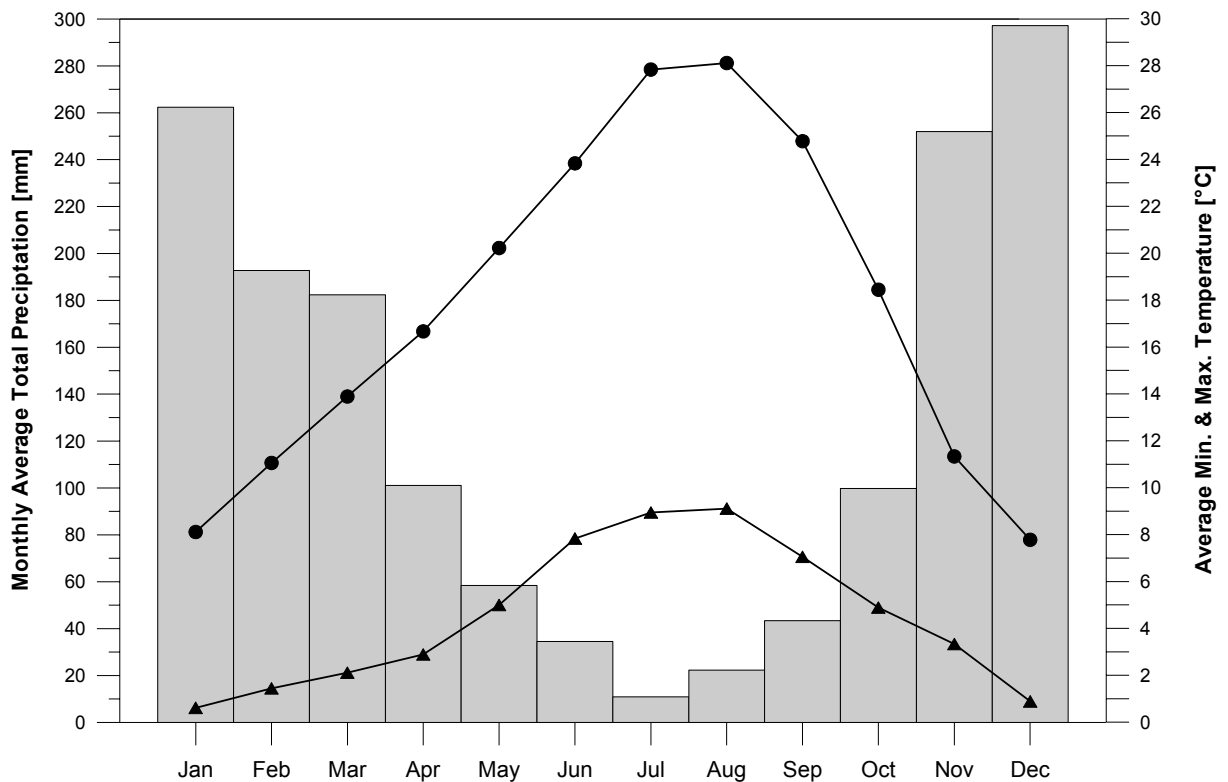


**Fig. 3.2:** Monthly climate summary for Noti. Monthly average of total precipitation indicated by bars, minimum (line with triangles) and maximum temperature (line with dots). Period of record: 4/ 1/1964 to 4/30/1991. From: WESTERN REGIONAL CLIMATE CENTRE (2003).

The average of monthly maximum temperatures at Noti is 17.7°C and 4.5°C for the minimum average temperature (WESTERN REGIONAL CLIMATE CENTRE, 2003). Another important factor for vegetation is the average frost-free season at the Lane Counties Coast Range (140 to 220 days; PATCHING, 1987). Mean annual potential evapotranspiration is 800 mm and actual evapotranspiration is 650 mm for this region in the Coast Range (LOY, 2001).

### 3.3 Geology and geomorphology

Bedrock of the Low Pass site is Eocene turbidite sandstone of the Flournoy formation (BALDWIN, 1974; WALKER & MACLEOD, 1991). This sediment rock is generally fractured in upper horizons. But not much is known about the depth and the conditions of fracture and permeability.

At some areas of the hillslope sabre growth of the trees indicates soil creeping or earth flow. This process occurred throughout a decade and is not a consequence of the excavated trench. This phenomenon is slightly visible in Fig. 3.4.1 and further more in Fig. A2a and A2b.

### 3.4 Soils

Doubtless soil properties are the most influential factors in this study. The procedure of soil characterisation orientated on AG BODEN (1996). It is based on the visible slope face of the trench below the hillslope (Fig. 3.4a), a cutslope along the forest road near the site (Fig. 3.4b) and the actual soil cores within the hillslope. The latter result from 16 auger holes (up to 250 cm deep) for the piezometer installation, distributed over the lower part of the hillslope in a grid (see Fig. 3.7). The drillings did not reach any bedrock supposing the total soil depth to be greater.

The soil order for Coast Range soils is that of an Inceptisols, which occurs in humid regions and have altered horizons which have lost bases or iron and aluminium but retain some weatherable minerals (UNITED STATES DEP. OF AGRICULTURE, 2003). A closer look at the soil cores (see Fig. 3.4c) characterised the series Bohannon sandy loam (PATCHING, 1987). This is a moderately deep, well drained soil, which was formed mainly in colluviums and residuum derived from sedimentary rocks.

Typically, the surface is covered with a mat of needles, leaves, and twigs about 2.5 cm thick. The surface layer is dark brown mineral soil with high live root content. This A-horizon is about 25 cm thick. Distinctive of the top layers of the B-horizon is the loamy sand with sandy-skeletal properties. That changes with increasing depth towards sandy loam with a subangular blocky structure. Also characteristic are loess/sand concretions reaching up to 2 mm in diameter. Highly fractured, weathered sandstone is at a depth of 180 cm. Depth to the weathered bedrock extends > 250 cm.

Moderately rapid permeability characterises this Bohannon soil. Available water capacity is about 0.09 - 0.2. Water supplying capacity is about 38 cm (PATCHING, 1987). The effective rooting depth at the site was 50-100 cm.

Detailed information on the individual piezometer core profiles are attached in Tab. A1.1 – A1.16. Coos Bay soils, where TORRES et al. (1998) and ANDERSON et al. (1997) described their experiments at Haplumbrepts of the Bohannon series, can be used for comparisons, although they mentioned that the sandy loam there is free of significant pedogenic structures that may favour preferential flow. They summarize that burrows and root holes become significant avenues for bypassing only if rainfall intensities are extraordinary high.

At the trench face, in particular, a lot of macropores were observed. These ranged up to 8 mm in diameter, with visible length up to 20 cm, and covered almost the whole trench face. An earlier dye tracing experiment of vertical infiltration, in the same vicinity, showed pathways with a length of 40 cm (M. WEILER, personal communication). A strong occurrence of macropores was found in upper horizons, where bioturbation is the main cause, followed by old roots. With greater depth, now in the sandy horizon, shrinking cracks as a result of saturated and dry conditions in this vadose zone become more important. Abundance of macropores declined towards a depth of 150 cm, where almost none of those structures could be identified.



**Fig. 3.4a:** Soil characterisation. Beside forest road is the trench excavation with visible soil face (cutslope) of hillslope investigated. Photography was taken prior to the installed roof construction.



**Fig. 3.4b:** Cutslope along the forest road about 200 m further away of the hillslope. The vertical distance of the picture is 2 m.



**Fig. 3.4c:** Soil profile of P\_B4 up to a depth of 120 cm. Note MUNSSELL colour scale 7.5 YR. Soil exceeding 120 cm depth did not show obvious colour variation to this photographed section and is not shown here.

Important features at this site were some prominent, natural soil pipes, occurring within the soil. Three soil pipes ended at the soil face in the trench and released water. The distance between these three outlets was several meters (see Fig. 2.5.1) and their alignment was almost horizontal. The shape and discharge pattern of the soil pipes is explained in Tab. 5.1. These soil pipes were probably developed from macropores and erosion forces, as mentioned above (UCHIDA et al., 1999).

A soil moisture characterisation along the trench or rather the visible soil face, shows the following features: The southern part of the trench (area of soil pipes openings) has obviously a wet surface. This general pattern is seen in Fig. 3.4.4. where the moss on the face just above the soil pipes indicates moist conditions. This section was the moistest part along the whole trench and contrasted to the north section, where the soil is dried out completely (see Fig. 3.4.1).



**Fig. 3.4d:** View of trench below hillslope. Note the location of the three soil pipes indicated by “x” (big one for SP1). The runoff gutters (subsurface flow collectors) did not have any use in this study.

### 3.5 Vegetation

The increase in precipitation from the Pacific towards the Coastal Range divide is the basis for coastal temperate rain forests, occurring along the North-American west coast (ELIAS, 1980). However, not many autochthonous forests survived and most are included in profit-oriented forest management schedules. So is most of the woodland at Low Pass under the management of the Forest Service, the Bureau of Land Management, or large private companies. The Oregon State Department of Forestry regulates many of the woodland practices used within the area (PATCHING, 1987).

Generally the hillslope is covered with a young stand of forest portrayed in Fig. 3.4.1. The site was harvested and yarded in July 1983 and replanted in 1984 with mostly Douglas fir (*Pseudotsuga menzeisü*). Other species were western red cedar, and salal. The vegetation on ground, hinted in Fig. 4.1 is dominated by sword fern (*Polystichum munitum*) and alder (*Alnus spec.*). The density of the canopy differs naturally with the some included light spots. Another feature is the existence of buried and semi buried branches and trees in the soil vegetation layer. These extended up to 1.2 m in diameter, and are remnants of former logging actions.

### 3.6 Overview of the hillslope site

The hillslope selected is a zero-order watershed or a headwater. The width of the investigated site is 30 m and upslope length ranges from 64 m (south) to 114 m (north), compare Fig. 4.1b. The probable drainage area of the soil pipes, or even an area of watershed, could not be determined explicitly. Instead, a maximum contribution area was calculated (see section 4.5.4).

The maximal vertical difference of the selected area is 60 m and the mean slope amounts to 21%. The general topographic pattern of the hillslope shows a concave hollow topography along the width. This site would be expected to have many confluent flow paths, a situation that might support flow path studies. Further the lengthwise topography shows a steeper bottom and a flattening out towards the ridge. The main part of hillslope is located above the forest road. A map of the hillslope plus the capture of the first order stream is shown in Fig. 4.1b.

### 3.7 Conclusions

The mountainous hillslope at Low Pass site in the Coast Range is predestined for the hydrological study of subsurface flow. Aforementioned characteristics of mostly lateral occurring macropores and presumably in some ways horizontal aligned soil pipes enhance the interest of studying the connection of these doubled domain preferential pathways.

In order to allow comparisons with other hillslopes where soil pipes occur, findings from the Low Pass site can be integrated in a wide range of results already presented (e.g. Toinotaini zero-order valley watershed in UCHIDA et al. (1999) or other a Coast Range site in TORRES et al. (1998)).

## 4 Methods

This chapter particularly shows the major field methods, the methods at the experimental hillslope table, the tracer experiments, the data analysis, and finally gives a brief summary of the basics of laboratory work. It also outlines some of the innovative technical installations which successfully drove process for the investigations at the hillslope table.

### 4.1 Field methods

Here, a description of the field methods, mostly on measurements techniques used at Low Pass site is provided. For a picture of the most centred installations see Fig. 4.1a. Note the black pipes in the back which delivered pipe flow to the tipping buckets (metallic boxes). After tipping the water ran along the diagonal pipe towards a white bucket. This is where the bromide probe is slightly visible at the very left edge in the picture. The three remarkable tubing and bottle units belong to the automatic sampling setup. For general orientation the map in Fig. 4.1b shows an overview of various instrumentations and the features of the field site.

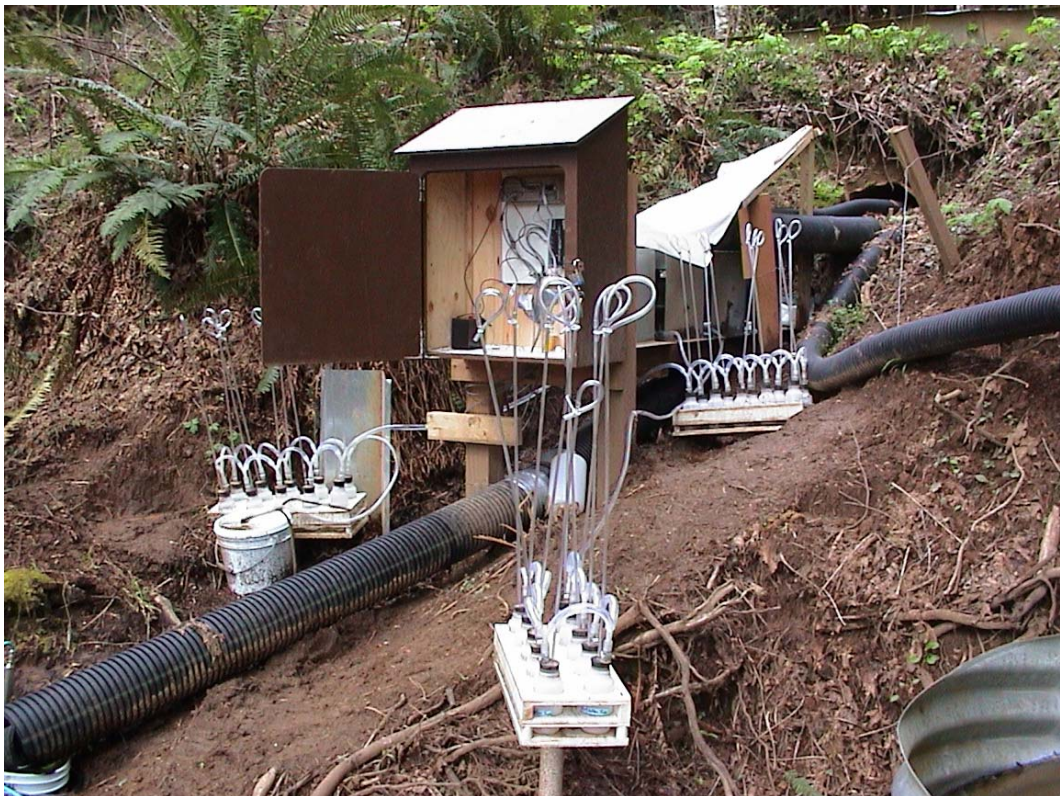
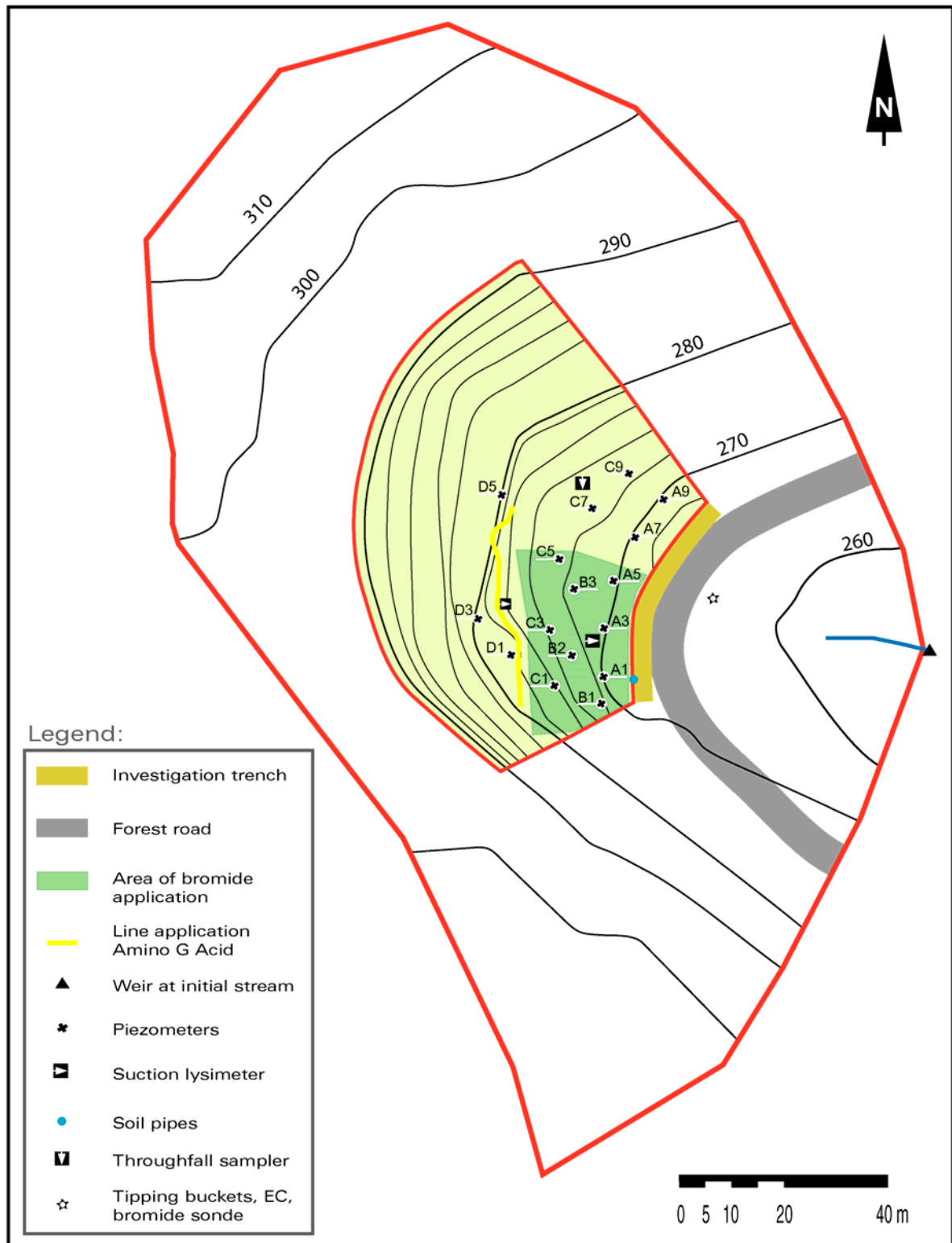


Fig. 4.1a: Overview of instrumentation around data logging unit at Low Pass field side.



**Fig. 4.1b:** Overview on investigated hillslope with instrumentation and extended catchment of a first order stream. Note that the isolines of the selected area show higher resolution because of internal survey. Piezometers are assigned by alpha-numerical identification codes.

The installation of a trench at the bottom of the hillslope enabled more precise observations of soil processes. This approach for the detection of subsurface flow mechanisms was described by WOODS & ROWE (1996) and various others. The vertical face (1.8 m high and 30 m long) was cut across the toe of the hillslope by a power shovel and backhoe. In this way the soil pipes were excavated in a formerly moist area along the forest road. The cut did not smear the surface structure of the soil face too much. In order to protect the surface and to supply a proper discharge sampling of the soil pipes the whole trench was covered by a plastic roof construction (Fig. 3.4.4). Any observations of the face after rain events (change in soil moisture, wetting increase) were easier to make under the roof's shelter.

#### 4.1.1 Determination of precipitation

The experimental hillslope is forested with a 19 year old mixed population of coniferous and deciduous species (see section 3.5). Here, open land precipitation differed from the effective precipitation reaching the soil because of interception. For Douglas fir stands (NW America at 45° Latitude) studies have shown 24% interception loss of gross precipitation, for Douglas fir and others 32%, and for Douglas fir and hemlock 34% (DINGMAN, 2002; ROTHACHER, 1963). Although these values represent old-growth stands, there is still an interception loss for young stands situated at the field site.

Dealing with interception losses and in order to quantify good data about the input, throughfall was measured. A classical rain gauge aperture with a modified top was installed below the canopy layer. The two extended sampling troughs and the rain gauge itself are shown in Fig. 4.1.1. Each of the 2 m long white plastic pipes had a slit of 19 mm widths on top, large enough to prevent blockage by conifer needles. Both branches were installed at an angle of 22.5° (which is slightly less than the angle of the collector funnel in a standard rain gauge). The area of the two troughs projected to the horizontal exactly doubled the normal catch area of the 20.32-cm-diameter gauge. The collected water reached a standard gauging tipping bucket system, where intensity data was recorded. The resolution of this system equals 0.127 mm throughfall per tip, which is calculated relying on the doubled area ( $=0.254 \text{ mm} \cdot 0.5$ ). The tipping bucket is logged on a HOBO data logger produced by ONSET, Co. LTD. Data collected needed a special post processing, as they are stored based on events (event samplers). The temporal disaggregating towards 10 min intervals was done with an algorithm (see appendix C7). The rain gauge was located on the ridge of the investigated hillslope, 120 m north of the north-west edge of the drainage area and did not fit on the map extent (Fig. 4.1b).

In addition to the gauging of throughfall a further aperture was set up to collect samples of rainwater. For this installation the same kind of collector head was used, supplemented by a RUBE-GOLDBERG sampler (see section 4.1.4) below which allowed taking continuous and flow proportional samples. This sampling of throughfall took place in the middle of the investigated hillslope (see Fig. 4.1b). For convenience, the terms throughfall and precipitation will be used interchangeably as most data deal with these values. In contrast the term "open land precipitation" is used at the beginning of section 5.2 in one case.



Fig. 4.1.1: Throughfall gauging below canopy layer of mixed forest.

### 4.1.2 Tipping buckets

Discharge running out of the four soil pipes was collected by a small steel barrage (see Fig. 3.4.4) and introduced into a pipe. Pipes lead the water then underneath the forest road and direct it into a tipping bucket. A roof covered the tipping buckets to prevent direct precipitation.

The determination of discharge quantities that occurred at the field site was most feasible by the use of tipping buckets. This approach offered both, good accuracy and clear measurable temporal solution. The tipping buckets were manufactured in a limited edition (prototypes) on the assumption of about 1.5 l volumetric content per bucket. An accurate calibration was done afterwards, as the fine adjustment in balance changed. Overall no problems occurred with tipping buckets during the investigation period. For details on the construction see Fig. C1.

A reed contact recorded each tips and transferred the data to a CAMPBELL SCIENTIFIC, CR10 data logger. Here, flow was recorded at ten minute intervals. The tipping bucket at the field site was located below the forest road.

### 4.1.3 Electrical conductivity

Above the tipping bucket, a probe measured the electrical conductivity of the water, before it flew into the bucket. The concern for that was monitoring any tracer breakthrough curves.

This probe was built after sketch by CAMPBELL SCIENTIFIC and contained a temperature corrected ohmmeter with a PT 100 thermistor in its core. There was found just little deviation of 5  $\mu\text{S}/\text{cm}$  to a commercial, standard conductivity device. For details on the wiring and construction see appendix C5. The gauged data water temperature and electrical conductivity were stored with a CAMPBELL SCIENTIFIC data logger. In this study the storage module recorded an average of ten minutes.

#### 4.1.4 Automatic sampling setup

The collection of water samples after the tracer application was an essential part of the experiment. Besides taking manual samples at the soil pipes, a continuous sampling of the discharge was prepared. RUBE-GOLDBERG samplers are simple to produce, have low costs, and are also well functional and automatic. The most favourable advantage is their direct dependence on discharge quantities. This pattern is necessary for any calculation of tracer mass. Such a setup was installed at the outflow of the tipping buckets. Out of the set of three tipping buckets and sampling units, outlined in Fig. 4.1a, just one set was delivered by water from the soil pipes. The water ran out of a bucket onto a flow splitter (pipe with a tiny opening on its convex top). The small diameter allowed 1.5 ml (about 1/1000 of total content tipping bucket) to enter the pipe which ran towards the first bottle of the automatic sampler. One bottle's capacity within a series of six was 270 ml. If this amount had passed through, the next bottle was filled automatically. For an illustration of the RUBE-GOLDBERG sampler see Fig. 4.1a. Full sampling bottles were replaced by new ones every day (at the start of the experimental period) and every seventh day (towards the end).

#### 4.1.5 Bromide probe

The constant monitoring for bromide concentrations was done with a ion-sensitive bromide probe, manufactured by INSTRUMENTATION NORTHWEST, Inc., Kirkland, USA. It is a TempHion Submersible Water Quality Sensor called T2, built in 1998 (INW, 2003). This ion specific electrode (ISE) works based on direct potentiometry, which means that there are two electrodes that read simultaneously, one sensing electrode and one reference electrode (submersed in the silver chloride filling solution). These two electrodes act like a dry cell battery, where the measurement is made after there is difference between the two electrochemical "half-cell potentials." The NERNST-equation is used to determine half-cell potential of the sensing electrode, given a stable reference potential (provide by the AgCl); then that was temperature compensated. All of the equations assume activity of bromide and not concentration. The installation needs to be vertical, why it was placed inside a bucket, where outflowing water of the tipping buckets constantly ran through. An additional shelter prevented algae growth caused by radiation. The monitored data was stored by a CAMPBELL SCIENTIFIC data logger every ten minutes.

### 4.1.6 Piezometer

Right from the start piezometers were seen as a key tool on the hillslope study. The distribution of piezometers over the hillslope is concentrated in the lower section, closer to the trench and the soil pipes. The installation had one first row closely parallel to the trench and three more following, the last of which had a distance of 35 m to the trench. The grid arrangement of the piezometers is presented in Fig. 4.1b and exact locations are attached in Tab. A1.1 to A1.16. From now on the abbreviations tell about the location (row and number of the piezometer, e.g. P\_A5; see Fig. 4.1b)

The initial core hole for the piezometer was made by a hand drill of 8 cm diameter. Drilling and drawing up the particular soil profile are done simultaneously. An extension enabled to reach depths of 250 cm, although this could not be achieved at all spots because of local bedrock formation. In those conditions the minimum achieved was 110 cm. After completion of drilling, surrounding PVC-pipes were fitted into the hole. As this application focused on water tables in the saturated zone, the arrangement of slits in the PVC-pipe is just in the lower part. See appendix C2 for further information.

The recording of water table height in the soil was achieved by installation of a piezometer in the PVC-pipe. Water table recorders WT-HR, produced by TRUTRACK, Co. LTD, New Zealand were installed. Further details on this tool provides appendix C2. In this study averages of 10 minutes were recorded.

Finally the successfully installed piezometers were tested on their connection by a slug test. An analysis of slug test data offered the calculation of the hydraulic conductivity using the method of BOUWER & RICE (1980). The method can be used on semi-confined aquifers that receive most of their water from leakage from the upper confining bed and unconfined aquifers. The solution is based on the THEIM-equation and assumes negligible drawdown of the water table around the well and no flow above the water table. The solution is described by the following equation:

$$K = \frac{r_c^2 \ln(R_e/r_w) \ln(y_0/y_t)}{2 t L_e} \quad (\text{E. 4.1.6a})$$

where:	K	= hydraulic conductivity [m/s]
	$r_c$	= radius of well section where water level is rising [m]
	$R_e$	= effective radial distance over which the head difference $y$ is dissipated [m]
	$r_w$	= radial distance between well centre and undisturbed aquifer ( $r_c$ plus thickness of gravel envelope) [m]
	$L_e$	= height of perforated, screened, uncased or otherwise open section Of well through which ground water enters [m]
	$y_0$	= $y$ at time zero [m]
	$y_t$	= $y$ at time $t$ [m]
	$t$	= time since $y_0$ [s]

Additionally the simplest interpretation of piezometer recovery is that of HVORSLEV (1951), which was used for comparisons:

$$K = \frac{r_c^2 \ln(L_e/r_w)}{2 t L_e} \quad (\text{E. 4.1.6b})$$

where: *see above*

### 4.1.7 Suction cup lysimeter

The purpose of these was to sample the draining water in different soil depths. The available sampler constructions offered either ceramic suction cups or in-situ lysimeters (constructed from fibre glass cylinders). According to WEBSTER et al. (1993), both showed same bromide tracer concentrations for a sandy loam. But contrary to these findings indifferent phosphor concentrations (4.6 times higher) were found in lysimeters than in Teflon suction cup samplers for a macroporous layered sandy soil (MAGID et al., 1992).

However this study goes along with the first one and so totally six suction cup samplers were distributed along the hillslope. In the following no distinguishing is done between the different terms mentioned above.

The soil water samplers (Model 1900) were manufactured by SOILMOISTURE EQUIPMENT CORP., Santa Barbara, USA. The method of suction cup samplers was reviewed extensively by LITAOR (1988). They are simple but do provide important insight into the infiltration process. One clustered arrangement, consisting of three lysimeters, was located just below the line source tracer application while the other one is within the first row of piezometers measuring tracer applied over the area (see Fig. 4.1b). Hence, both are referred as either upper lysimeter (L\_U) or bottom lysimeter (L\_B). Each set contained soil water samples of 30, 50, and 70 cm depths in order to focus on a tracer gradient and its temporal movement through the soil. Thus giving an idea how far the tracer went. Further details and a figure of the lysimeter are attached in appendix C4.

The time ahead the first sampling was 9 days (which is less) to settle the new erected lysimeter. For the collection, a vacuum between 50 and 60 kPa was created by using a vacuum test pump with a dial gauge. ANDERSON et al. (1997) and LUXMOORE (1981) used a suction vacuum of 8.5 kPa in particular for mesopores, although the gradient drives water from a wider range of pore sizes. Of course pressure head is somewhat arbitrary. No significant difference in the composition of soil-water solutes was found by BEIER & HANSEN (1992) when they compared a 40 kPa falling head vacuum with a continuous vacuum of 10 kPa. Therefore no systematic error was seen in the 50 to 60 kPa used in this study under the assumption of sampled pore sizes < 5 µm.

After the vacuum was applied, the closed pinch clamp sealed the sampler under these conditions. This caused the moisture to move from the soil through the porous ceramic cup into the lysimeter. During the experiment the intervals for the suction time were set to

24-48 hours. ANDERSON et al. (1997) used a time step of 6 – 20 h. However this longer time step provided an integrated sample over the time and avoided water samples too small. The required quantity for the analysis was 20 ml; this would have been more difficult to achieve in some drier periods with smaller intervals, just set up on the particular sampling visits. On the other hand a smaller time interval would provide more exact information. To remove the soil water sample from the piezometer a plastic tube, a two-hole rubber stopper, a flask or bottle and the vacuum hand pump were used. Before and after each sample collection, the tube and the bottle were rinsed twice with deionised water.

#### **4.1.8 Mini v-notch weir**

For the first order stream a weir was installed and a related catchment proposed. Generally the triangular shaped weir of Fig. 4.1.8 stated below was installed for additional information on the understanding of whole hillslope response to rain events. At this low altitude in the gully, most of the hillslope's runoff was assumed to pass by. This enhances the descriptive data on the initial stream related to the runoff processes at preferential pathways at the soil pipes.

The advantage of the flume installation, instead of another tipping bucket, was an easy and quick installation. Especially in gauging discharge of smaller quantities they offer accurate results. The shape of the opening is a "v"-notch with an angle of 60°. The water height in the notch was recorded by a water height recorder WT-HR, mentioned earlier in this section. Data is arranged in 10 min intervals. In general, uncertainties of the flume are larger than the one of the tipping bucket, measuring the soil pipes. Although the data logger had a one mm resolution, high maintenance was required in this forested catchment to receive confident data. Any branch being in a cleft stick at the "v"-notch resulted gauge errors. So the data processing needed much effort. Most obvious single errors were corrected manually. Some remaining data were not corrected due to uncertainties of true or false data. Further details on the weir and the discharge calculation are discussed in appendix C3.



Fig. 4.1.8: Flume with WT-HR water height recorder.

#### 4.1.9 Soil moisture probes

At a representative location of the hillslope three soil moisture probes were installed in 30, 50 and 70 cm soil depth. Unfortunately, there occurred a battery error with a loss of major data. A reason here fore was the high required voltage for the three probes connected to the same battery supply. This problem was solved with an installed 12 V battery instead of one with a smaller capacity. The series of available data is very restricted and does not allow expressive conclusions to be presented here. For further information on the installation and technical details see section 4.2.6.

## 4.2 Experimental hillslope table

Artificial, physical experiments in science demand to simulate the natural processes. Although the simplified approach can not capture the entire complexity of natural systems there is still evidence about the gained process understanding. To achieve perfect identity between natural processes and simulation must fail. Moreover the goal is merely to get best possible reflection of the natural processes, particularly as hydrologic modelling is most credible when it does not pretend to be too sophisticated and all inclusive (KLEMEŠ, 1986).

Runoff development on hillslope scale is complex and often includes a combination of several processes. Regarding the physical modelling the outstanding difficulty is to arrange the soil structure at the experimental setup in its original pattern.

### 4.2.1 Table itself

Performing experiments on an artificial hillslope table needs a particular geometrical affinity to truth hillslopes. The dimensions were 198 cm width, 395 cm length and 20 cm depths (18 cm effective soil depth). Unchanneled headwater basins often show roughly about these three dimensional ratios (GUTKNECHT, 1996; TORRES et al., 1998). Most important in this study was the similarity of the Low Pass field site and the experimental table. The length and width there for the more detailed section was about 40 x 80 m, and the approximate soil depth until the bedrock showed at least 2.4 m. Another affinity was the slope. Following the Low Pass field site, the tables slope was set to 25% (respectively 14°) to provide similar environments.

The presented Fig. 4.2.1 shows the table, including the soil filling and the nozzles of the rain simulator. The black plastic nearby the table helped to minimize the errors of spray, where the irrigation failed the table. This error was very little, but nevertheless was collected by the galvanized gutters. On the soil, little tubes belonging to the little water sampling wells (see section 4.2.5). Furthermore a black cable is visible which belongs to a soil moisture sensor, buried underneath.

The base of the table was a heavy steal frame with four legs. Above, the basin (rectangular parallel piped) was lined out with smooth PVC boards and sealed properly. The outflow side wall contained wire netting (mesh size: 2 mm) over the full width, where the water was able to pass through. Then water was divided into eight chambers (sediment trapping), which each contributed towards a tipping bucket. See Fig. 4.2.3a for the arrangements of tipping buckets.



**Fig. 4.2.1:** Artificial hillslope table and rainfall simulator. Note that the centred gutter does not fit into the setup, this is a protection against splash effects on the soil from nozzles after the run.

## 4.2.2 Soil filling

Filling up the empty table was presumably the major challenge within the work on the experimental hillslope. Natural conditions of soil features at the field side are most subtle and change a lot. The detailed transfer of structures, developed throughout many years to an artificial hillslope, using manpower and a shovel is impossible. Outstanding changes find expression in soil density, water holding capacity, predefined pathways for water, etc.. A literature review on soil packing found very less records about the filling for bigger volumes, whereas much was found for soil columns and porous groundwater aquifer modelling (OLIVIERA et al., 1996).

It is apparent, that a raining method with free falling sand passing through a sequence of sieves before reaching the surface of the sand body was used at different groundwater experiments (STAUFFER & DRACOS, 1986). In general literature elucidated two different ways of filling the soil in order to get close to original conditions. One is described by wet filling. Here the sand is washed in, most suitable the sand water blend runs through a hose. For this process gravity is less dominant, which causes a different particle distribution and erection of layers. The wet sand is dried out afterwards. The other way is dry filling (OLIVIERA et al., 1996).

However, as this study had to deal with loamy sands instead of homogeneous sand, things were more difficult (YARON et al., 1966). Soil physiologists, who were included into the

question, recommended the dry filling technique. Here, theory incorporates a reduction of velocity for heavy soil lumps. This is commonly achieved by a designed construction of a vertical pipe with horizontal nails in randomly chosen arrangements throughout the length of the pipe. This little tool has great similarities to a 'rain stick' manufactured by the aborigines. The effect is a slow down of soil lumps, which does provide a homogenous soil arrangement in both, area distribution and soil depth profile.

In contrast to the recommendations the "delaying tool" could not be used for these experiments because of the loamy soil of the Low Pass site. Most of the soil was dense compacted. The actual distribution of the soil was undertaken by a rake, levelling layer after layer. No additional procedure was used to adapt soil density. The major concern about the soil treatment was to aware surface runoff. Therefore a minimal micro relief with tiny raked contours (plowing structures) was added on the top of the surface. The dry soil bulk density of the table was determined at two representative locations and varies around 1.1 g/cm.

### 4.2.3 Rain simulator

A rain simulator triggered the artificial rain for the table. Inflow quantities running in from the tab were measured by a flowmeter (accuracy:  $\pm 0,378$  l) at the tab. Sprinkling used water from the public water supply which was not demineralised. The simulator consisted of seven nozzles, fixed on a moving guide rail which moves along the length of the table. This was forced by an electrical, linear accelerator (rotating spindle). The brass nozzles sprinkled minute drops in a spraying angle of  $100^\circ$  towards the soil. The nozzles had an adjacent distance (centre to centre) of 40 cm. The elongation of the guide rail was equal to the distances of the nozzles; this means no overlapping of the spraying. As the motor moved linear, stopped at the end and returned linear no periodically distribution (e.g. sine function) traced the spray (WEILER, 2001). The impact energy of the produced sprinkle was small except for the time after the simulator was switched of and the remaining water run out. For those events a separate gutter was used.

To prevent undefined losses at the borders, a black plastic collected the spray-induced variations. The error of evaporation was assumed to be negligible. The finally deposited rain within five minutes was investigated in a test phase by nine beakers (diameter 5 cm) spread out at the table on a 3x3 matrix. Later these values were extrapolated to hourly intensities. The result showed lengthwise uniform artificial rainfall with a little asymmetric pattern along the width of the table (see Fig. 4.2.3b). Summarizing this pattern is defined as too small to result any influence on the goal of this study. The overall mean was 38 mm/hr, meaning on this hourly basis (although these experiments applied 5 and 10 min intervals). This intensity (on 1 hour duration) has a return period of about 100 years at the Oregon Coast Range (GOARD, D.L., in prep.).

The triggering of irrigation intervals relayed on the prevention of surface runoff. The irrigation rate for the table remained in 5 min on- followed by 10 min off-intervals. Towards the very end of the investigation the sprinkling quantity was raised up and a few runs took 10 min rain followed by a 10 min break.

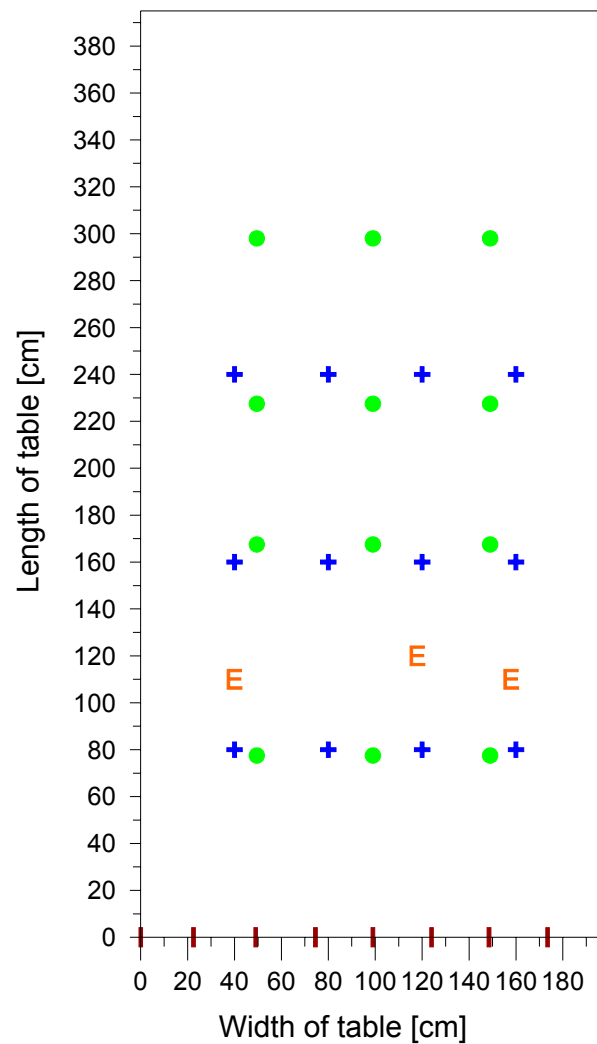


**Fig. 4.2.3a:** Shape of table, dividing for collection chambers of tipping buckets (vertical strings), piezometers (points), soil moisture sensors (E) and location of sampling wells (crosses).

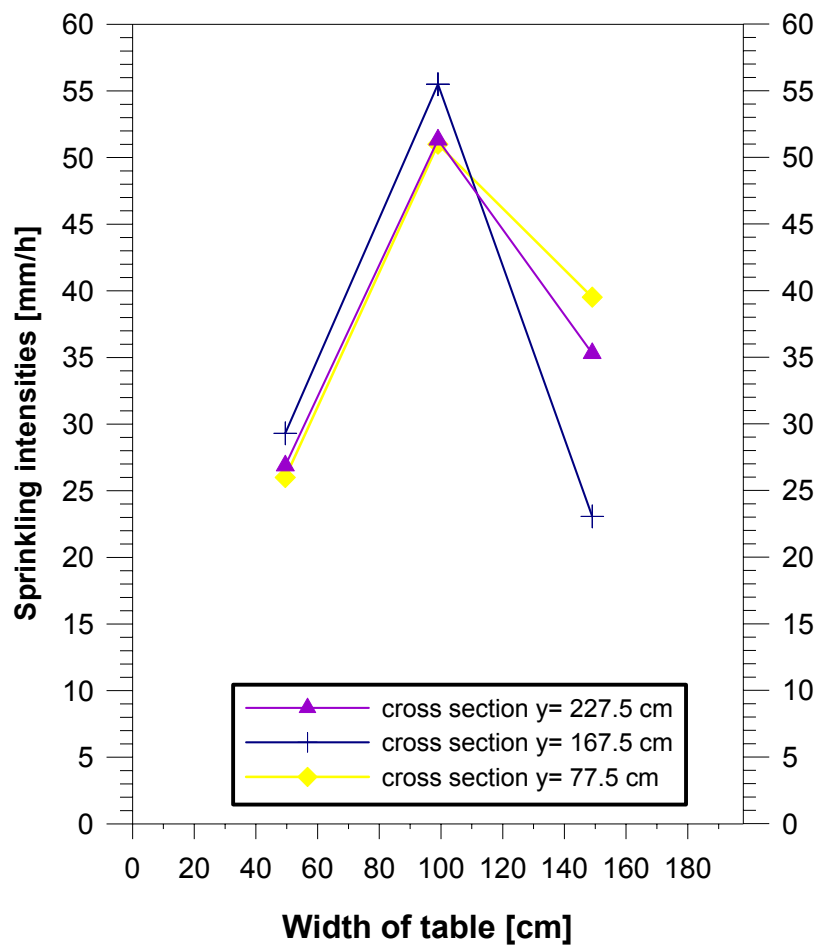


Fig. 4.2.3b: Distribution of sprinkling intensities (mm/hr) along different transects of table.

#### 4.2.4 Tipping buckets at table

The discharge quantities at the hillslope table are different from those in the field. While planning the experiment the same blueprint as for the tipping buckets in the field was scaled down to a volumetric content of 75 ml (see appendix C1). However, the small tipping buckets were arranged in a series of eight, to provide discharge measurements over the total transect of the tables outflow. A couple of problems raised from the downscaling of the tipping buckets and had to be solved. First, the weight of the bucket was heavy in relation to the weight of water. Second, the friction within the axis made accurate tipping initiation of the buckets impossible. However the problems could be solved by using ball bearings and going ahead with a general tuning. So, installation of the contact switch was modified and updated. After fine adjustments, the rating was investigated for the eight tipping bucket as a mean of 80 tips. Finally the volumetric content ranged from 53 -89 ml for the particular buckets (mean: 70 ml/tip). Final data went to a CAMPBELL SCIENTIFIC data logger, stored by sums over two minutes. Tipping bucket one (TB1) is on the left hand side of the table and captures the width 0 -22.5 cm. Tipping bucket eight (TB8) is at the end of the series at 173.5 -198 cm (see Fig. 4.2.3a).

### 4.2.5 Mini-wells for water sampling

Measuring tracer concentrations directly in the soil water was an important concern because this provided more detailed information on the movement of the tracer through the soil. For the spatial investigation of the line source tracer application (see section 4.3.2), twelve mini-wells were installed in a grid, shown in Fig. 4.2.3a. The constructional challenge for the mini-wells in the soil was high, in order to be aware of any rapid water passing by vertical closely. The sampling should exclusively include water from the lower centimetres of the soil layer. Therefore the construction is similar to the piezometers in the field with an additional suction pipe in the centre, which allowed the sampling of small water quantities out of the bottom close zone with a syringe. These small volumes were important in three ways: First, to keep as much water in the system as possible; second, to obtain real time samples, no former tracer concentration had firstly to be flushed out (amount of water) before taking the samples; third, low disturbances of the soil system. All constructional features are documented in appendix C7. The sample interval for these twelve mini-wells was 15 minutes.

### 4.2.6 Piezometers at table

The arrangement of piezometers at the table was different from that in the field. Furthermore the setup might be special, even for the first time described. The initial challenge was to establish a mechanism to get water table data within the shallow soil of the table (height 18 cm) without minimal interference. To be aware of any sprinkling water bypassing the piezometers, the decision went towards a minimal impact approach. Therefore a hole in the bottom of the table allowed pressure transmission in a connecting hose. This hose is permanently filled with water and ran towards a water level recorder WT-HR (previously mentioned in section 4.1.6). The connection between hose and WT-HR was established with some garden hoses and silicon work (Fig. 4.2.6). So the water height in the table and in the piezometer was connected by the hose. It was assumed simplistically that the water table within the soil matrix is equal to the non-soil conditions (plain column of water). This was the case as reference measurements were too difficult to obtain, although there were indicating data from the ECH<sub>2</sub>O probes (see later) about the soil moisture content. Medical gauze (bandage available at pharmacies) serves function of sediment protection at the entrance on the bottom of the table. The piezometers were arranged in four rows by each three (Fig 4.2.3a). This grid distribution was sufficient for the investigated phenomena of spatial water tables. The distance between the outflow and the piezometer rows was 77.5, 167.5, 227.5 and

298 cm. Out of totally 12 piezometers just two did not response properly after water table establishing. This was caused by either a clog up at the start of the hole of the table, or by any non-equal soil condition or lack of water from leaking at the PVC pipe and its connections. The data was recorded in two minute intervals.



**Fig. 4.2.6:** Three water table loggers at the side of the experimental table. Note the kind of fit from connecting hose to standard WT-HR 500.

### 4.2.7 Soil moisture probes

In addition to the water height in the table, useful information was gained from the soil water content. The applied ECH<sub>2</sub>O probes, manufactured by DECAGON DEVICES, Pullman, WA, USA, (DECAGON, 2003) are based on dielectric. They return volumetric water content. Out of the two available models, the EC-20 (thin strip of 20 cm length by 3 cm width) was used at the experimental table. In order to avoid any locally saturated conditions the arrangement of the probes was chosen to be vertical standing on their long axis, allowing water flow with no obstruction. The location of the three distributed soil moisture probes on the table is indicated in Fig. 4.2.3a. In relation to expected changes in water table levels, the depths of these differed. So had the left one a soil depth of 9 cm (respective 9 cm above bottom), the middle one 4 cm (14 cm above bottom) and the right one 8 cm (10 cm above bottom). The data was stored in a CAMPBELL SCIENTIFIC data logger at two minutes intervals.

For a final calibration two soil core devices (diameter: 97 mm) were used to sample soil close to the probes, weighted, oven-dried at 105 ° C for 24 hr, and weighted again. By that volumetric water content of ECH<sub>2</sub>O probes and water content are linked.

### 4.3 General information on the applied tracer

It is primarily proclaimed that concentration dimensions of parts per billion (ppb) equals µg/litre.

Bearing in mind the goal of soil water tracing, the decision in this study went towards the use of two artificial tracers. In general, specific investigations in the unsaturated zone are confronted with the high potential of sorption. First, Amino G Acid was applied as a fluorescent dye tracer for a line application in the ground, second was a salt tracer for the extensive distribution on the hillslope (vegetation cover close to the surface). Both Amino G Acid and bromide are commonly used in unsaturated zone studies (SCHUDEL ET AL, 2003; FEYEN et al., 1999). For general information on fluorescence tracer and analysis see SCHUDEL ET AL, 2003; MIKOVARI et al., 1995). No proof was found about interfering of bromide and Amino G Acid as co-tracers (whereas e.g. lithium bromide and Rhodamine do; JONES & JUNG, 1990).

For experimental runs at the hillslope table, those two tracers were applied, too. However, the bromide was added to the sprinkling water, an easier and clean way to do. To obtain further information on the flow paths the third tracer experiment contained a Brilliant Blue FCF line source application. Now, separate viewing follows:

#### **Line Source: Amino G Acid (Techn: 7-Amino-1,3 Naphthalenedisulphonic Acid Monopotassium Salt)**

Amino G Acid belongs to the group of functionalized polycyclic aromatic hydrocarbons. Various productions are available (e.g. CAS # 86-65-7, 842-15-9). For this study a composition with CAS # 842-15-9 by ACROS ORGANICS, Fair Lawn, New York was used. The appearance of the substance is almost white powder and the molecular weight comes to 341.4 g/mol.

Fluorescence tracers are easy to handle, simple to detect and rapid to analyse quantifiably using fluorometer techniques. Here, an exposure or an excitation with light reacts in the tracer's light emission peak of particular wave length afterwards. This pattern is significant for the substance. SMART & LAIDLAW (1977) report 355 (310) nm for maximum excitation and 445 nm for maximal emission wavelength. However, BEHRENS (1986) reported 359 nm for maximum excitation and 459 nm for an approximate maximal emission wavelength. This appeared to be closer of different productions. Emission spectra in our analysis showed peaks at 455 nm in the fluorometer. Using an emission peak set to 455 nm, there two excitation peaks occurred in the fluorescent spectrum at 310 (large peak) and 350 nm (smaller).

The chemical structure of Amino G Acid is shown in Fig. 4.3.1a.

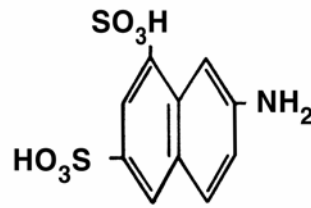


**Fig. 4.3.1a:** Structure of Amino G Acid. From: SMART & LAIDLAW (1977).

Important for any tracer is the chemical and physical interaction with the media, the so called effect of adsorption. This was of interest for humus, where the tracer was applied and for the soil itself, where tracer supposed to travel toward the soil pipes. Investigations on that with humus, where the dye suffers high adsorption losses, showed a loss of 61% from initial concentrations of 100 µg/l at sediment to solution ratio of 20 g/l (Tab. 4.3.1). For smaller sediment concentrations (2g/l) loss reduced to 25%. For an overview on Amino G Acid adsorption with humus see Fig. 4.3.1b. More recent studies ran experiments where concentrations were as low as possible where adsorption is equivalent less. This was a cause to minimize tracer input mass. Available data on the adsorption in mineral material was restricted to Kaolinit and Limestone. Tab. 4.3.1 shows the overall little adsorption losses for these. Amino G Acid is less adsorbed than Lissamine FF (and significant less than Rhodamine WT) (TRUDGILL, 1987). Although Amino G Acid is very little absorbing, it is seen as the best tracer for the requirements of the Low Pass field experiment.

Amino G Acid loses fluorescence below pH 6.5 and is generally more absorbed in alkaline soils. The loss in their studies remarks tracer loss for acid red earth (pH < 5.1) with 0.5-3%, for brown earth 64-66% and for brown calcareous earth 62-80%. Desorption ranged from 3% (for initial solution concentration of 2000 ppb) to 26% (initial solution concentration of 500 ppb) (TRUDGILL, 1987).

**Tab. 4.3.1:** Amino G Acid adsorption on mineral and organic materials. Figures are percentage of tracer remaining in a solution from 100 ppb initial concentration. From: SMART & LAIDLAW (1977)

Sediment Concentration [g/l]	Mineral		Organic	
	Kaolinit	Limestone	Sawdust	Humus
2	99	95	66	75
20	97	96	17	39

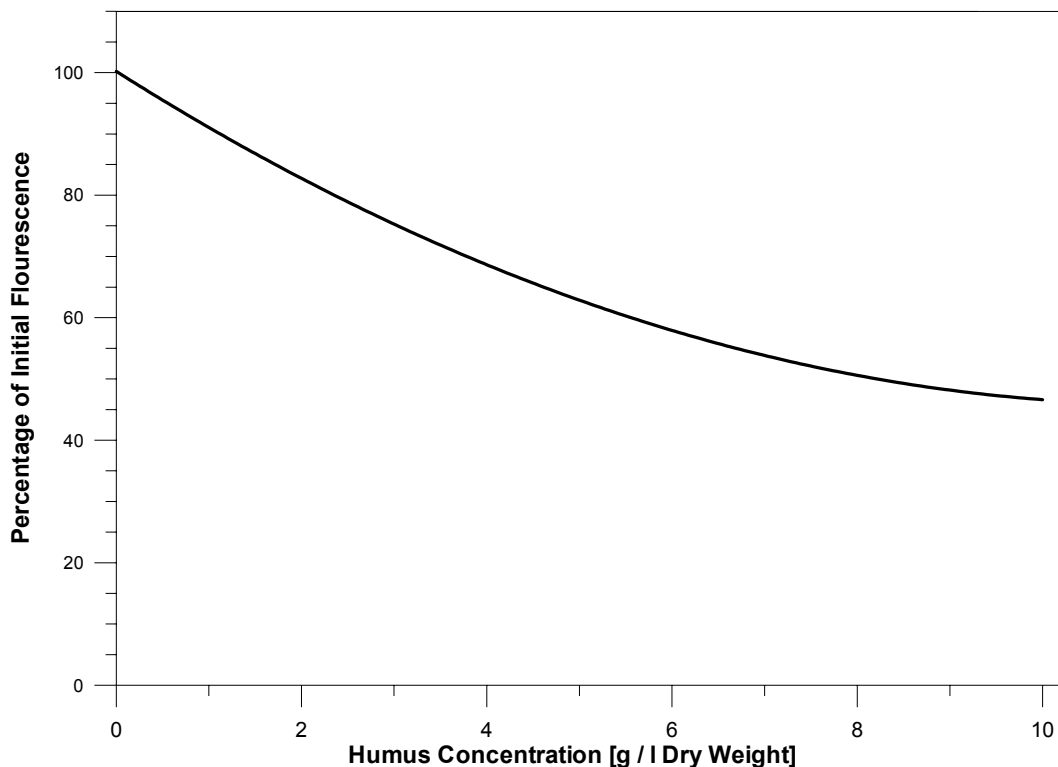


**Fig. 4.3.1b:** Adsorption of Amino G Acid on humus sediment. Initial concentrations were 100 ppb. From: SMART & LAIDLAW (1977).

Background fluorescence of Amino G Acid at brown calcareous earth for streams shows 20-100 ppb and for suction cups 200-800 ppb (TRUDGILL, 1987). Amino G Acid is subject to photochemical decay over a period of days. Thus dye solutions should be shielded from light before use and during collection and analysis. The photochemical decay for a setup of 100  $\mu\text{g/l}$  exposed six hours during sunny conditions amounted to a decay coefficient of  $1.6 \text{ E-}2$ . The same concentration for the same time under a 60 W lamp got a decay coefficient of  $3.7 \text{ E-}4$  (SMART & LAIDLAW, 1977). A covering of heavy duty polythene is recommended for water sampling apparatus.

No column test or batch test was performed with the soil at Low Pass field site in order to get better information on the sorption of this particular soil.

#### **Extensive application: Bromide**

The use of bromide in hydrology takes advantage of the circumstance that bromide does not occur naturally in most of catchments (FLURY & PAPRITZ, 1993). Bromide is not included in the nutrient cycle and there is no intake of micro organisms. Therefore excellent conditions for the detection of the tracer are provided. Concluding, bromide is considered as a conservative tracer in mineral soil (FLURY et al., 1995); Although there is evidence that in humic soil layers anion adsorption might occur (LANGE et al., 1996).

For these experiments a lithium bromide solution was used, manufactured by FMC CORPORATION, Bessemer City, New York (product CAS number: 7550-35-8). The purity of the colourless liquid is 75-80% (calculated with 77.5%) and the molecular weight equals 86.84 g/mol.

### Line Source: Brilliant Blue FCF

For the line source the food dye Brilliant Blue FCF (CAS # 42090; N-Ethyl-N-[4-[[4-[ethyl[(3-sulfophenyl) methyl]amino]phenyl](2-surfophenyl) methylene]-2,5-cyclohexadien-1-ylidene]-3-surfobenzenemethanaminium hydroxide inner salt, disodium salt;  $C_{37}H_{34}N_2Na_2O_9-S_3$ ) was used. It adsorbs weakly on soils but in relation to Amino G Acid it has a stronger isotherm sorption (FLURY & FLÜHLER, 1995). But due to its low toxicity, high visibility and high mobility it is one of the best compromises available up to date as dye tracer to visualize flow the pathways in vadose zone (GERMÁN-HEINS & FLURY, 2000; WEILER, 2001). Any tracing experiments with Brilliant Blue have the recommendation of high concentration input to ensure that the dye is still visible after adsorption. In this study they were employed to provide quantitative results on the covered distance of tracer movement.

## 4.4 Characteristics of the tracer experiments

The tracer input mass determination had the philosophy of a minimal impact in the system. Any positive record of tracer should not and is not allowed to be obtained by an excessive tracer input mass. Further, as the solution ratio is limited for substances a smaller input mass needs smaller quantities of water. This aspect is not to neglect for smaller systems like the hillslope table. A rough estimation of tracer input mass was done considering the following factors: lowest detectible tracer concentration in the outflow, expected time between injection and arrival of the peak, size of the soil volume that will be involved in transporting the tracer, water content of the soil and finally expected pipe flow. Another approach to calculate tracer input mass is provided by LEIBUNDGUT & WERNLI (1984):

$$TIM = \frac{t \cdot C \cdot Q \cdot Adc \cdot f}{2 \cdot E 6} \quad (E. 4.4)$$

where:	TIM	= tracer input mass [kg]
	t	= estimated time of tracer break through [h]
	C	= max. concentration at sampling site [mg/m <sup>3</sup> ]
	Q	= pipe flow [m <sup>3</sup> /h]
	Adc	= adsorption coefficient [-]
	f	= factor of safety [-]

But still any calculation of tracer input mass is to be treated as assumption as the variables rely on the characteristic results explored by the experiment.

The tracer applications of bromide and Amino G Acid were conducted simultaneously in each of the study locations.

### **Line Source: Amino G Acid**

Despite several available formulas, which allow to calculate the dimension of input mass experience is also needed for the determination of tracer input mass. We included weather forecast data and based our calculation on a simple assumption of an upcoming event similar to ID 2+3. A first approach estimated mass to 150 g (see Tab. A4) and a second using E. 4.4 got about similar results. For the latter an adsorption factor of 0.3 was included and also the advice of SCHUDEL et al. (2003) who suggest for experiments in the unsaturated zone a double to triplet tracer input mass in relation to saturated conditions (implicated in factor of safety). Thus for the in-line application at the field site on April, 2 an input mass of 150 g was applied. This was seen as a representative value, which was in the range of similar experiments (MCGUIRE, personal communications). For the hillslope table experiment water volumes were calculated in the table using soil volume and drainable porosity. Further, a peak concentration of 150 ppb was aimed to prevent sorption losses. The finally applied tracer input mass amounted to 0.1 g.

The subsurface line source was applied at the field site in a virtual line, indicated in Fig. 4.1b. Here injections of 20 ml were set each 20 cm. At the table the line (length: 100 cm) was located centred in the width of the table at a distance of 285 cm from the outflow. Concerning the humus layer in the field of about 5 cm the tracer injection had to be in this depth, as sorption reduces without organic matter (see above). In both cases needles, fitting to the front of medical syringes were used for the injection. Needles got clogged up every now and then by soil particles and were replaced. Beside that, the method is very clean and does shield from contamination in a good way. Prior to injection no pre-wetting was done!

### **Extensive application: Bromide**

Here, determination of input mass relied on a maximal concentration of 10000 ppb and the portion of initial mobilisation was assumed to be 100% for the spraying of the area (Tab. A4). For the application at the field site on April, 2 a total quantity of 8 kg bromide diluted into 50 l was sprinkled close above the soil cover over the hillslope. For the proceeding of manual sprinkling a spray gun and a pressure canister (used at planting or crop spraying) rendered the service. The nozzle outflow was regulated for an equal distribution of the 50 l and achieved a constant spray. To avoid spraying overlap in the forested, dense vegetated environment little amount of Brilliant Blue FCF was added to the transparent solution. With that a visible check helped to distinguish between zones already sprayed and zones with spraying to go. The sprayed area is shown in Fig. 4.1b and was of course selected by the spatial proximity to the outlet of soil pipes. The application area was 493 m<sup>2</sup>.

The hillslope table experiment used 5 g bromide in liquid phase. This was placed in a tool to admix fertilizer (available at farmers supply), which is screwed in between tab and the hose. As the water ran through, it gathers proportionate bromide. It was assumed that all of tracer mass was delivered towards the nozzles within the initial irrigation interval of 5 min.

### **Line Source: Brilliant Blue FCF**

The line source of Brilliant Blue FCF was restrictively applied at the table. It was the third and final tracer experiment as the sampling required excavation of soil. The tracer input mass of 100 g was diluted by 500 ml deionised water (about the maximum solubility). This liquid was applied in the same procedure than the Amino G Acid with syringes. The centred line of 100 cm length had a distance of 290 cm to the outflow.

### **Sampling and analysis in general**

All water samples were collected in HDPE bottles. Water samples at the weir, the soil pipes, the lysimeters and the piezometers were collected daily (beginning) to 4<sup>th</sup>-daily (towards the end of the study).

Samples were stored below 4 °C until the analysis. The unfiltered samples were settled a few days, to deposit the little sediment. The detection of Amino G Acid was done with a TURNER DESIGNS Model 10 AU fluorometer. Only a couple of samples were influenced by clouding or higher background concentration. Unfortunately interfering by the cork, used to seal the glasses, occurred at some samples. Using this aperture the detection limit was 5 ppb.

The analysis of the bromide samples is processed with a DINONEX 2000 ion chromatograph. This process required a filtering of the samples, as a lot of the field samples contained sediment. The execution of that is managed by a suction filtering aperture and paper filter. This process also needed extra care as the cleaning with deionised water is of major importance. According to the lack of time the parts were rinsed twice and reused directly again, without air drying of the glassware. Some of the samples bottles were already filtered with GEHLMANN GHP Acrodisc 0.45 µm, located on top of a syringe. The detection limit of bromide in an ion chromatograph was at 1 ppb.

Electrical conductivity was used as a tool to monitor bromide breakthrough at the soil pipes runoff. The increase of electrical conductivity (EC) is well connected to the increase of bromide concentration, as the mean natural conductivity at the hillslope is very low (previous long range mean: 40 µS/cm) and no other artificial intake occurred. For the final determination of bromide concentration in the flow continuous measurements of EC were combined with the hand samples with laboratory based bromide determination.

## **4.5 Data analysis**

### **Centre of mass**

The distribution of rainfall can be wide spread with many events over the time interval investigated. To get a referring point for the analysis the temporal gap between rainfall and runoff, the centre of mass was determined for the rainfall distribution. This was calculated based on daily values, for intervals including several days and in the other case for single day events based on 10 minutes values.

### **Seven day antecedent precipitation index, API<sub>7</sub>**

Previous studies at the Oregon Coast Range suggested the integration of antecedent rainfall characteristics under conditions of low intensity rainfall to predict the amount of runoff (ISTOK & BOERSMA, 1986). This index is also a helpful indirect indicator on soil moisture. This calculation was done as a simple summation rather than a weighting summation as described by MANIAK (1997). The daily totals of the seven days before a hydrograph rise were included. Amounts of precipitation as well of API<sub>7</sub> were rounded to integer values.

### **Hydrograph separation**

For a simplified separation of base flow the start of event flow in the hydrograph was set at the hydrographs obvious rise. The determination of the events ending point contained more difficulties. Even the easiest way by using an empiric formula (e.g. LINSLEY) must fail as the catchment area is not known. More common methods focus on the different storage coefficients of fast and slow responding components (DYCK & PESCHKE, 1995). Here, the obvious change of slope or turning point in the recession curve of the hydrograph tells about the ending point of the event. A visual check of the graphs, plotted in a semi logarithmic scale was done for a hydrograph separation on event components and base flow components. The final separation was achieved with a direct connecting line of the starting point and the end point (trapezoid). In this case the shape of hydrograph did not allow any detection of a turning point, a horizontal line starting at the rise of flow did the separation towards the ending point (result: rectangle).

### **Timing of flow**

The time shift of flow is calculated between the rainfalls centre of mass and the runoff peak. The time to flow includes the time between the rainfalls centre of mass and the start of flow. This index is positive for following runoff reaction and negative in case the start of flow is ahead the rainfalls centre of mass.

### **Recession analysis**

In order to determine turnover times and storage feature recession branches are analysed on the assumption of a single linear reservoir by the MAILLET-formula. The event series were selected on condition that three to four days ahead didn't get any rainfall and the series until the next rise of discharge contained at least five days. These strong demands on the data were performed following base flow investigation methods (DYCK & PESCHKE, 1995). Results are presented individually and are not combined to a master recession curve.

### **Runoff coefficient**

Index is calculated as follows:

$$\psi = \frac{R_d}{P} \quad (\text{E. 4.5a})$$

where:  $R_d$  = runoff coefficient [-]; 0 1  
 $R_d$  = direct runoff, stormflow [mm]  
 $P$  = precipitation [mm]

### Dynamic contributing area of soil pipes

An approach for an arithmetic estimation of the drainage area of a soil pipe lead back to DICKINSON & WHITELEY and CALVER et al. (both in JONES, 1997). A first step towards is a base flow separation (already explained in the previous chapter). The formula then offers the calculation of a surrogate 'catchment area' based on the maximum contributing area. These were selected from the dynamic contributing area (DCA) for each storm, according to:

$$DCA = \frac{\text{total storm discharge in pipe}}{\text{total storm rainfall}} \quad (\text{E. 4.5b})$$

This is based on a runoff coefficient of 1.0 in a given storm. It is a summarised calculation for all three soil pipes, for sure with a dominating representation of SP1. The authors there recommend a large sample size of about 20 complete storm records. As this study does not have such this formula can not ensure a reasonably representative result.

### Velocities of tracer experiment

The description of a black box system with tracer techniques uses relevant parameters, which are presented in the following. Various velocities are determined of the tracer break through curve:

$$V_{a \max} = \frac{x}{t_{\max}} \quad (\text{E. 4.5c})$$

$$V_{a \text{ peak}} = \frac{x}{t_{\text{peak}}} \quad (\text{E. 4.5d})$$

$$V_{a \text{ med}} = \frac{x}{t_{\text{med}}} \quad (\text{E. 4.5e})$$

$$V_{a \min} = \frac{x}{t_{\min}} \quad (\text{E. 4.5f})$$

where:  $x$  = Distance between input and sampling location [m]  
 $t_{a \max}$  = Time between input and first tracer contact [s]  
 $t_{a \text{ peak}}$  = Time between input and concentration maximum [s]  
 $t_{a \text{ med}}$  = Time between input and median [s]

$t_{a \min}$  = Time between input and end of tracer break through [s]

### Tracer recovery rate

The calculation of the relative tracer recovery rate at time t is:

$$TRR(t) = \frac{Q}{M_0} \int_0^t C(t) dt \quad (\text{E. 4.5g})$$

where: Q = discharge [l]  
M = mass of tracer [g]  
C(t) = tracer concentration at time t [g/l]

## 4.6 Conclusions

Most of the methods applied in the research at this Low Pass field site are common and widely used in experimental hydrology. The Low Pass field site was well equipped with instrumentation in order to achieve the objectives of the study. The best choice of tracer regarding conditions at the field site was made on bromide and Amino G Acid because of their sorption characteristics and their use in soil water tracing.

## 5 Results and discussion: Field investigations

In this chapter the results of the field experiments are presented and discussed. The following does include sections on throughfall, pipe flow, water tables and results of the tracer experiments. Digital time is converted in relation to the tracer injection on the second of April 2003 which has the date value of zero. The following results presented are mainly from the period between February, 13 (day no. -48) and May, 27 (day no. 55). This may be regarded as the total field study period, although some data-gathering only started shortly after March, 2, when additional instrumentation was put into operation (high intensity study period).

In this study calculation of specific discharge was not undertaken, because an accurate determination of the soil pipes drainage area would not have been successful.

### 5.1 Description of soil pipes

The information on the soil pipes already provided in section 4.3 is now supplemented with essential data. Investigation of the shape and size of the outlet was made by digging to a depth of a few centimetres. Tab. 5.1 provides data of the various discharge patterns observed. Soil pipe one (SP 1) was a well established one and got the main emphasis. Pipeflow of all three endings contained little sediment.

**Tab. 5.1:** Features of soil pipes

	Size pipe outlet	Shape	Discharge pattern
Soil pipe 1 (SP 1)	Diameter: 12 mm	Inside colmated surface	Perennial until summer drought (mid of June)
Soil pipe 2 (SP 2)	13 x 4 mm + diffuse	Above a dense soil-rock piece	Running up to 3 days after storm events
Soil pipe 3 (SP 3)	Two outlets: 5 x 5 mm + 3 x 3 mm		Running up to 4 days after storm events

The outlet of respective pipes is at least 1 meter above the soil bedrock interface, according to the core analysis of the piezometer. A detailed survey of surface topography did not provide any hints on the subsurface shape of SP1. This complies with JONES (1997) who mentioned that surface depressions are poor indicators of pipeflow contributing areas. The

data on discharge presented mainly involves water running out of SP 1, since SP 2 and SP 3 started up only in wet conditions.

No interflow occurred at the soil face in the trench throughout the study. For the already moist conditions in the southern part of the trench (area of soil pipes), the additional visible wetness after rain events was very small. However, this wetness of the surface was still not enough to produce seepage. Hence, outflow in the soil profile under investigations (to a depth of 1.8 m) was totally restricted to the soil pipes. Previously constructed gutters to collect interflow, shown in Fig. 3.4.4, were not involved as they appeared to be useless.

### **Discussion of soil pipe features**

A similar observation where pipe flow was responsible for 95% of the outflow of a small granitic headwater and almost no interflow occurred was reported by TSUMAMOTO et al. (1982). The observations of the site made in Tab. 5.1 show that the pipe outlet seemed not to be located close to the soil bedrock interface (MCDONNELL, 1990) or within a narrow band above the soil bedrock interface (UCHIDA, 2002). The results go more along with a study in north-coastal California where pipe outlets occur near the soil surface to a depth of about 2 m and are commonly situated at gullies or sinkholes (ZIEMER & ALBRIGHT, 1987). More precise information about the shape and location of the soil pipes might be possible using ground-penetrating radar, as HOLDEN et al. (2002) did in peat soil. This may also provide data about the depth of soil-bedrock interfaces. A fibrescope examination on morphologic features was not undertaken, but provides potential to detect triple-junctions (TERAJIMA et al., 2000).

## **5.2 Precipitation**

Before presenting the data measured at the hillslope, the general context of the investigation period is analysed. Because of annual variations, the winter 2002/2003 got less precipitation than in the long-range mean. Available data of the long-term climate station Eugene (see Fig. 3.1) are shown in Fig. 5.2a. This had an influence on the long-term water balance of the field site Low Pass with effects on the results of the soil pipe study.

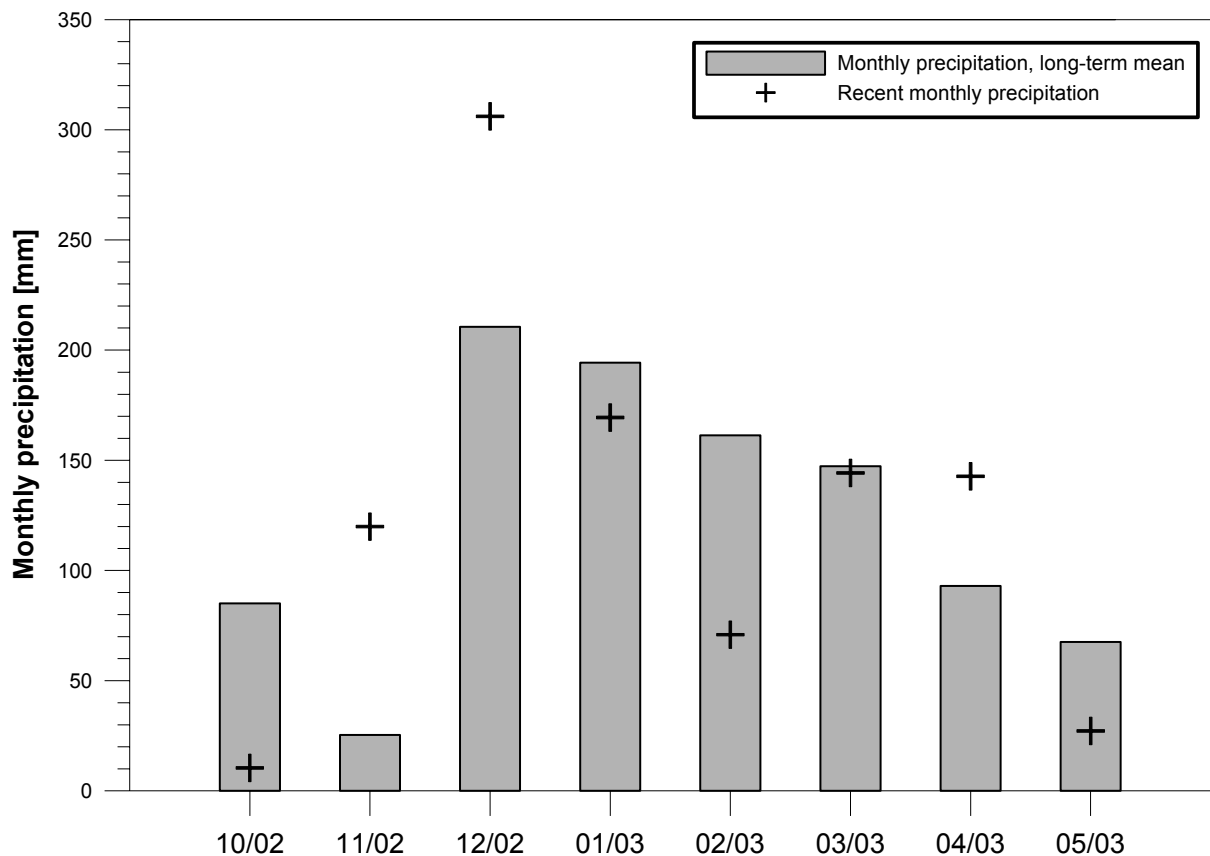


**Fig. 5.2a:** Open land precipitation at the climate station Eugene, for overall investigation period (October 2002 to May 2003) and long-term mean.  
From: OREGON CLIMATE SERVICE (2003).

After this general context, the data of the throughfall measurement at the hillslope itself are presented: Despite a data gap around day -3, the hillslope received a total throughfall of 392 mm for the period February, 13 (day no. -48) to May, 14 (day no. 42). Decreasing of rainfall towards summer, mentioned in section 3.2, is traceable by the negative trend of daily values. Daily measurements of precipitation are presented in Fig. 5.2b. Daily totals reached up to 51 mm. Summarising daily values in amounts of multiple days (e.g. pacific fronts passing through) helped with the analysis. Those were calculated as sums between days with no rain. Therefore, Tab. 5.2 presents rainfall data for time intervals, which range between 16 and 131 mm and showed resulting flow events.

Changing the objective from daily amounts to smaller time steps, for example 10 minutes, an analysis of events focuses on intensity. Here, a mixture of mostly low rainfall intensities interspersed by some high spikes was obtained. The maximal intensities are listed in the third column of Tab. 5.2 for a series of selected intervals. The maximal intensity observed was 5.2 mm/10 min (equals 32 mm/hr), followed by 2.83 mm/10 min (equals 17 mm/hr). The context of the second peak, as well as general variation of intensities are shown in Fig. 5.2c. Furthermore the API<sub>i</sub> is provided in Tab. 5.2 for events, as an indirect indicator on soil moisture. This value will be used in section 5.3 about flow to relate responding runoff start with its rain conditions seven days before.

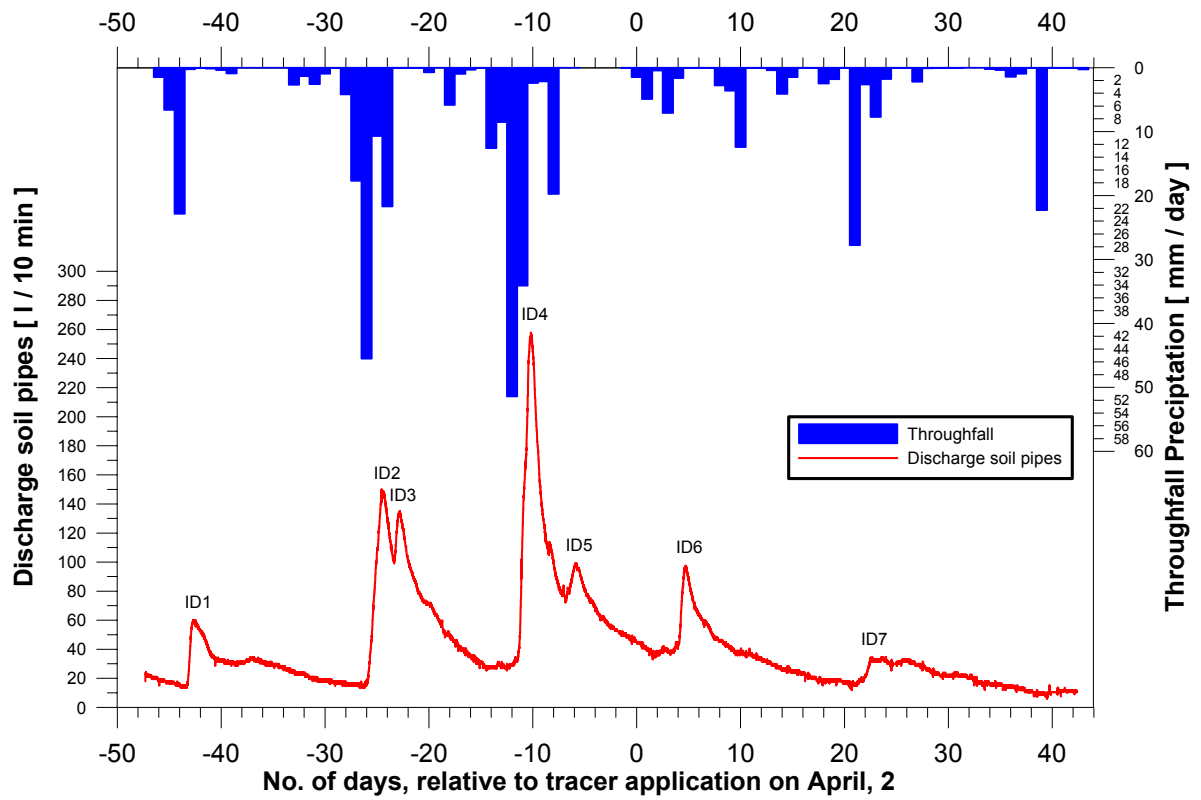


Fig. 5.2b: Daily rainfall at field site Low Pass and pipe flow (addition of SP1, SP2, SP3) for study period.

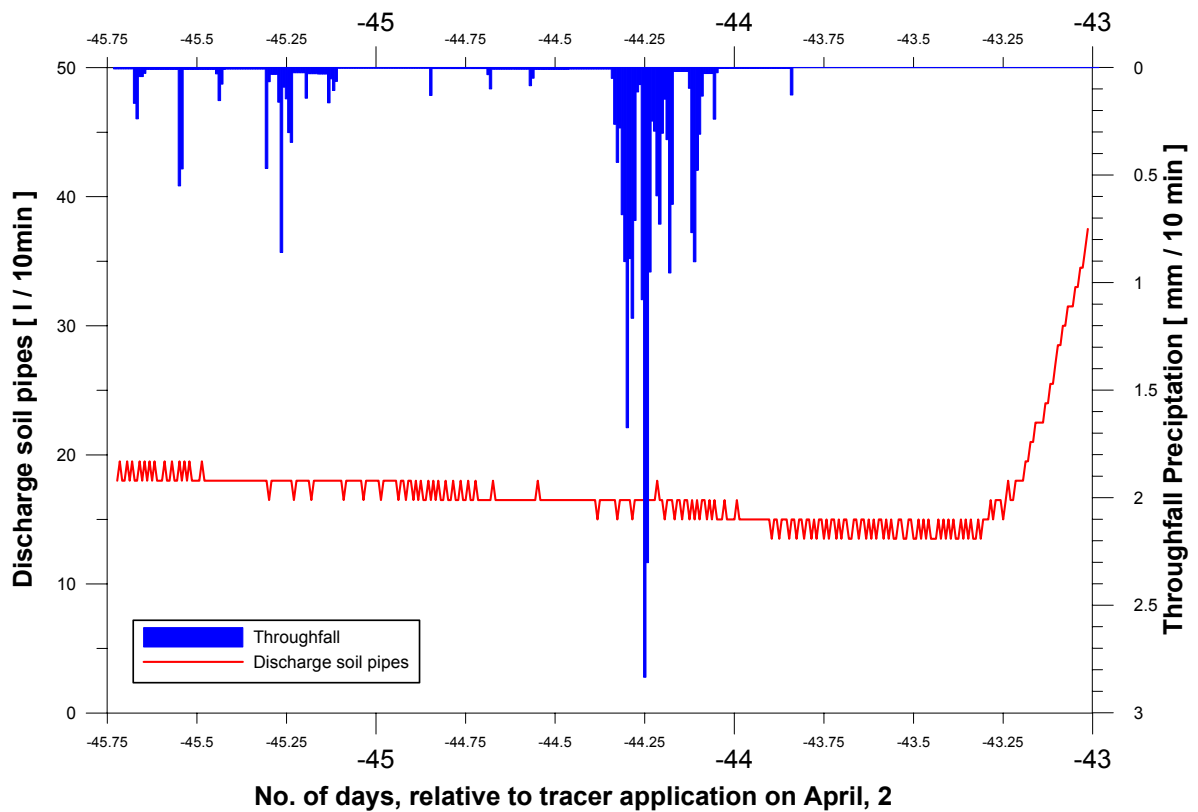


Fig. 5.2c: Rainfall intensities per 10 min for selected interval, additionally hydrograph (pattern of tipping buckets).

**Tab. 5.2:** Selected characteristic of rainfall and runoff attributes for the hillslope and pipeflow. Note the relation between rain interval and peak ID, a reason to merge the two table parts

<i>Rainfall; section 5.2</i>				<i>Runoff; section 5.3</i>				
Rain dominated interval [day no.]	Pre-precipitation [mm]	Max. intensity [mm/10 min]	API <sub>7</sub> [mm]	Peak ID	Total event pipe flow, without base flow [m <sup>3</sup> ]	Peak flow soil pipes [l/10min]	Time shift: rain to flow [hr]	Time to start of flow [hr]
-46 to -43	31	2.83	gap	1	74	60	38	26
-28 to -24	100	1.03	8	2+3	446	150	28	-3
-14 to - 8	131	1.75	8	4+5	760	258	27	-7
0 to 4	16	0.74	gap	6	152	98	61	46
8 to 10	19	0.68	14	-	-	-	-	-
21 to 24	40	0.99	10	7	87	35	47	14
39	22	5.2	3	-	-	-	-	-

## Discussion of precipitation

The precipitation event on day 39 became a little suspicious as the distribution of 10 min-intensities clarified. A large intensity of 5.2 mm/10 min occurred at the very first time step of the event on that day and afterwards intensities went down to about 1.5 mm/10 min. But also a check on one of the additional open area precipitation recorders (closely located) showed the same outstanding intensity and daily amount. Thus the data seems to be correct. In order to get an idea about the rainfall occurred that day, a look on nearby climate stations at Eugene city and Alsea fish hatchery revealed 0.5 and 0 mm respectively (OREGON CLIMATE SERVICE, 2003; G.H. TAYLOR, personal communication). Two Stations further away (Corvallis city and Guin Library Weather Station at the Hatfield Marine Science Centre in Newport, Pacific Coast) recorded daily totals of 7 mm respectively 0 mm (AGRIMET, 2003; HATFIELD MARINE SCIENCE CENTRE, 2003). Although the gradient of rainfall in this luv-lee system is superposed by another pattern, it was conducted: Considering the amount of rainfall of 22 mm with a maximal intensity of 5.2 mm/10 min (equals 32 mm/hr), on day 39 surrounded by low rainfall amounts, indicates a very locally extended convective storm cell with a heavy burst.

Despite this maximum the dominant low rainfall intensity observed is characteristic for the Coast Range, as ISTOK & BOERSMA (1986) found that intensities of 12.71 mm/hr were exceeded very rarely.

### 5.3 Soil pipe flow

To ease of understanding and handling, ID numbers for the peaks following rain input were assigned (see Fig. 5.2). Hence, it is not distinguished between flow of the three different soil pipes and present flow as summarized number.

The overall mean for the period was 41 l/10min. A hydrograph separation was performed for ID 1 to ID 7 and full results are attached in appendix A3. In the whole study period total flow running out of the soil pipes was 5448 m<sup>3</sup>. On the basis of the hydrograph separation, total event discharges (without base flow) were calculated and are presented in Tab. 5.2. These lay between 74 m<sup>3</sup> and 760 m<sup>3</sup>. The maximum peak flow which occurred was 258 l/10min at ID 4.

Towards dry summer conditions, after the investigation period, flow was zero (day no. ~73). This recession towards the end, as well as recessions following rain events [-46;-43] and [-28;-24], only fit with the strong demands outlined in section 4.5. These were analysed on the assumption of a single linear reservoir by the MAILLET-formula in order to determine mean turnover times and storage features. The results of the recession branches, highlighted in Fig. 5.3a, are presented in Tab. 5.3. All three do show good fits as  $r^2 > 0.9$  (non logarithmic calculation). Additionally, further recession branches were included, which do not fit with the strong demands. These are indicated separately and were added for the objective of enlarging the total number for a further statistic.

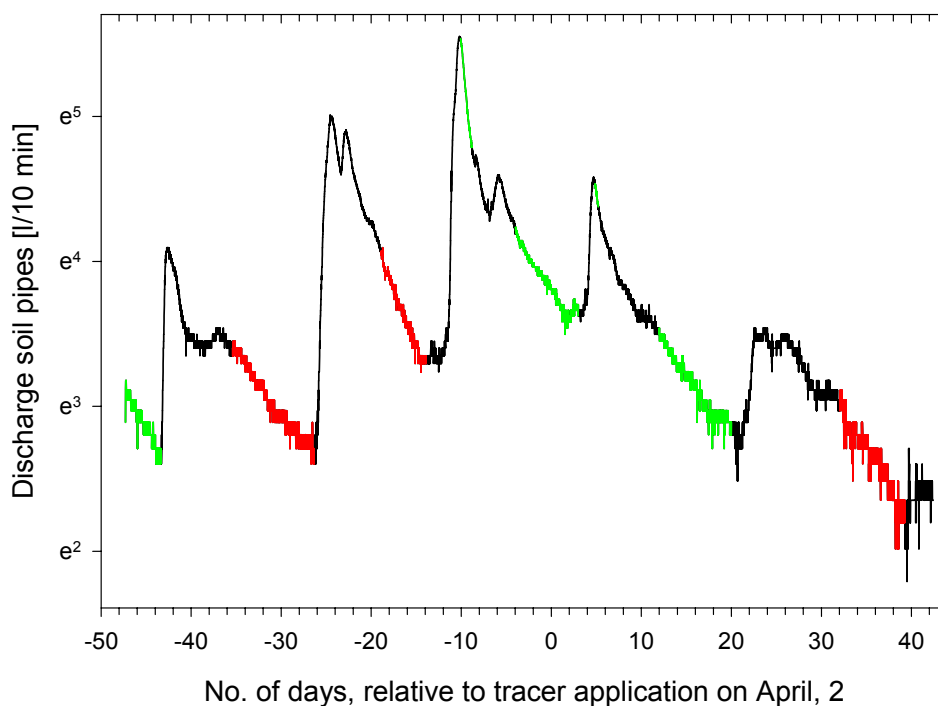


**Fig. 5.3a:** Pipe flow shown in logarithmic scale and branches used for recession analysis. Red intersections indicate strong demands on data; green indicate series with low demands.

**Tab. 5.3:** Recession analysis of selected events and storage coefficient of the system

Rain event ahead [Day no.]	Demand on data	Corresponding peak ID	Coefficient $\alpha$ of MAILLET-formula $Q(t) = Q_0 \cdot e^{-\alpha \cdot t}$ [1/d]	Regression coefficient, $r^2$ [-]	Storage coefficient $k$ , mean turnover time $\bar{t}_R$ $k = \bar{t}_R = \frac{1}{\alpha}$ [d]	Mean discharge over recession branch [l/10min]
-47.3 to -43.4	low	-	0.013	0.92	76	18
-46 to - 43	high	1	0.014	0.94	69	25
-28 to - 24	high	2+3	0.043	0.97	23	44
-10 to -8.8	low	4	0.774	0.97	1	176
-4 to 3	low	5	0.029	0.93	34	48
4.84 to 5.2	low	6	0.259	0.97	4	87
12 to 20	low	6	0.013	0.93	77	23

To interpret this information table, it is important to know that the mean turnover time chiefly provides information on the dynamic of the system. For true residence time tracer information depending on the mobile phase is required. Now the extraction of table information shows: During low flow conditions at the soil pipe (flow < 25 l/10min), storage coefficients greater than 69 days illustrate the slow outflow out of the system and imply a slow dynamic. For the event [-28;-24] the amount of water in the system is different as the second highest discharge peak occurred just some days ahead of that recession. Runoff then was still quickly driven and different fluxes were active during this mean discharge of 44 l/10 min (see Fig. 5.2b). For the enlarged number of events investigated, the dependence of mean turnover time on mean discharge is presented by a linear recession analysis (generalisation of the MAILLET-formula) in Fig. 5.3b. This graph shows the pattern of quick turnover times for high mean discharge conditions, whereas the dynamic of the system is slow for small discharges. As the recession time constant varies systematically with discharge, there is a consistency with a nonlinear storage-discharge model.

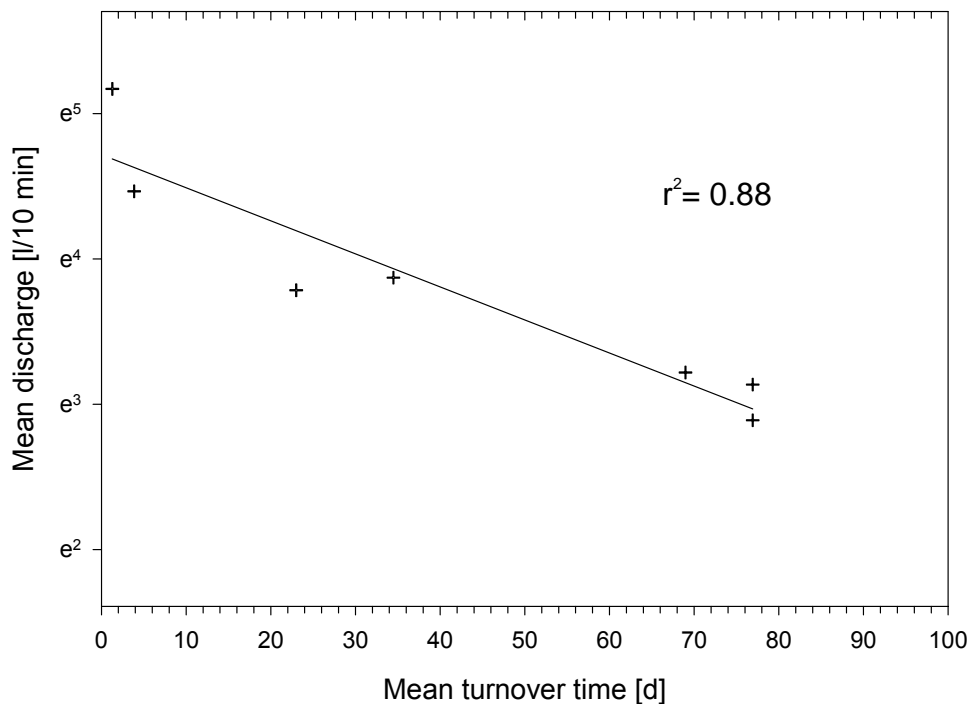


**Fig. 5.3b:** Recession of mean discharge over recession branch and mean turnover time for selected events outlined in Tab. 5.3.

### 5.3.1 Timing of soil pipe flow and flux

The time shift between rainfall and runoff ranges from 27 to 61 hours for the events selected in Tab. 5.2. Plotting the time shift against the precipitation quantity showed a negative linear trend ( $R^2= 0.74$ ). Although harder to detect, a focus on the start of flow instead of peak flow showed delay times of -3 to +46 hours. Negative times occurred here in case of wide spread rainfall distribution with double peaks, then start of flow was ahead of the centre of mass in rainfall.

The response of soil pipe flow volume to a given quantity of precipitation was variable and depended on  $API_r$  (listed in Tab. 5.2) representing the total water content of the system. Here, the total number did not allow conclusions on any dependence.

### 5.3.2 Discussion of soil pipe flow

#### General:

To set up a water balance for the study period is hard to achieve as the investigation period remains short, respectively shorter than a hydrological year. A short term comparison for the investigation period of total flow ( $5448 \text{ m}^3$ ) with total throughfall (392 mm) is linked to the

uncertainty of an unknown catchment area. The issue of catchment area will also be discussed in section 5.4.

A look at the rain events [0;4] with 16 mm of rain and [8;10] with 19 mm of rain surprised because of the different reaction they generate. In one case a discharge of 148 m<sup>3</sup> is prominent compared with no obvious reaction for the even bigger, second event. This seems to be the start of the dryer system conditions, which got more obvious on day 39, when no system response at all occurred after heavy rainfall input. Although for an annual series, comparable results were obtained at a similar Oregon Coast Range site, where 44% to 93% of all the rainfall events produced no measurable runoff (ISTOK & BOERSMA, 1986).

The results of Fig. 5.3b are distinct from processes relevant to DARCYS law where turnover times would not change for different mean discharges. A highly heterogenic system, with a runoff generation mechanisms that differ from DARCYS law is summarized. This is in particular because those processes are valid within cm-scale, but not within a scale of decametre, to be assumed here. Additional different mean discharges in Fig. 5.3b are also connected to different conditions of water content in the system. Thus turnover times also represent the hydrologic connection and finally determine the dynamic of the system. Quick turn-over times for high mean discharge conditions are likely to be interpreted by no water resistance in wet soil environments or a possible water table. But there is also the possibility that higher soil moisture produces pressure transmission. The response dependence on water tables in the hillslope will be shown in section 5.3.

Observations that bypassing preferential flow (respectively pipe flow) became more important when rainfall intensities were extraordinary high could not be confirmed in this study (observations at similar soil type by TORRES et al., 1998).

### **Timing:**

The phenomena of different lag times in forest soils under wet and dry conditions are widely described (e.g. TURTON et al., 1992; MCDONNELL, 1990). Generally, the response times indicated a fast acting mechanism (e.g. Tab. 5.2). Obviously, SP1 acts as a preferred path mechanism. Similar responses of subsurface flow in forest soils have been observed by MOSLEY (1982), MCDONNELL (1990) and TURTON et al. (1992) although the latter focused on subsurface flow in general, rather than a soil pipe mechanism operating.

Concerning lag time and time shift the results here are not very consistent. A comparison of the events [-28;-24] and [-14;-8] seems difficult. They both had about similar starting conditions ( $API_7$  and total precipitation), which resulted in about the same flow lag time (3- 7.5 h).

Stepwise multiple linear regression using rainfall amount,  $API_7$  and mean intensity as independent variables and total flow as dependent variable were achieved, but appeared critical as the total number of events is too small. However, regressions for time shift were more significant than time to start of flow. These findings go along with ZIEMER & ALBRIGHT (1987). As well an analysis using SPEARMAN rank order correlation failed because of the small data total.

The  $API_7$  did not help much to explain flow mechanisms as the values were too similar and the availability low. Conclusions point towards the major importance of the soil water content, especially the water table rather than the antecedent rain index.

## 5.4 Dynamic contributing area of soil pipes

The dynamic contributing area (DCA) was calculated in Tab. 5.4 for the events linked to peak ID, according to equation E. 4.5b. The maximum DCA occurred on peak ID 6. Here, throughfall showed the smallest value and the border issues of the hydrograph separation are added in Tab. A3. However, the maximum amounted to 1 ha and the reach of the soil pipes was assumed to that with already mentioned uncertainties.

Further the table presents runoff coefficients of the different events based on an assumed catchment area equal to DCA. The average runoff coefficient calculated for the peaks ID 1-5 and ID 7 amounted to 0.375.

**Tab. 5.4:** Pipe flow records, DCA and runoff coefficients

Rain dominated interval [day no.]	Pre-precipitation [mm]	Peak ID	Total event flow, without base flow [m <sup>3</sup> ]	Peak flow soil pipes [l/10min]	DCA [m <sup>2</sup> ] according to E. 4.5b	Runoff coefficient $\psi$ , based on max DCA = catchment area
-46 to -43	31	1	74	60	2387	0.239
-28 to -24	100	2+3	446	150	4460	0.446
-14 to -8	131	4+5	760	258	5802	0.580
0 to 4	16	6	152	98	9500	max! 1
21 to 24	40	7	87	35	2175	0.218

### Discussion of contributing area

The maximum contributing area amounts at least to 9500 m<sup>2</sup>. Regarding the fact that a runoff coefficient of exactly one is hard to obtain, the area is presumably bigger. Including the uncertainties of the hydrograph separation of ID 6 (see appendix A3) the large contributing area should be treated with scepticism. However, it differs in the order of magnitude from the bromide sprayed area (highlighted in Fig. 4.1b and section 4.4) with its 493 m<sup>2</sup>, which was expected primarily to be the contributing area. Finally, even a large DCA does still not include evidence about the shape and predominant direction of the soil pipes.

For the size of pipe outlet (assumption: SP1 as most dominant feature) the contributing area seems to be very high. UCHIDA et al. (1999) presented values of 158 m<sup>2</sup> for a soil pipe diameter of 5 cm in a similar forested catchment.

A comparison of pipe flow runoff coefficients, based on DCA, shows the same order of magnitude as the Maesnant basin ( $= 0.4$ ), where soil pipes show similar maximum DCA and quantity of storm flow is comparable (DUNNE, 1978 cited in JONES, 1997). Runoff coefficients on subsurface flow for the Toinotaini zero-order watershed differ little from the Low Pass ones ( $= 0.24$ ; UCHIDA et al., 1999). However, looking at the magnitude of  $\alpha$ , both are still distinguishable from through flow ( $= 0.11$  according to DUNNE, 1978 cited in JONES, 1997) by the higher coefficient. Thus it is another indication that pipe flow here is to be assigned to a different category.

## 5.5 Piezometer results

The visual check of the slug test results did not show anything suspicious, why the piezometers were rated well connected to the surrounding soil (Fig. A4). Out of the slug test data the hydraulic conductivity was calculated (by E. 4.1.6a and 4.1.6b) to  $1.4 \text{ E-}07 \text{ m/s}$  respectively  $2.1 \text{ E-}07 \text{ m/s}$ .

### 5.5.1 Water table levels

Data of the water table is presented in depth below surface topography rather than height in the piezometer drillings. Series are discontinuous because some recorder's offset was not deep enough! Tables showed the general pattern of a greater response in lower parts (piezometer row A) than in higher elevations of the hillslope (piezometer row D), where slope was higher. Furthermore, even within a row the development was different, for example piezometer P\_A5 to P\_A9 had good response to rain events with great amplitude whereas P\_A1 and P\_A3 did not. This fact is surprising because it was mentioned earlier that the southern part of the trench in the neighbourhood of P\_A1 had moist trench faces, plus the mouths of the soil pipes were 2 m below P\_A1 and P\_A3 and in contrast the other part of trench face was always dry. Therefore the trench face does not represent wetness in hillslope behind.

Fig 5.5.1a gives an overview of selected piezometers. The focus is primarily on the water table variation in interaction with the biggest runoff event ID 4. Here the maximum amplitude (in relation to the individual offset of each piezometer) occurred at P\_A7 with 588 mm followed by P\_C9 with 487 mm (Tab. 5.5.2). Therefore a well responding area is identified in that region of P\_A7 and P\_C7.

Generally the saturation of soil as a post-rainfall process happened in soil depths of up to 80-100 cm (for row A) below surface topography. The saturation zone for upper piezometer rows was deeper, at about 1.4 m or even around 2.2 m (see Fig. 5.5.1a and Fig. A5).

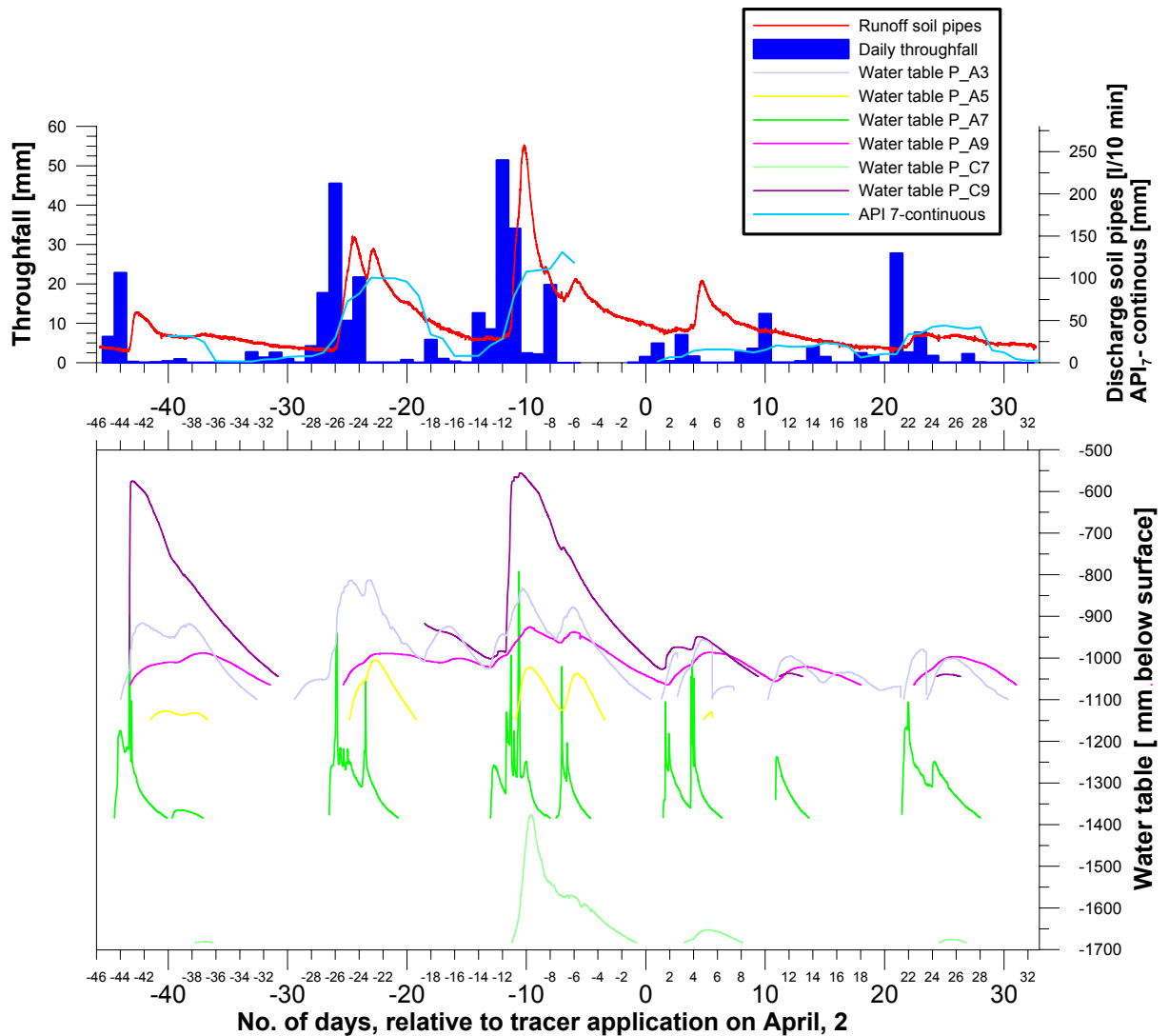


**Fig. 5.5.1a:** Water table at various piezometers, pipe flow and throughfall. Series of P\_C9 includes missing data. Note the different offset of the individual piezometers.

Another observation at P\_A9 is the rain event (20 mm) at day minus eight, where under API, conditions of 109 mm a second peak of the water table was established. Here, the system responded rapidly because of the already moist conditions. Precipitation input is traceable throughout water table and discharge data.

Coming back to the water table levels connected to ID 4 a mapping of the different water levels in the spatial context of the piezometers is performed for the well-responding area around P\_A7 and P\_C7. The time steps included showed maximal or minimal levels for at least one piezometer or any other outstanding feature. Fig. 5.5.1b shows again the heterogeneity of the piezometers in row A, whereas Fig. 5.5.1c presents row C.

To show the relation between water table height and discharge, correlations were performed. However, the received hysteresis did not provide much information as discontinuous data series were included. The pattern of hysteresis is hard to interpret and is attached in Fig. A6. Therefore, the next section focuses on timing.

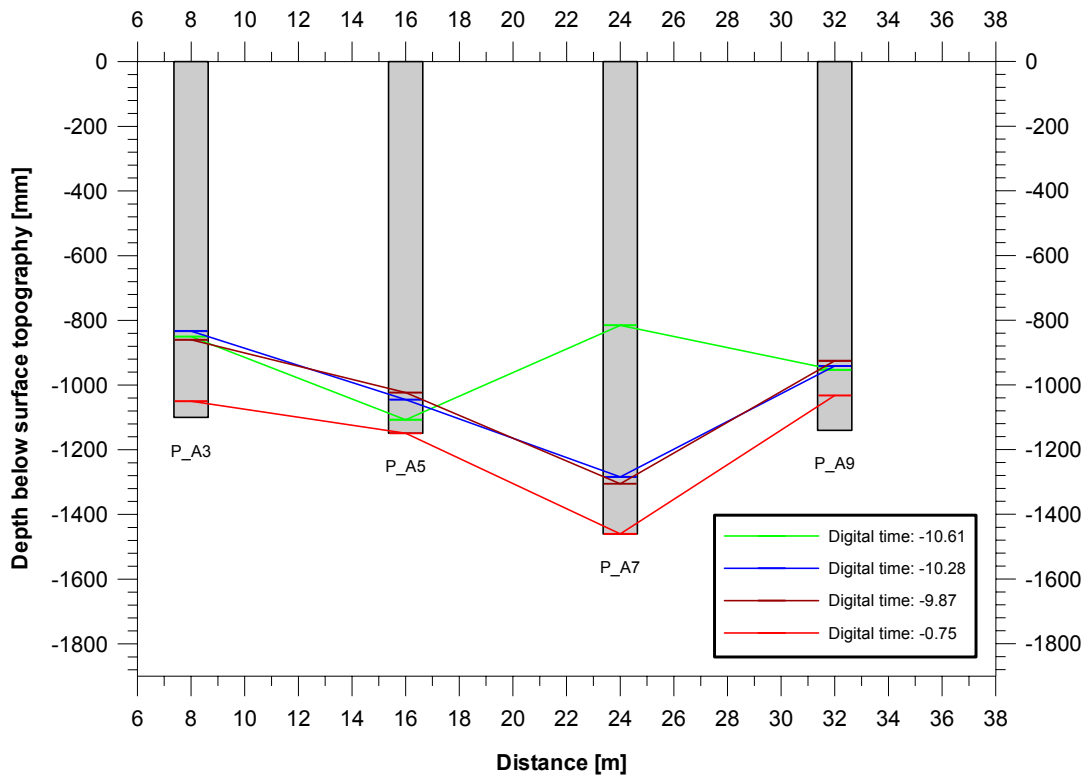


Fig. 5.5.1b: Water table levels at piezometers in row A ahead, while and after ID 4. Piezometer offset is indicated by grey bars.

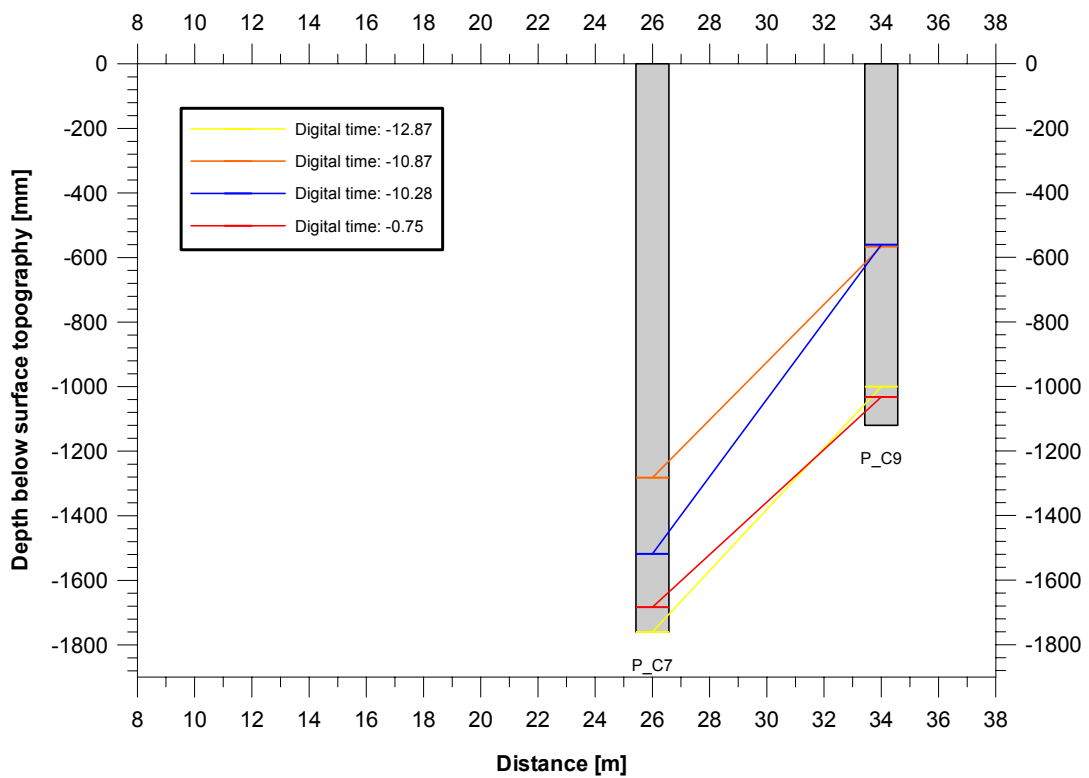


Fig. 5.5.1c: Water table levels at piezometers in row C ahead, while and after ID 4. Piezometer offset is indicated by grey bars.

## 5.5.2 Timing of water table establishment

Referring to the special features of P\_A7 and P\_C7 indicated above, the timing of those is once more significant. Both water table series also show the bigger time lags with the hydrograph, in comparison with the others. Furthermore, the deviation towards the major discharge peak on day minus ten is 11 hours ahead for P\_A7 and 11 hours back for P\_C7. The time shift for other events is presented in Tab. 5.5.2. The rising time is sometimes hard to separate as the graphs showed some previous peaks.

**Tab. 5.5.2:** Data of selected piezometer on selected events, including time shift

Piezometer	Event [day-No.]	Corresponding peak ID	Time shift (peak hydrograph to peak water table) [hr]; convention: $\oplus$ = water table ahead of hydrograph	time to rise [hr]	Remarks	Rise of water table [mm]
P_A3	[-24;-23]	3	+6	52		238
	[-10]	4	+2.5	70	on top of recession branch	181
	[5]	6	+1	50		137
P_A5	[-10]	4	-11	27		122
P_A7	[-43;-42]	1	+11	1.9	on top of recession branch	316
	[-24;-23]	3	+32	15		304
	[-10]	4	+11	2.6		588
	[5]	6	+19	1.2	on top of recession branch	308
P_A9	[-36;-32]	-	-69	87	further event on top	52
	[-24;-23]	3	-60	70		74
	[-10]	4	-11	76		94
	[5]	6	-12	82		76
	[24]	7	-81	88		66
P_C7	[-10]	4	-11	35		305
	[5]	6	-19	45		28
P_C9	[-43;-42]	1	+11	3.5		449
	[-10]	4	+6	30		487
P_C3	[-10]	4			too little	10

					response	
--	--	--	--	--	----------	--

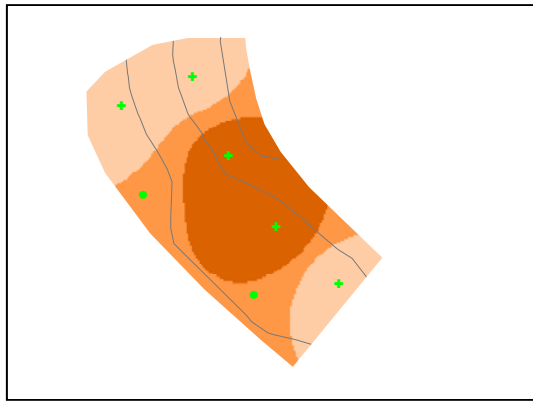
The pattern of P\_A3 shows the smallest time shift between flow soil pipe and water table. Additionally the shape of the water table graph is similar to the hydrograph (Fig. A5). This is explained by the proximity of P\_A3 and the soil pipes.

Pointing to Tab. 4.4.2 the positive time shift of P\_A7 is conspicuous. In relation to the rainfall input the water table established faster than discharge occurred, a pattern shows in Fig. 5.5.1.b. This raises the question about the overall dominating process and which is first?

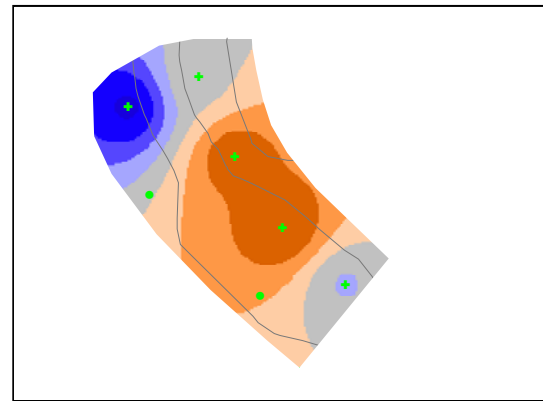
### 5.5.3 Spatial presentation of water table

Illustrating the spatial distribution of the water table over the hillslope is difficult, as the last section showed. The heterogeneous response generated by the individual connection of each piezometer to surrounding groundwater caused problems. These show up in particular there, where no response occurred. However, the water table was spatially interpolated for the biggest runoff event (peak ID 4). This seem to be of interest as water tables showed the biggest amplitudes, with spatially the most expanded water levels, around day no. -10. Data source were the few piezometer data of Fig. 5.5.1b+c. The calculation included five selected well responding piezometers (indicated by green crosses) as point values which were interpolated by the „Inverse Distance Weighting” (IDW) method. This is based on the assumption that each point value has a local influence, which declines with increasing distance from the reference (BURROUGH & MCDONNELL, 1998). The area of the applied interpolation was selected by field experience, data availability and the interpretation of data presented in the chapter above. Time steps were chosen non-linearly and correspond to the individual maxima or minima of the different piezometers used and relayed also on the hydrograph.

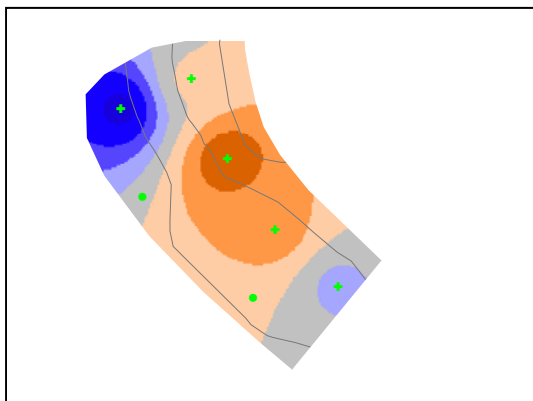
The spatial change in water levels over time is presented in Fig. 5.5.3. However, the depth of water decreases with an expansion of those saturation zones 900 - 700 mm close to surface. The most extended area with probable highest water levels (and thus water content) is detected for the digital time -10.6. This development occurred about 12 hours before pipe flow peak. At that moment the extension had already declined (see digital time -10.2). Despite the water table at the north part having a wide distribution in a depth of 900 – 700 mm and beeing even wide distributed, no interflow could be seen there (previously mentioned). The decline in spatial distribution and absolute water level towards time -9.63 and -0.75 is similar contrary to the rise which happened before. Generally, heterogeneity, side effects, and the interpolation method blur the spatial presentation the most, why Fig. 5.5.1b+c is more clear.



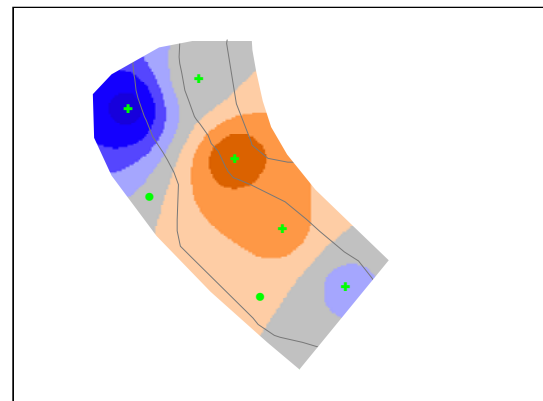
Time step: 03/20, 4:40 h, (digital time= -12.8)



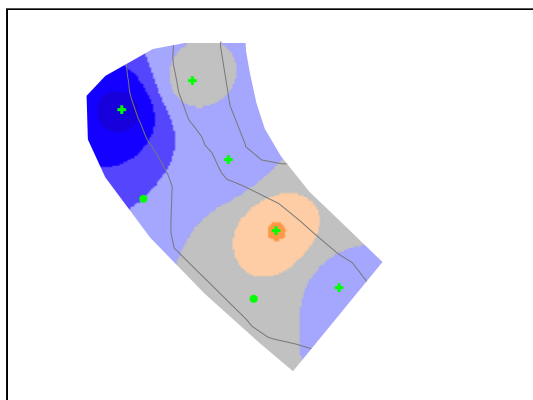
Time step: 03/21, 21:30 h, (digital time = -11.1)



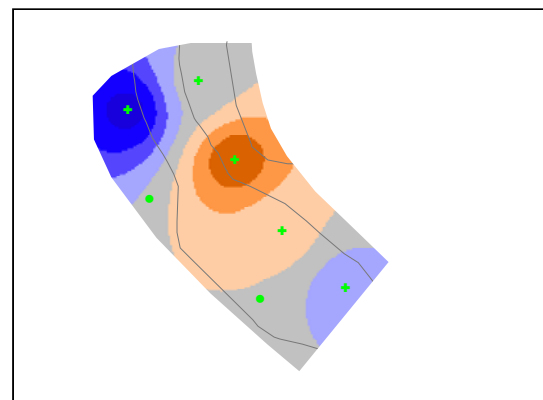
Time step: 03/22, 4:40 h, (digital time = -10.8)



Time step: 03/22, 7:10 h, (digital time = -10.7)

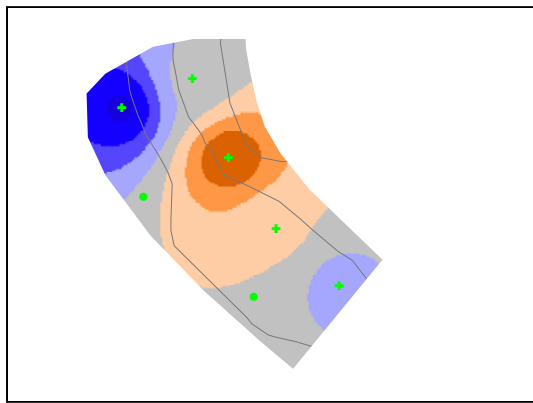


Time step: 03/22, 8:30 h, (digital time = -10.6)

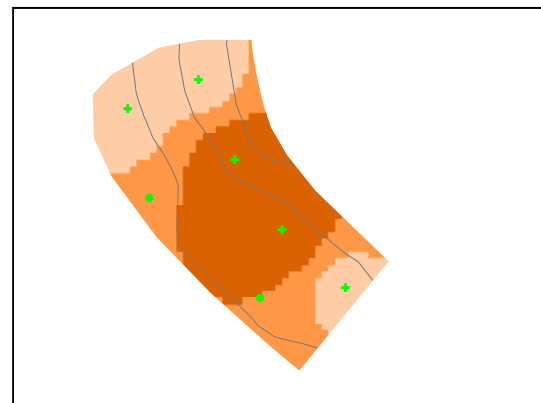


Time step: 03/22, 19:10 h, (digital time = -10.2, about peak hydrograph)

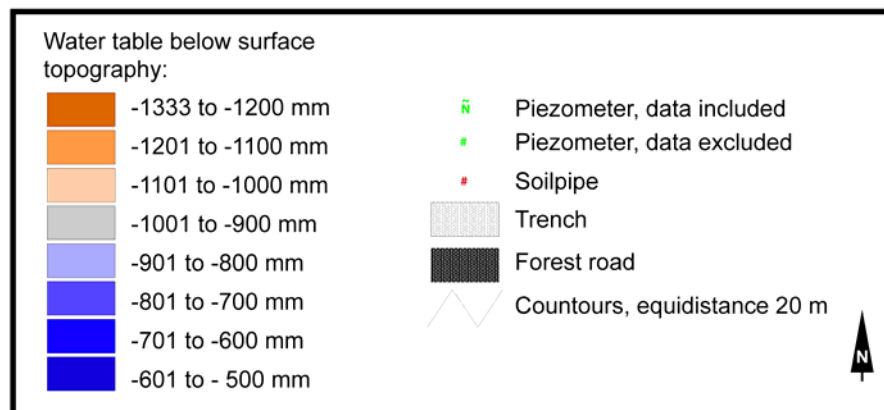
**Fig. 5.5.3:** Spatial distribution of water table at lower part of hillslope ahead, while and after ID 4. For legend see following page.



Time step: 03/23, 7:40 h, (digital time = -9.68)



Time step: 04/01, 6:30 h, (digital time = -0.75, runoff amount equal to starting conditions of ID4 event on digital time -12.8)

Fig. 5.5.3: *continued*

## 5.5.4 Discussion of water table and flow mechanisms

The data here does not show any diurnal changes as did the piezometers of TORRES et al. (1998) but those did have smaller depths. Although water table and discharge in general show that there in some way is a connection between them, a great variability was observed for different events and piezometer locations:

A comparison of the two bigger events [-28;-24] and [-14;-8] is made, including water table data. The open questions were a.) where does the difference in peakflow response come from and b.) what is the reason for the difference in total flow ( $760 - 446 = 314 \text{ m}^3$ )? Starting conditions for both were similar as  $API_1$  is the same, and the baseflow starting point is about equal for both events ID 2 and 4. Beside that, the precipitation input varied by 31 mm and the piezometer starting height and total height were different (Fig. 5.5.1a). These facts were found for P\_A9, P\_C7 and P\_C9 where nothing else was detected for piezometers close to

the soil pipe outlet. In relation to the questions the more distinct response at [-14;-8] can be explained with the different water tables in the system and therefore with the different water content. This is also supported by the events [0;4] and [8;10] with an equal rain input (see Tab. 5.2) where the remaining water table in the system at starting conditions differed and so total response differed (Fig. A3). However, the different pipe flow response on rain events throughout the study is well linked to soil moisture. For early events in the period water content was close to field capacity which resulted a flow response. Whereas water content towards the summer was far away from field capacity and resulted no response. Because of the gap in soil moisture surveillance, no more data can be investigated regarding this topic.

An explanation for the wet surface, in spite of the little response of the piezometers in the southern part (around SP1 and P\_A2), might be the possible earlier occurrence of land slides, which had dehomogenized the soil. Further, each piezometer seemed to react, in some way individually because of possible heterogeneity (e.g. occurrence of differently fractured sandstone, proposed higher availability of water and higher porosity). These are simultaneous reasons for the well responding area around P\_A7 and P\_C7 rather than the individual setup installation.

Worth considering is also that water table development on the slope may be controlled by depressions in the bedrock topographic surface. This was corroborated by MCDONNELL (1998) but does not seem to be valid at this site where high fractured and permeable sandstone underlies the soil. Further, the influence of surface topographic features (convergence and divergence) of the hillslope was taken into account (described by WOODS & ROWE, 1996). Very little differences in the shape of the north and south part of the hillslope were found, although it is probably not decisive for the different moisture content at the trench face.

A further question remains open: How does the drainage area of the soil pipes change when water tables (saturation) change? Despite the hysteresis curves were hard to interpret, any hidden data about the drainage area is still expected. Following the idea of a dendrite pipe network the slope of each water level point includes information on the characteristic flow patterns regarding on the individual height. To join this idea into a drain system, a hypsometric curve of the pipe network could be calculated.

Although we found a hint of a possible lateral groundwater wave propagating downward, indicated by the periodically rise and fall of water table, no pressure wave effect can occur in this soil/bedrock formation. Such kind of subsurface storm flow was identified by TORRES et al. (1998) and WENNINGER et al. (*submitted*) in non-open systems but is not relevant at Low Pass field site.

In order to get an idea of the drainage network of the soil pipes a land drainage approach was used, which is commonly applied for the installation of drainage pipes in wetlands and agricultural areas. The HOOGHOUTD-equation includes two terms, one for groundwater movement below the drainage (possible upwelling) and a second for groundwater movement from above. The initial calculation cited in EGGELSMANN (1981) results a guide number for the distance between draining pipes:

$$a = \sqrt{\left( \frac{4 \cdot K_2 \cdot d \cdot h^2}{s} + \frac{4 \cdot K_1 \cdot h^2}{s} \right)} \quad (\text{E. 5.5.4})$$

where:	a	= distance between draining pipes [m]
	$K_1$	= hydraulic conductivity above pipe level [m/d]
	$K_2$	= hydraulic conductivity below pipe level [m/d]
	d	= factor, relating on the depth of soil horizon below soil pipe [-]
	h	= height of ground water table above pipe level [m]
	s	= maximal outflow to be drained by the system, pipe flow [m/d]

For this this approach the first term (contribution from below) was neglected. Including the hydraulic conductivity determined by the slug test, the maximal specific pipeflow (determined by max. DCA) of different events, and the piezometer levels it was possible to get a rough assumption on the distance between draining pipes. This value is based on parallel installed drainage pipes but can be related to the drainage network of the natural soil pipes.

Calculations were performed for peak IDs 4 + 5 and 6, for different assumed hydraulic conductivities, for different elongation of water tables, and for different DCAs. The results obtained in Tab. A5 for the distance between draining pipes varied around 1 m. Although it is unlikely to come across parallel pipes the area of interpretation was extended towards the shape of the network. This is finally interpreted in the way that the soil pipes network is well connected and out branching does occur within the scale of 1 m. If this knowledge is transferred to the field site, there is a hint on the occurrence of many soil pipe draining structures along the width of the investigated hillslope (30 m).

## 5.6 Discharge at weir

The weir measured the initial stream running out of the proposed well at the lower hillslope. Obvious graph characteristic are the gaps of the series. Reasons here fore were the branch jams in the notch, which provided error data. This was likely to occur in a forested environment even under high maintenance.

As the weir was installed later, the first available data capture the response on rainfall event [0;4]. Peak discharge of the flume, 640 l/10 min, was about 6.5 times higher than the peak of the soil pipes. The total flow amount for this event ID 6, according to the limitations in Tab. A3 was 4110 m<sup>3</sup>. This was shown to be 26 times higher than soil pipe total event flow volume. Because the determination of a drainage area was difficult, no specific discharge was calculated for this peak event. The turquoise graph presented in Fig. 5.6a is standardized based on the maximum peak of soil pipe discharge. This helps to make comparisons between the response of soil pipe and weir discharge.

The data presented in Fig. 5.6a also show a second peak for weir flow around day 24. Although these data are discontinuous, the general response according to the rainfall input is more strongly pronounced than the soil pipes hydrograph during these dry conditions of the system.

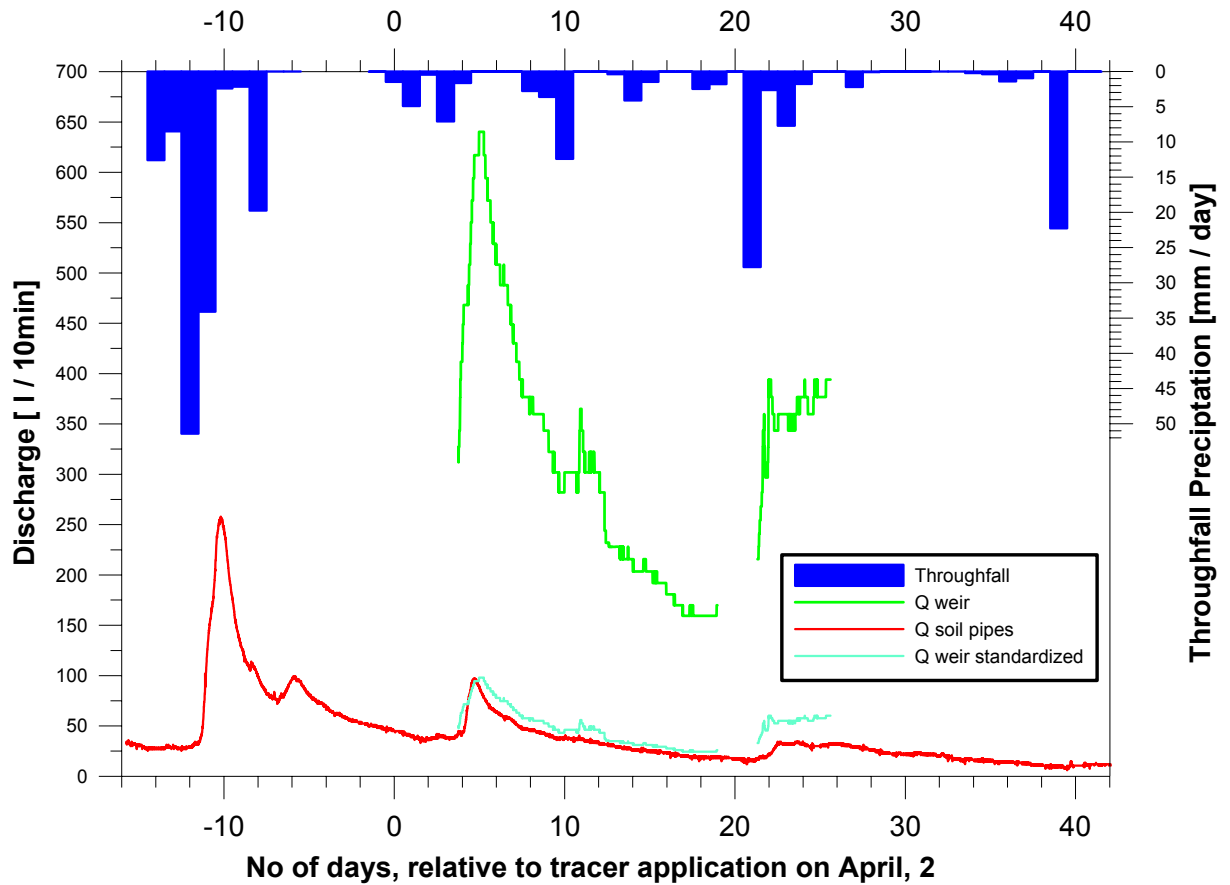
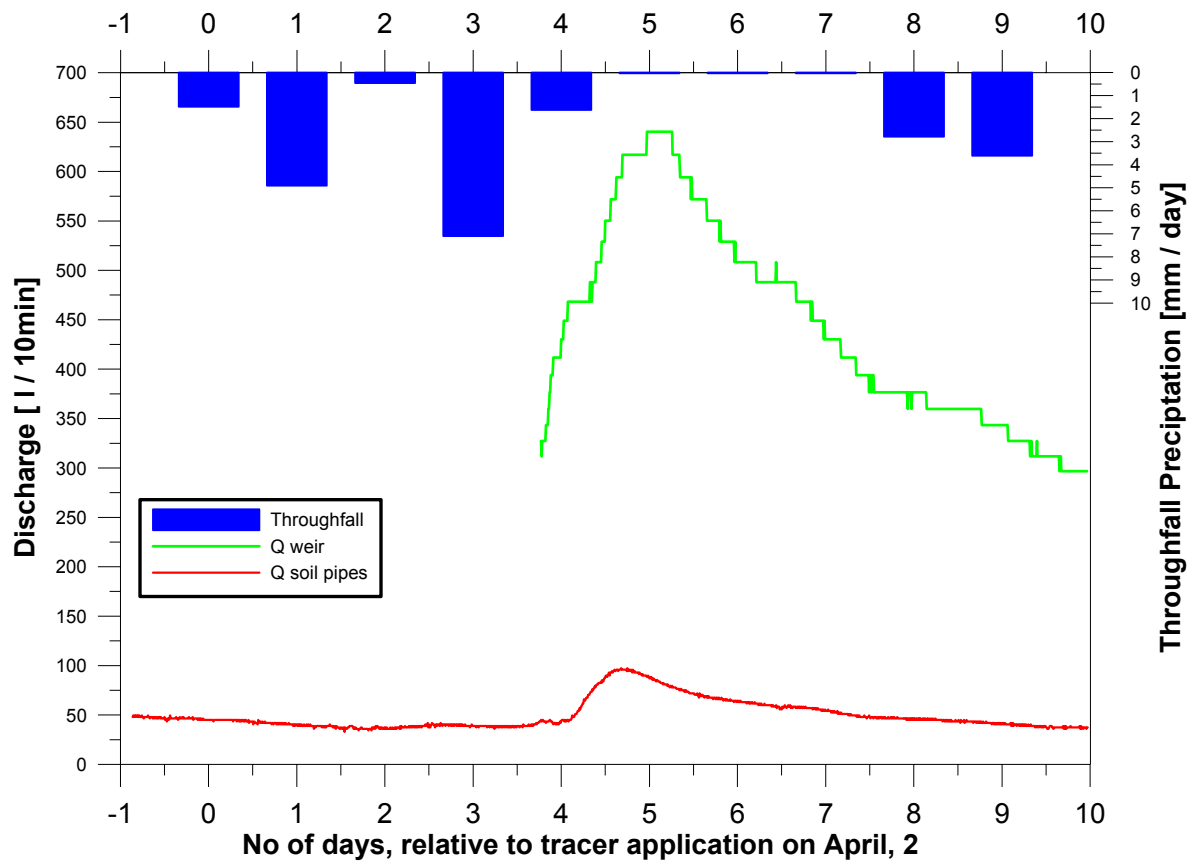


Fig. 5.6a: Discharge of weir, soil pipes, and standardized weir flow.

Finally the temporal delay between the soil pipe hydrograph and the hillslope hydrograph (weir) are illustrated for the event ID 6. The peak of the weir hydrograph was delayed by 7 hours compared to the pipe flow peak (Fig. 5.6b).



**Fig. 5.6b:** Time shift of pipe flow and weir hydrograph for event related to tracer injection (peak ID 6).

### Discussion of weir flow

Based on the portions of pipe flow and stream flow for event ID 6, the percentage of streamflow generated by pipeflow of the studied soil pipes is 3%. This result is consistent with the observations of TURTON et al. (1992), where subsurface flow at a plot scale contributes little to quickflow. Nevertheless, for this view it is important to outline that there are probably more subsurface flow paths, like other soil pipes, which could not be included in this comparison. Concerning these different drainage areas the percentage might be higher and should be treated with scepticism.

Furthermore, the forest road has important influence. Here, a great deal of literature focuses on these runoff generation processes summarised by LUCE (2002). The behaviour and dependency of cutslopes interception and its contributions is still not clear. The subsurface portion of flow contribution is strongly connected to a seasonally high water table. Observations from the Oregon Coast Range show that some roads intercept subsurface flow even when the water table is below the road (LUCE, 2002). Former studies at the Low Pass field site addressed this focus on the road section. However, the influence of the forest road with its extended contribution area and the amount of the already measured uphill pipeflow has an effect on the interpretation of the weir hydrograph. E.g. take into account that the already measured tipping bucket outflow was served into the catchment of the weir.

Looking beyond the end of the visible initial stream, where old trees hide the water at some stages, the true origin of the stream would be expected. This might be a spring with even similar characteristics to the soil pipes, and would lead to some discussion about the difference and the terminology in general. This may be called confluence for the catchment area and raises questions about the water origin at this opening. The much lower altitude suggests a strong domination of groundwater rather than any interflow (see definition of “spring”). To what extent this water differs from the soil pipe water could not be investigated in this study. In conclusion weir discharge presumably includes a majority of groundwater. Further possible interpretation and general conclusions are demonstrated later in Fig. 5.8.

## 5.7 Results tracer experiments

### 5.7.1 Amio G Acid

#### Lysimeter

To begin, it is important to note that the measurements represent integrated data, as the suction was kept for one to three days. The upper suction lysimeter (L\_U) reported basically the movement of the tracer front through the soil. This is presented in Fig. 5.7.1 for soil depths of 30, 50, and 70 cm. Data smaller than 30 ppb are treated as fuzzy data, as background concentration in the humus layer is able to achieve such values.

The first detection of tracer in the 30 cm suction cup occurred one day after the application. So the tracer went rapidly through the humus layer outlined in section 3.3. In the following days up to day 9 the full tracer breakthrough took place in the 30 cm depth. The thinned out concentration towards the end indicate a tailing of the curve.

The first arrived tracer 20 cm lower (at 50 cm total soil depth) is proposed to be at day 5 with 76 ppb. The following dry period did not cause much tracer movement. Not even a tailing of the first peak is visible. The second rise up on day 21 is explained by rainfall of 28 mm on that day which mobilized further tracer. Unfortunately further data could not be provided as the water content was too small to allow any sampling.

At a the soil depth of 70 cm no tracer occurred. The reason therefor might be the not yet detected entire breakthrough at a 50 cm depth.

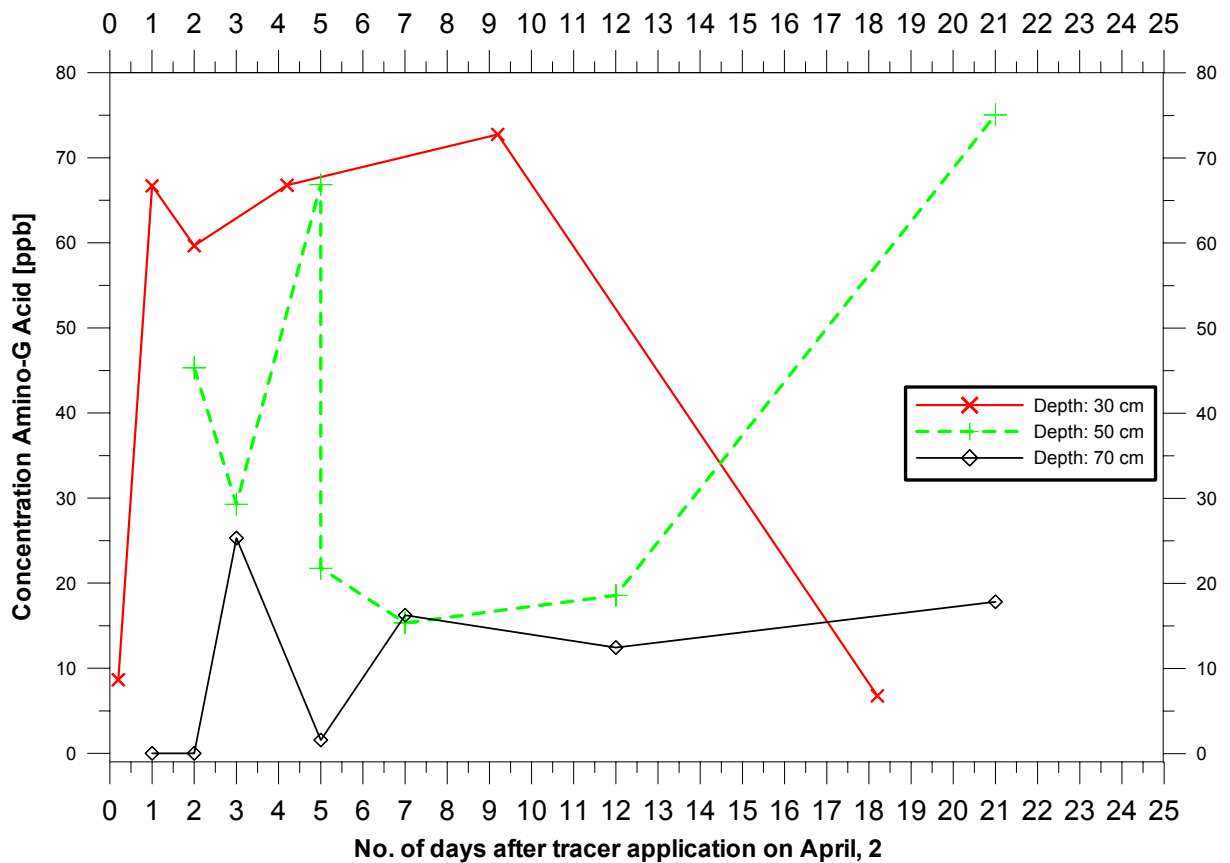


**Fig. 5.7.1:** Concentration of Amino G Acid at suction lysimeter below the line source tracer application.

### Piezometer

The samples sucked out of the piezometer are rare, because in a lot of cases not enough water was in there to provide the required sample minimum (see section 5.5). No significant tracer concentration was found within the grid capturing likely pathways. Background concentrations here were around 10 ppb, probably caused by high sediment content or interactions with the bitumen or PVC shavings (might have been some mistaken leftovers).

### Soil pipes and flow proportional samples at tipping buckets

The hand samples at the three different soil pipes endings did not show an Amino G Acid breakthrough. The detected concentrations were within the background or close to the detection limit and are classified as no tracer breakthrough.

The flow proportional sampler at the tipping buckets offered continuous surveillance for a tracer breakthrough. For the period investigated no breakthrough curve was detected.

### Weir

The hand samples at the weir resulted in a single peak (digital time 4.5) of 43 ppb. Besides that no other samples contained Amino G Acid. Therefore an error is supposed for the outlier. Summarizing this study has no evidence of any tracer arrival at the lowest point of sampling and presumes overall confluence.

## 5.7.2 Bromide application

### Electrical conductivity

The results obtained in Fig. 5.7.2a do not show an increase of conductivity in the pipeflow. The time series, starting on the day of tracer application, keeps the level of the long range mean with about 40  $\mu\text{S}/\text{cm}$ . Minor fluctuation was probably caused by the different salt content of the pacific originated precipitation, which passes through to the runoff. A measurement for precipitation conductivity was not installed, so no data is available on the variation of this input value.

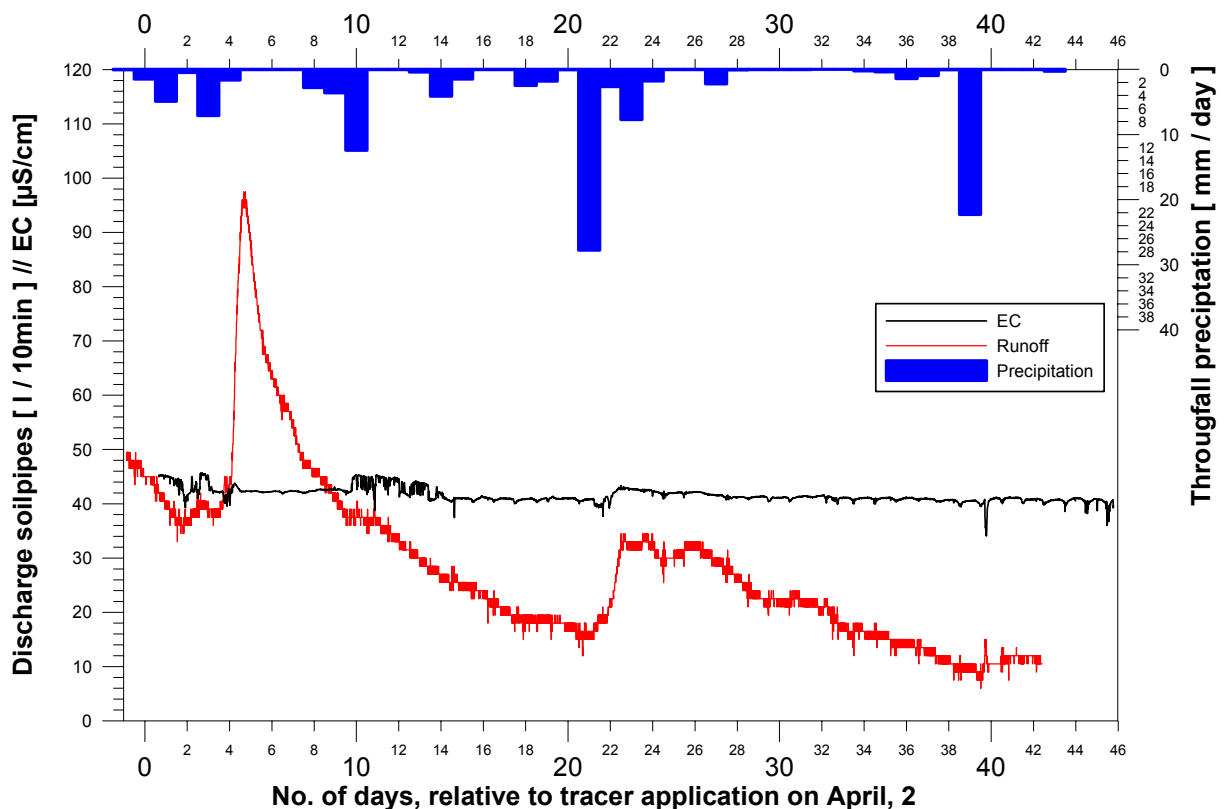


Fig. 5.7.2a: Electrical conductivity after the tracer application, discharge soil pipes and precipitation.

### Bromide sonde and bromide hand samples

The data series of the bromide sonde at the outflow tipping buckets did not show a tracer breakthrough. All stored ten minutes data ranged below 0.06 ppb, except two outliers. These amounted to 1.2 ppb (digital time: 2.6319) and 1.99 ppb (the following 10 min interval, digital time: 2.6388). No explanation was found for this pattern, which occurred together with very little variation of electrical conductivity (Fig. 5.7.2). The corresponding sequential samples at the tipping buckets and the selected hand samples from the pipe outlet did not show any bromide.

Samples of the piezometers and from the weir did not have any breakthrough of bromide, either.

Data about the remaining bromide provided the samples from the bottom suction lysimeter (L\_B). As concentrations here were very small this study refrained from using relative tracer concentrations ( $C/C_0$ ). The absolute concentrations for three different depths show the movement of the surface applied tracer on its way through the soil (Fig. 5.7.2b). The maximal concentration in 30 cm depth occurred 23 days behind the tracer application. Afterwards concentrations dropped and showed 8 mg/l. For soil depth of 50 cm there is a weak rise of detectable tracer concentrations. For the samples of the 70 cm depth there was no bromide detected.

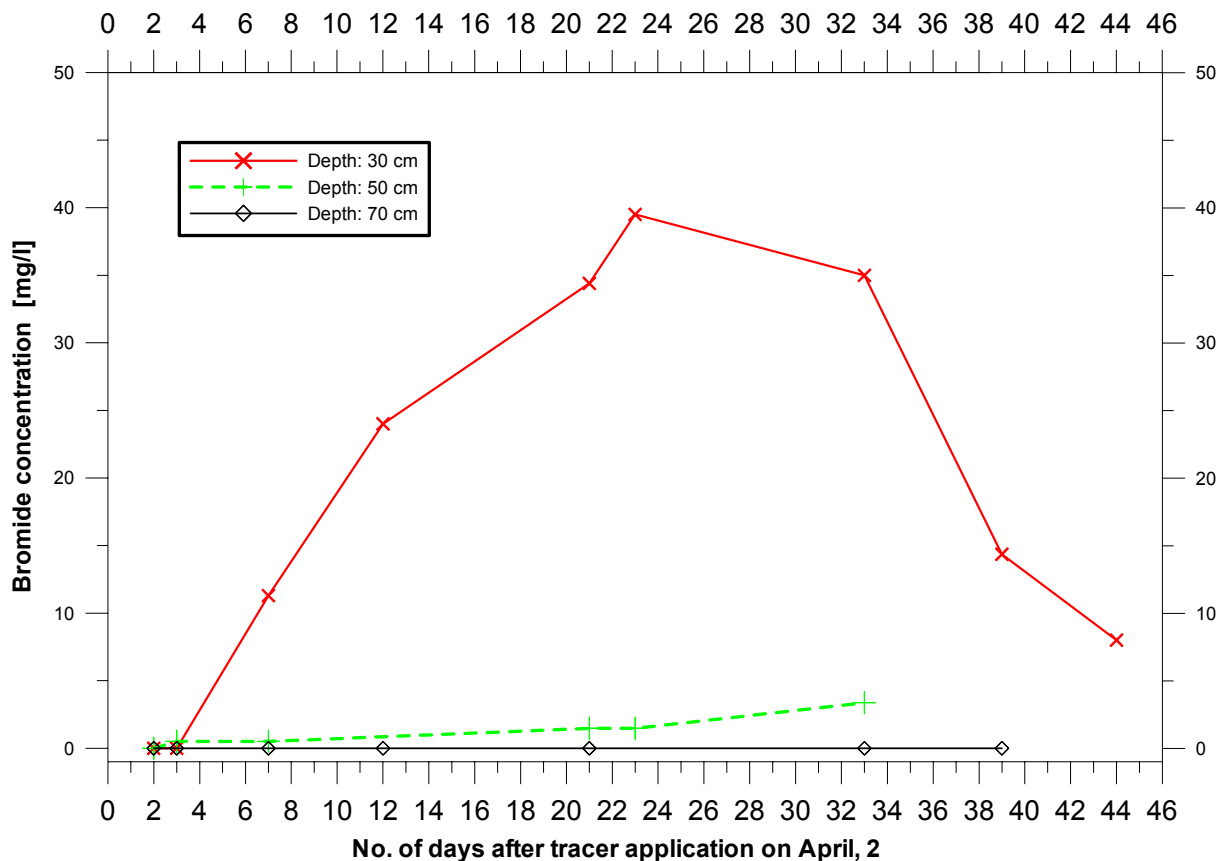


Fig. 5.7.2b: Bromide concentration at bottom suction lysimeter (L\_B).

### 5.7.3 Discussion of tracer results

The results of the performed experiments are linked to the conscious fact of no applied pre-wetting. Any speculative questions as to moisture conditions would have provided better breakthrough curves are left aside. Thus, the results presented by ANDERSON et al. (1997) include point injections into saturated material differ from this study. Their results are based on saturated zone flow which could not be established at the entire drainage area of the soil pipes. Tracing the flow in the vadose zone (extensive tracer application) they showed that 92% of the labeled water remained in the vadose zone after 3 days and ~140 mm of

sprinkling. However, their lysimeter observations with about the same installation and conditions (depth 0.87 m and 0.21 m) fit well to these ones.

For an interpretation of the suction cup data problems arised from the dissolved organic carbon, as in particular concentrations ranged low. Beside this background issue note that solute sampling is likely to miss bypass flow (FLURY et al., 1994). As bypass flow was proposed in this kind of soil (see above), it may also be valid that Amino G Acid (applied at 20 cm distances) used a macropore system to bypass the sampling cup. But as the data of the bromide movement showed very similar results a remainder of both tracers in the upper 50 cm of the soil is summarized.

### **Reasons for the absence of tracer at the soil pipe outlets and at the weir**

The transit times of the tracer up to the soil pipe did exceed the investigation period and remained in the system.

A major reason here is the reduced precipitation (113 mm) falling after April, 2 why further events did not mobilize the tracer enough. For the line source application and the extensive application it is shown that the tracer did hardly reach a soil depth of 70 cm. So the drained soil matrix had too little conductivity to enable faster tracer movement. On the evidence it is likely that most tracer was held up or stuck in the micropore system of the unsaturated zone. The status of saturated conditions with higher velocities could not be obtained. This was particularly difficult because piezometer data showed the unsaturated conditions during the whole period in the upper 70 cm soil depth (see section 5.5). Similar results where tracer 'stranded' in the unsaturated zone are apparently described by NYBERG et al. (1999) and WILSON et al. (1993). But within the logic of this interpretation a further process is not able to be described: How does it come that a little peak of discharge occurred (ID 6) and although a quick piezometer response after storm events indicates a fast acting water table establishment from above whereas there is no evidence of tracer movement?

Another further consulted interpretation focuses on the tracer input mass being too small. Two aspects appear to be relevant: Unexpected high sorption and dilution. Both phenomena are already detected for the restrictively applied line tracer in 70 cm depth (Fig. 5.7.1). And on its further path, even if little tracer reached saturated conditions a very strong dilution made a determination impossible. This effect also played out particularly at the weir, where a high portion of ground water contributed to runoff. Further, regarding the soil pipes, the maximal dynamic contributing area (section 5.4.1) outlined that a high solution is likely. Instead of a wider distribution of the area sprinkled with bromide (towards the higher gradient in topography in the south) a higher tracer input mass might be the better approach. Concluding, the assumed contributed discharge for the tracer input mass calculation was too small.

## 5.8 Conclusions of field investigations

The characteristic in Coast Range rainfall intensities distribution, with outstanding peaks throughout a low intensity (Fig. 5.2c), is assumed to be a trigger mechanism for runoff generation. Whether the pipe response is linked to higher intensities could not be investigated comprehensively.

The results of pipeflow imply that there was a component of rapid contribution from rising water tables as a consequence of a supposed dendritic network upslope with its spatial increase of drainage network. Taking the obvious response (rise of water table) into account, it might be questioned, why no tracer reached the saturated conditions? The answers on this topic about local groundwater recharge are discussed in two ways. First, regarding the water content of the soil, much water is needed to achieve field capacity. And even under macropore conditions preferential flow is inhibited by the unsaturated conditions. Thus, the rise of water table is caused by 'old' water rather than by 'new' water, which would have contained tracer concentration. Second, there has been no focus, whether interflow from the top hillslope area is able to cause a water table rise. However, there is a second component of groundwater, which is responsible for the long-term delivery. This is based on the ephemeral pattern of pipe flow and its summer drought. The impact of groundwater from below on pipe flow is e.g. supported by the position and horizontal alignment of the pipe outlets; and the temporal start up of SP2 and SP3 probably is created by a possible threshold mechanism. Piezometer data showed that the water table in the hillslope was highly variable in both magnitude and timing. And even neighbouring piezometers showed unexpected differences. But temporary water tables in the hillslope occurred up to 60 cm below surface topography and are well linked to the pipeflow hydrograph. Orientating on the question about the affection of topographic convergence on subsurface flow and water tables, the findings provide evidence for higher water tables levels and oscillation in the less convergent, northern part of the hillslope.

This might also be explained by the shape of the dendritic network and the connection of different areas to it. This hypothesis would explain the different piezometer response. However, verification of this network shape is e.g. possible by a fibrescope examination on morphologic triple-junction features (TERAJIMA et al., 2000). Nevertheless, an absence of this drainage mechanism of the pipes would otherwise cause a saturation of soil with occurring interflow components at the trench section.

Fig. 5.8 gives an outline on ideas about processes and conditions of flow. The proposed water table shows an annual magnitude and therefore the drainage area of the pipe network differs throughout the year. For the high water table levels during winter we see a water table rise supported by winter frosts with open cracks and strong stability of soil aggregates. A similar context is shown in the results of TSUKAMOTO et al. (1982) who reported that pipe flow did not begin until groundwater saturation reached the pipe level.

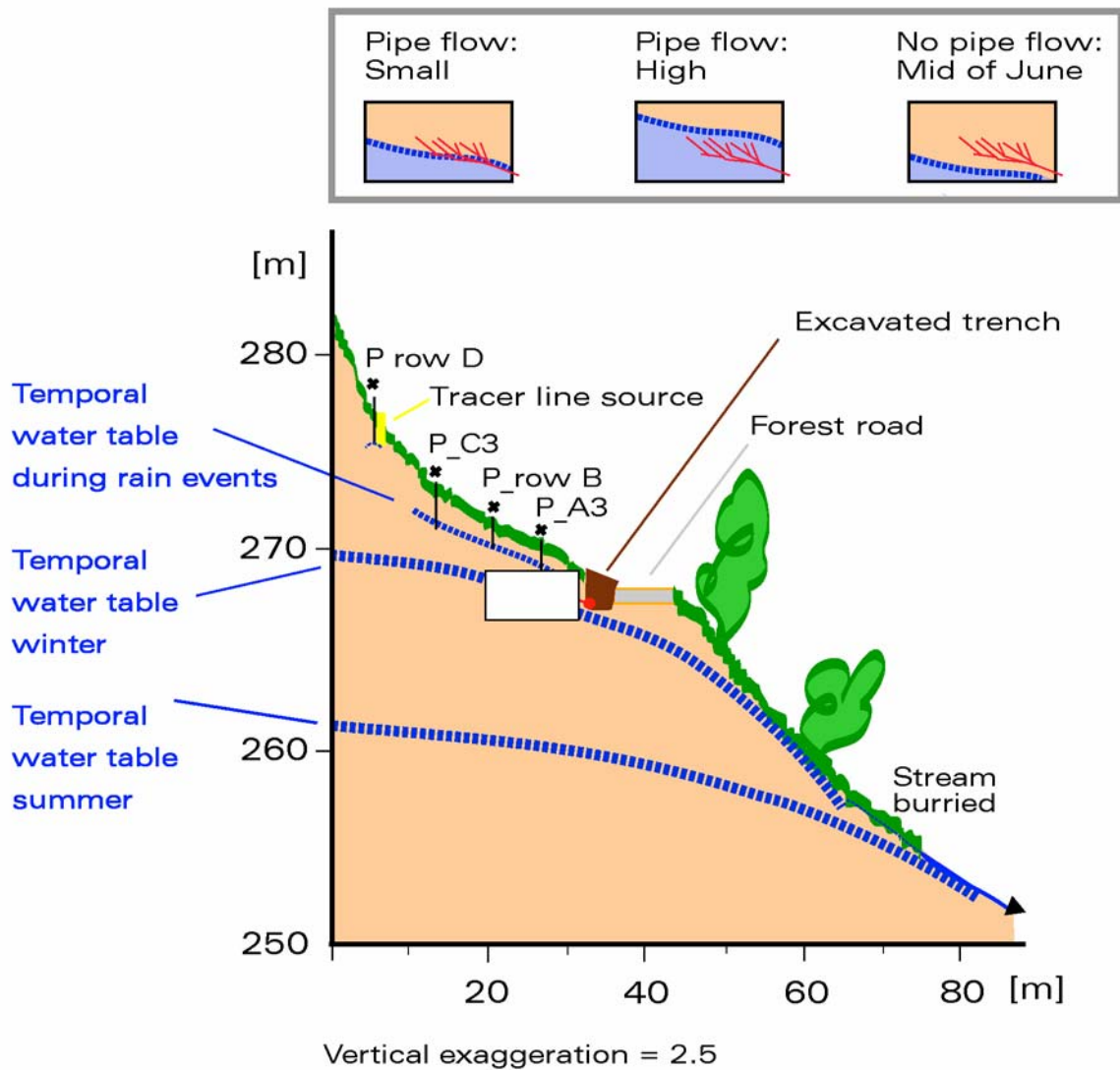


Fig. 5.8: Assumed processes and conditions along transect of the hillslope.

The role of bedrock is still not clear. However, there is a certain interaction between key-mechanism water table and the fractured underlying bedrock formation, with leaky properties. Further, there was found no hint about a connection of the water table in the slope and other indication of ground water.

The hydraulic connection of lateral flow in the macroporous soil and the horizontal dominated soil pipes (likely to be seasonal groundwater table) is still unsure, as the outcome of the tracer experiments provided no successful information. The pattern that flow begins only when soil is almost saturated is a well known fact for macropore flow (e.g. JOERIN et al., 2002) was supported by selected data presented above.

The question how old the dominating pipe flow is (dominated by 'old' groundwater or rather event water) is not clarified satisfactorily with this tracer study. Mean turnover times of recessions could also not help to solve this problem although residence time (tracer experiment) does outstrip mean turnover times (recession analysis) by far.

---

Estimated reasons for the unsuccessful tracer experiment are the reduced precipitation input and the dry conditions in the unsaturated zone. For the objective of the study the hillslope is still to be treated as a 'black box'. A proposed outlook may be the excavating of tracer for determination of already travelled distance or, alternatively, to wait for the next wet season. The results presented are a snapshot of conditions as soil pipes develop and change, visible in varying sediment discharge within years (UCHIDA et al., 1999). The reason here is the non-DARCY flow in a soil pipes with its acceleration and erosion. Moreover, WILSON & SMART (1984) predict that soil pipes modified their hydraulic properties to produce an efficient drainage network.

## 6 Results and discussion: Hillslope table

The availability of sophisticated hydrological models has greatly improved hydrologists ability to perform complex hydrological analyses. Models make it feasible to evaluate the impact of soil pipes on stream flow generation. This chapter follows the question of how an artificial simulation of the conditions of a field site actually operates in practice.

The results presented are the starting point for further studies, which will include artificially implemented soil pipe structures (see section 6.8). This physical modelling approach might help to gain knowledge about the connection of lateral and transverse macropores at the Low Pass field site and in general.

### 6.1 Short overall description of the experimental run

Preliminary initial experiments helped to assess the response and conditions of the table. The very first stages of the sprinkling experiment were performed at a slope of 5%, and resulted in a strong occurrence of Hortonian Overland Flow. An additional textile layer was placed on top of the soil, with the intention of improving the infiltration capacity by the enhanced roughness, which would hinder landed drops from transverse flow. But this did not reduce surface runoff either.

The final run was included at a slope of 25% and included the three days May, 19 to May, 22. In what follows, time is expressed as digital time.

### 6.2 Sprinkling

The sprinkling intervals were chosen small enough in order to prevent Hortonian Overland Flow and frequently enough to ensure steady state conditions at the outflow. A unit consisted of 5 minutes' irrigation, with an average of 2.338 mm or 18.23 l sprinkling. It was followed by 10 min draining. For a simulation a combination of looping units was applied. This was in order to catch up with the idea of mostly low rainfall quantities with high peaks included. After about five to six loops, there was a longer drainage period, which was also varied in its length. The schedule of irrigation runs and drainage stages for the whole experiment is reported in appendix B1.

At the end of the experiments a series of 10 min sprinkling events was performed with a 10 min break in between. The reason for this was a final mobilisation of any remaining tracer in the system. As a result of the extended sprinkling interval the occurrence of little HORTONIAN Overland Flow was taken into account.

The temporal distribution of sprinkling (on / off application) over the experimental period is presented in Fig. 6.2.

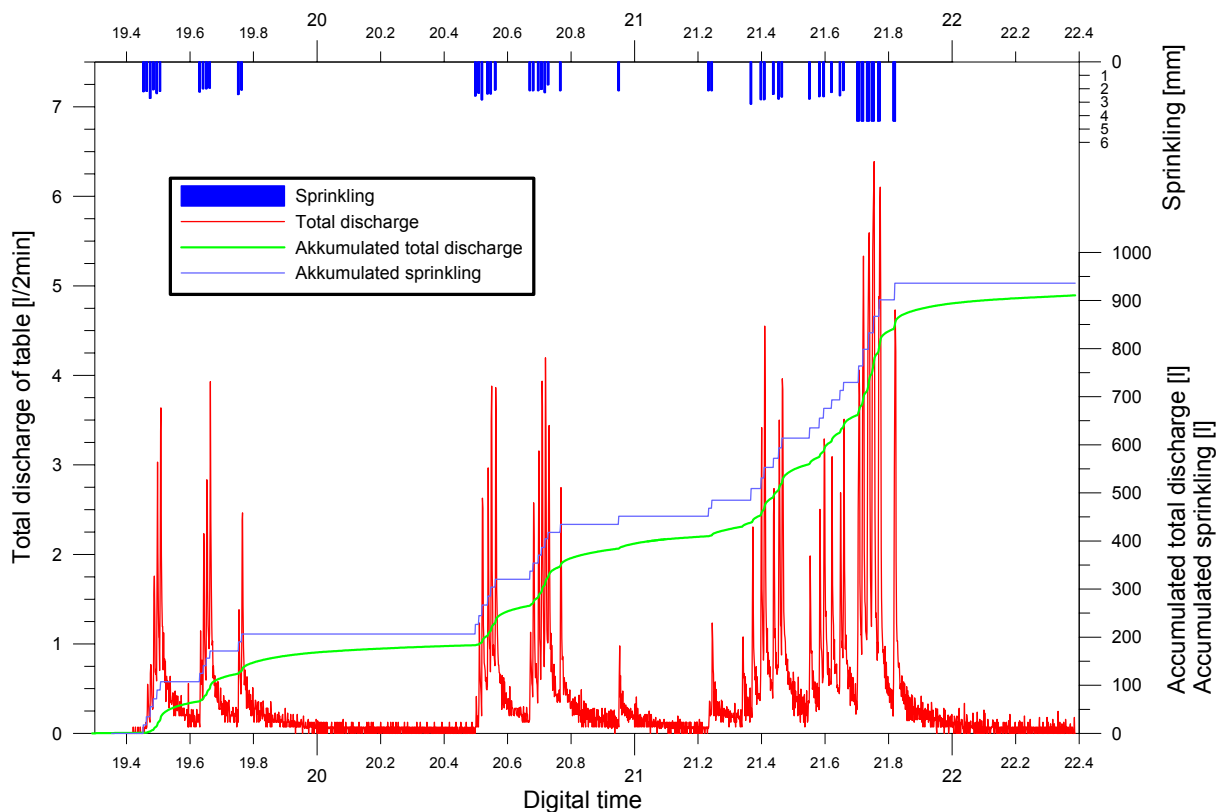


Fig. 6.2: Overview on sprinkling and runoff for the whole experiment at the hillslope table.

### 6.3 Runoff

First of all the individual eight tipping buckets (TB) were summarized to total outflow of the table. Surface runoff contributed only minimally to the total outflow. This hydrograph is presented in Fig. 6.2a with the resulting pattern of peaks following sprinkling events. The graph does not show strong steady state conditions at the TB. Drainage periods show a longer visible tailing, up to about 18 h beyond the last sprinkling. Maximal discharge for the ordinary 5 min-sprinkling events reached about 3.9 l/2min.

A closer look at the distribution within the array of eight tipping buckets showed a non-uniform distribution with a strong dominance of TB 8 followed by TB 1. Thus major portions of total discharge ran out of the table at the very right side. On the contrary, minor portions of the total discharge were produced from TB 2 and TB 5. This variation is presented in Fig. 6.3. The dominance of TB 8 also has a temporal pattern beside the quantitative. Here, the flow reaction past the sprinkling is much faster than at other TBs (see also Fig. 6.3).

Using the results of a hydrograph separation enabled to calculate runoff coefficients for the different runoff events according to E 4.5a. Here results varied between 0.007 and 0.028 (average= 0.014; n=14) for peaks following the 5-minutes sprinkling intervals.

## Timing

The time shift (according to section 4.5) between runoff peak and the 5-minutes sprinkling events ranged between 2.5 and 4.5 min, average was 3.46 min ( $n=36$ ). No significant relation with soil moisture data was found.

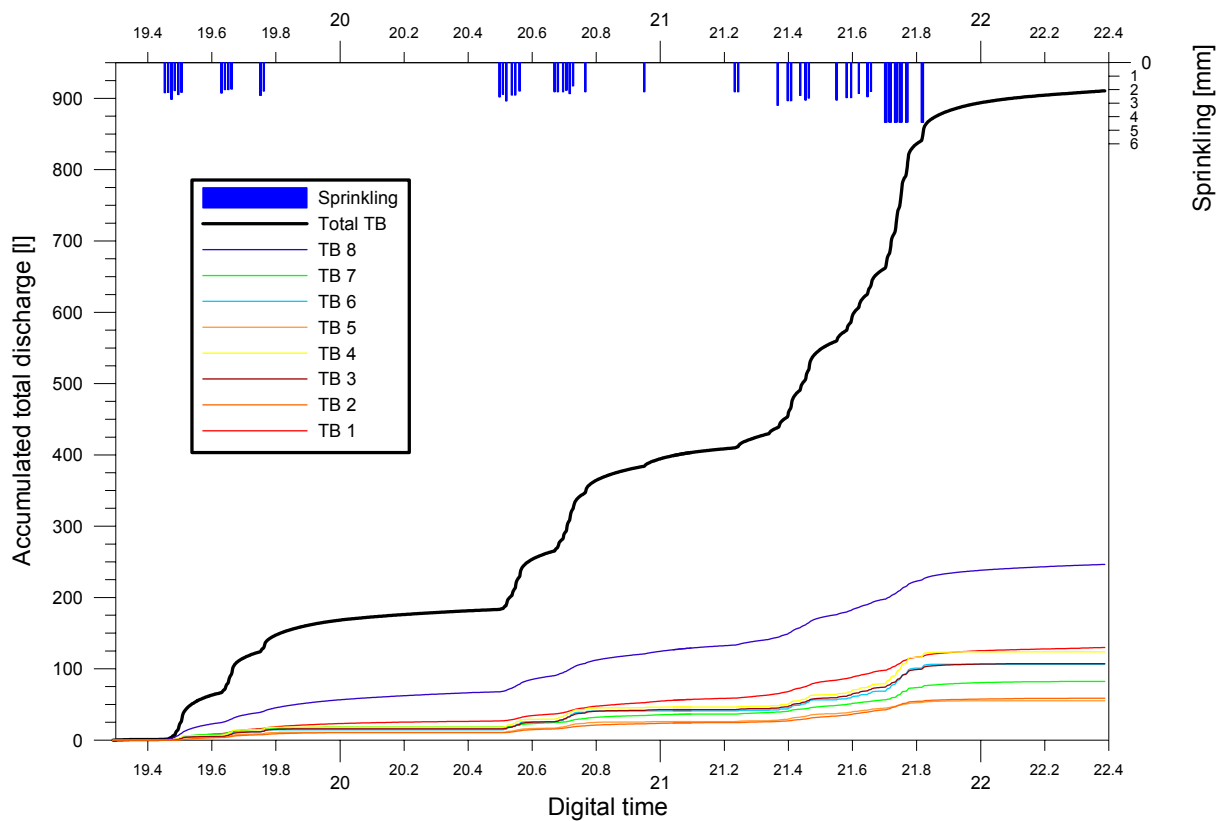


**Fig. 6.3:** Variability of accumulated discharge at different tipping buckets and sprinkling intervals.

## Discussion of Runoff

The non-uniform distribution of discharge at the TBs was not expected. In view of the homogenous rainfall distribution (mentioned earlier) and the horizontal alignment of the table ground, either a proportionately greater runoff might be expected at TB 3 to TB 5 (all in the middle) or else an even runoff for all TBs. For an explanation of the actual result importance has to be attached to soil properties. The irregularity is obviously caused by the soil filling, although this was done with maximum precision.

The occurrence of surface runoff is best explained by there is a missing vegetation layer and A-horizon. These findings contrast to other sprinkling studies on a comparable soil, with much greater slope angles ( $43^\circ$ ) and durations of 10 to 30 min where no surface runoff

occurred (TORRES et al., 1998). Both experiments highlighted that soil-water content does not influence the generation of HORTONian Overland Flow.

## 6.4 Water balance

For the overall run, which included three days of investigation, a total amount of 935.8 l of rain was applied to the table. The total runoff for the same period amounted to 910.6 l. Therefore the water balance shows a gap of 25.2 l, which is water remaining in the soil and a minimal portion of eventually evaporated water.

## 6.5 Soil moisture

The soil moisture data of three differently located sensors are presented in Fig. 6.5. During the experiment the volumetric water content of the soil ranged between about 25 and 35%. The calculated mean drainable porosity amounts to 8%. Using a piston core device at digital time 22.4 provided a soil water content of 0.61 g/cm<sup>3</sup> for the probe B. The linkage of volumetric water content (output logger) and absolute water content resulted in a water content of 0.87 g/cm<sup>3</sup> for saturated conditions of probe B.

The graph of the deeper probes A and C shows that the system was saturated for most of the time. Within the overnight drainage periods water volume reduced but still did not reach a limit. Contrary sonde B shows this very well. Here, four centimetres below soil surface, the rapid drainage even in short sprinkling breaks dominated.

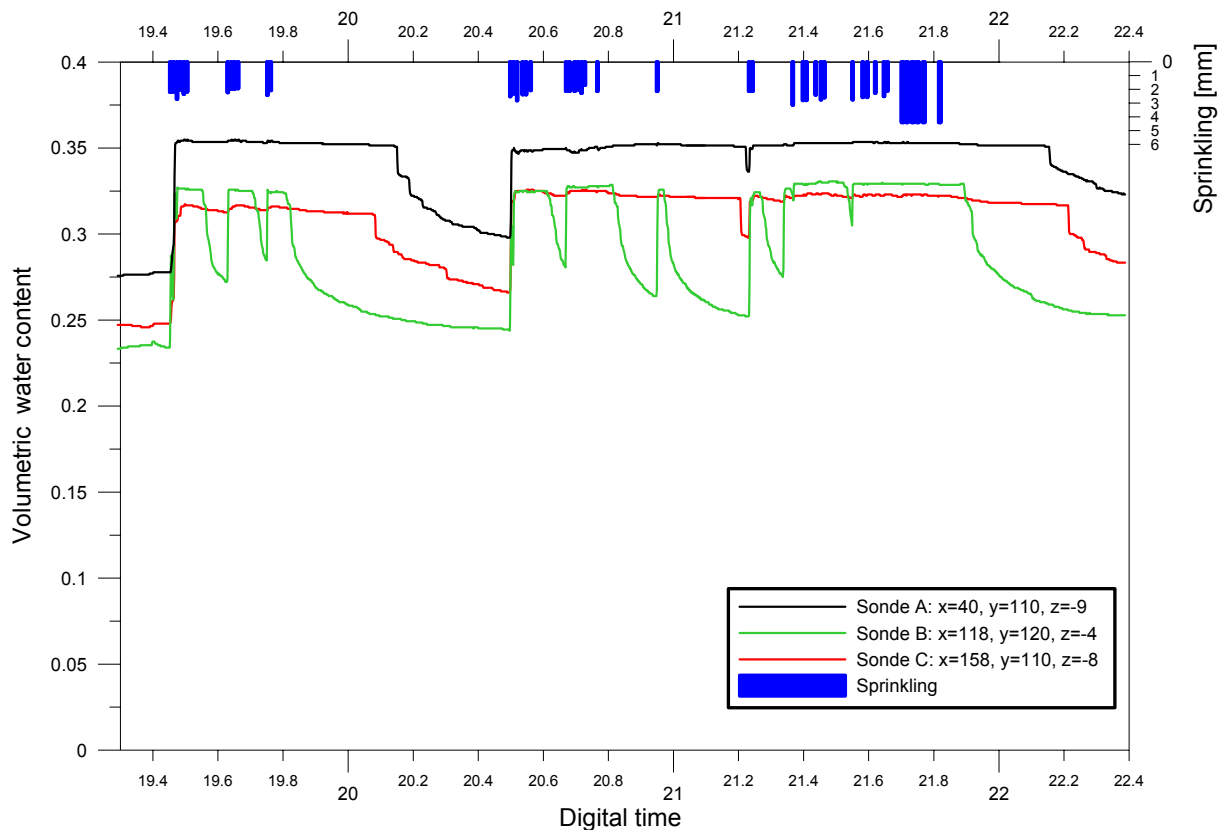


Fig. 6.5: Soil moisture at three different locations at the table for the period of experiment.

### Discussion of soil moisture

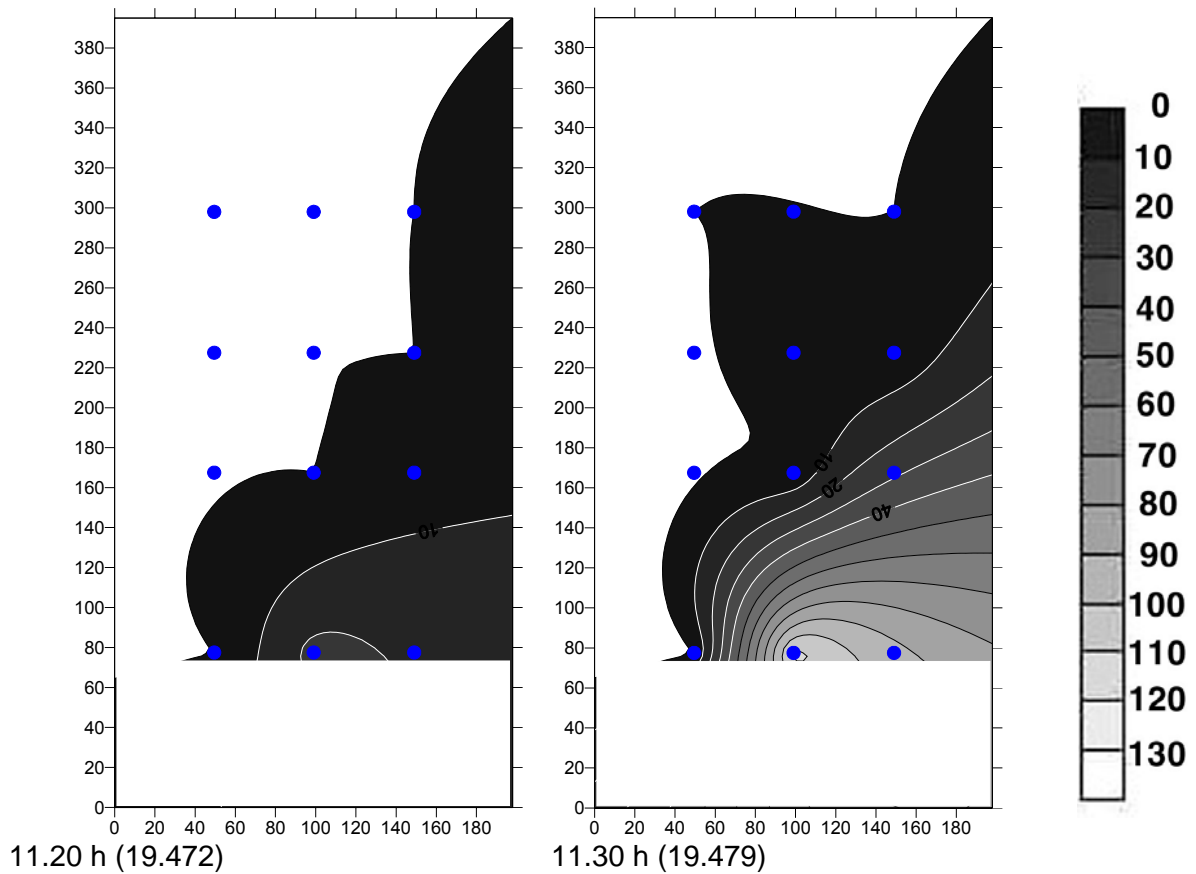
Constant soil moisture content is typical for steady state irrigation. Although this was not obtained perfectly, approximate 'steady state' conditions were achieved. These results are consistent with FEYEN et al. (1999) for example, who sprinkled a muck plot

## 6.6 Water table and water volume

To visualize the water table levels a spatial distribution was chosen. The data of the mini piezometer was interpolated by the Kriging-method. Length numbers where  $y$  is  $\in [0, 78]$  were excluded from interpolation. Because of that, there was an illustration much closer to reality than the one with the border issue zero instead. This would result in a declining water table towards  $y=0$  which is contrary to the natural conditions. Because the table was actually sloping, a small extended water table was 'backed up' from the outlet and rose disproportionately in this not interpolated zone. A complete saturation of the soil - with water level with the surface of the soil - was observed in this area rarely (especially at the 10 min sprinkling intervals).

The spatial interpolation was prepared for the first day of experiments on selected time steps (Fig. 6.6a). Generally, the water table moved slower than the runoff response. The water table was established from lower regions, where water was backed up on the sloping table. This process is more or less uniformly and reached up to a water level height of 13 cm. After

the rise of the table around digital time 19.5 the maximum in both height and extension was obtained. The subsequent decline towards the next day happened slowly, in particular between digital time 20 and 20.45. This underlined the characteristics of the system. The decline of the water table during the recession period, starting at 19.82, was not uniform and showed priority at the left hand side of the table (TB 1).



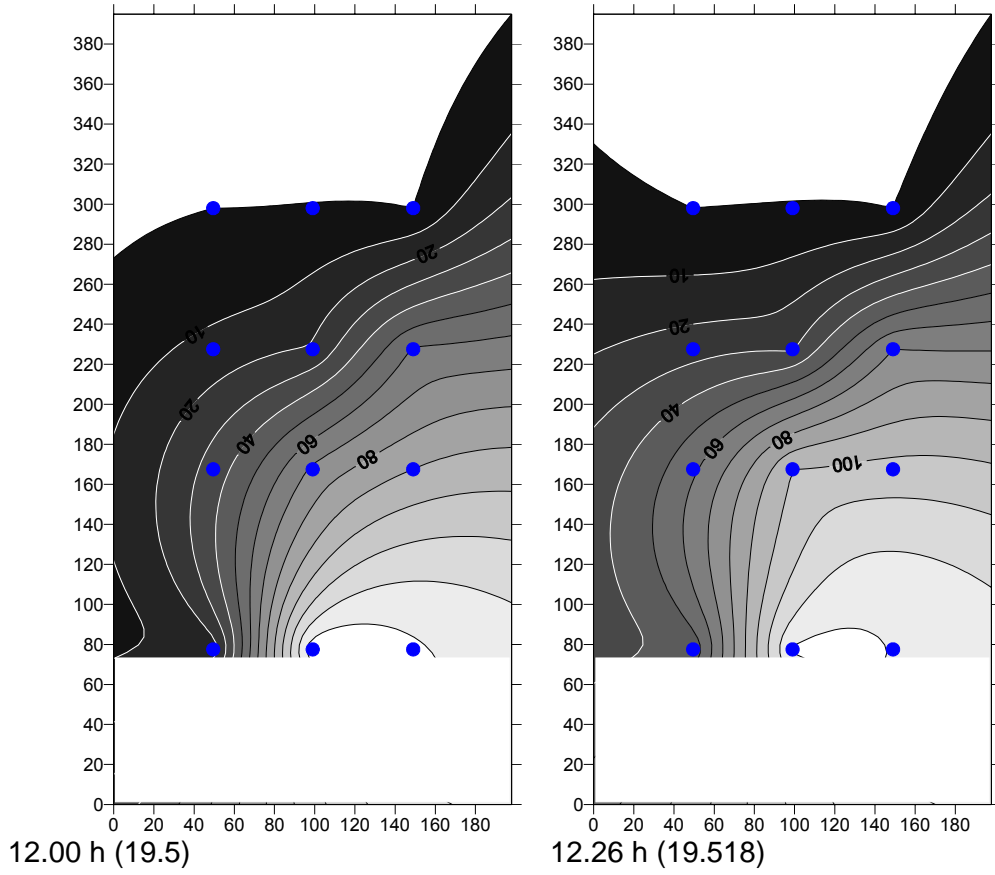
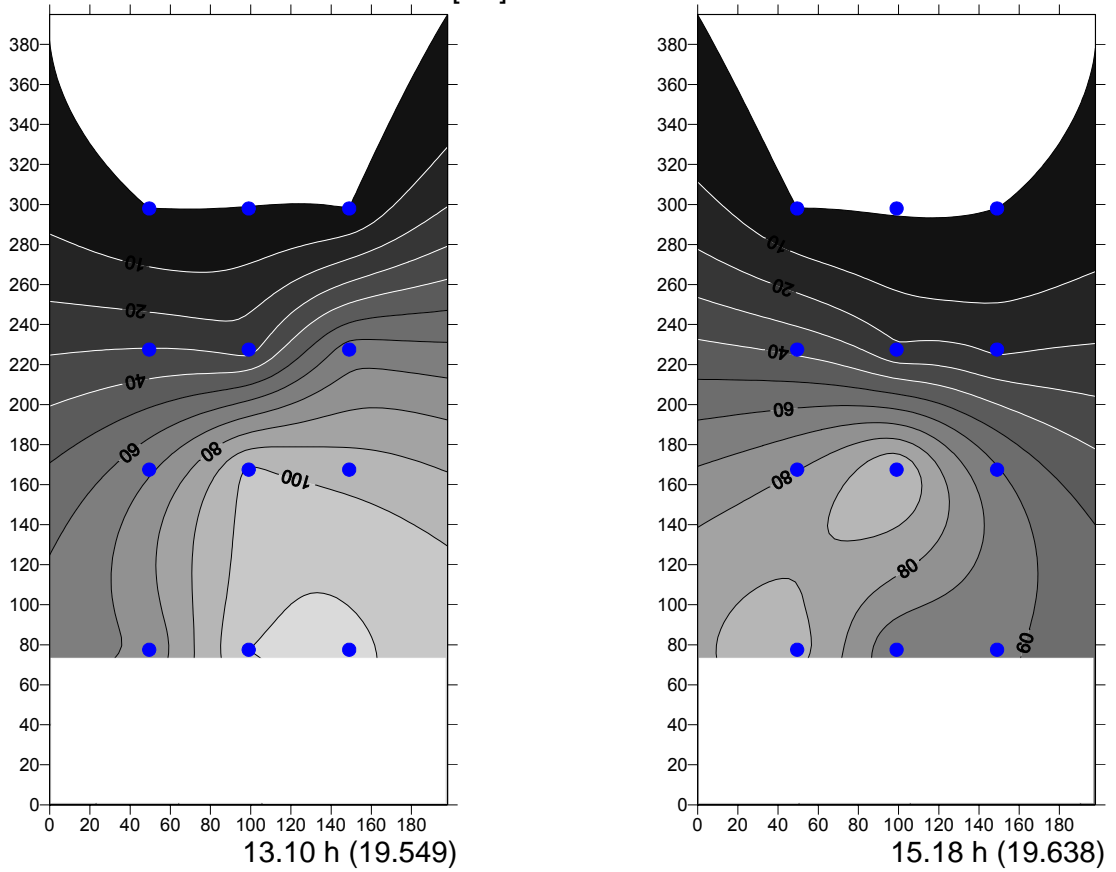


Fig. 6.6a: Height of water table [mm] at different time steps. See legend on right for details. Dimension of table [cm].



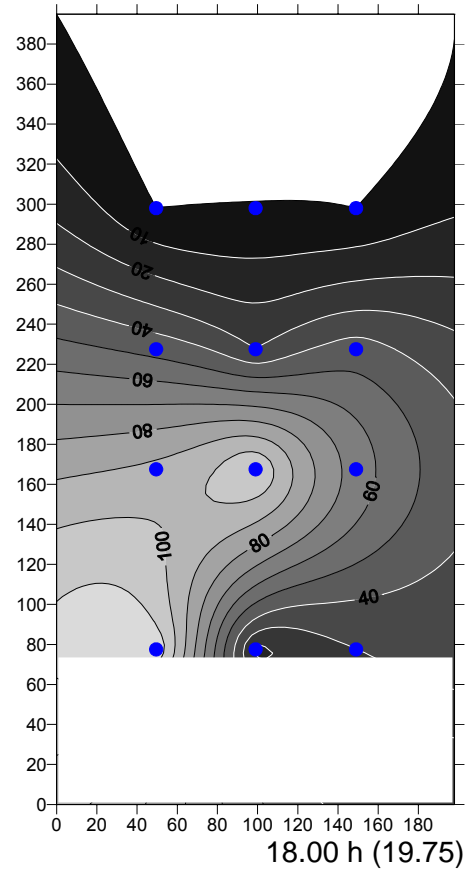
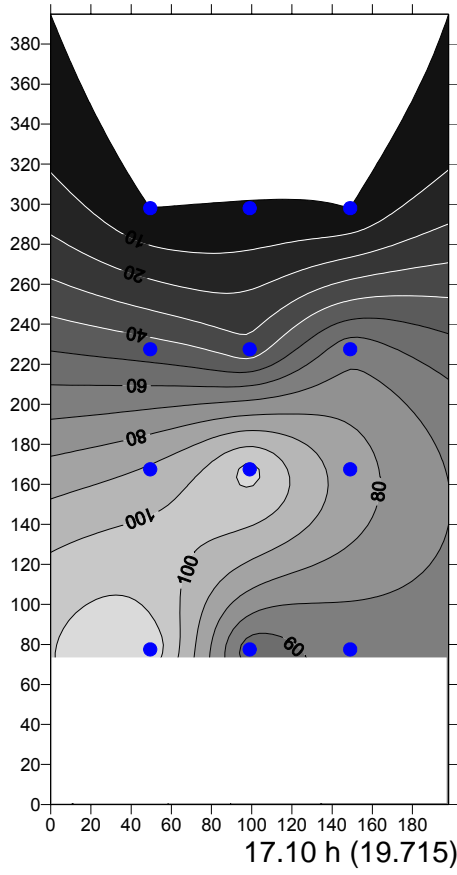
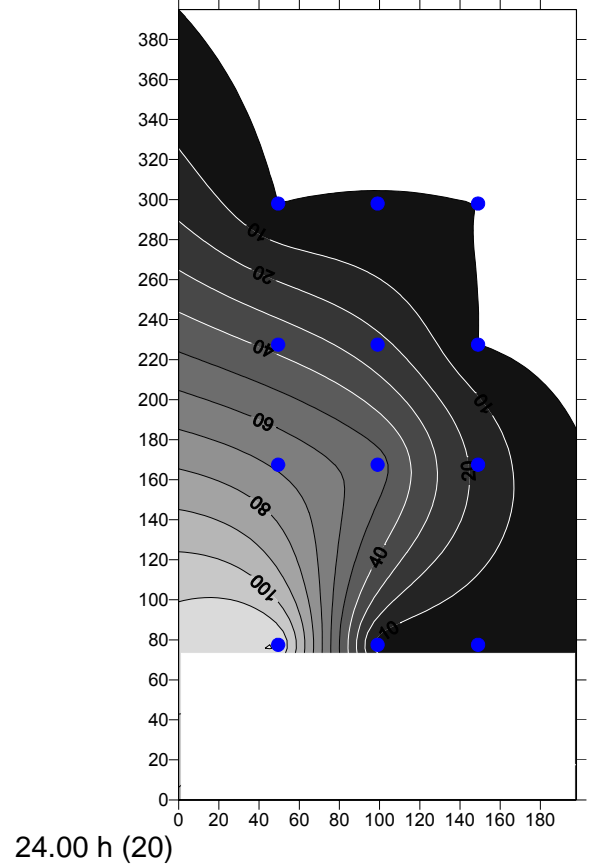
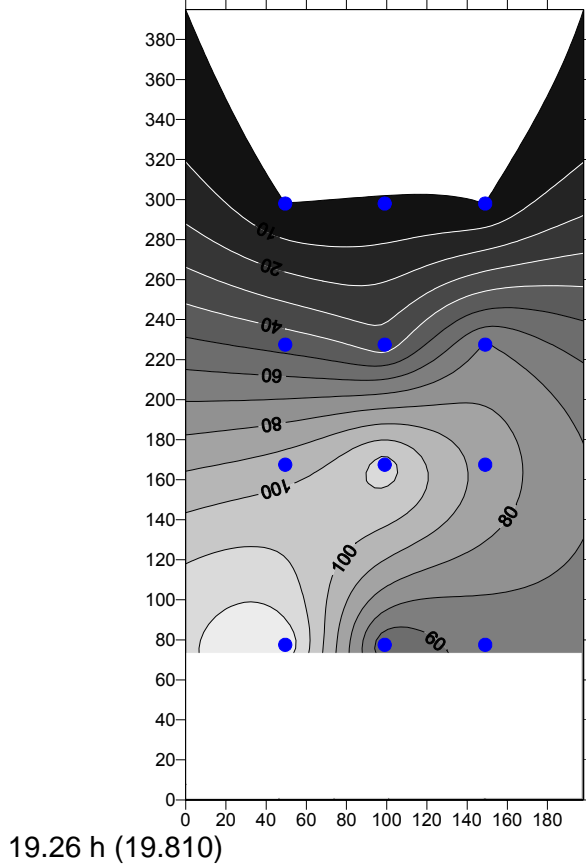
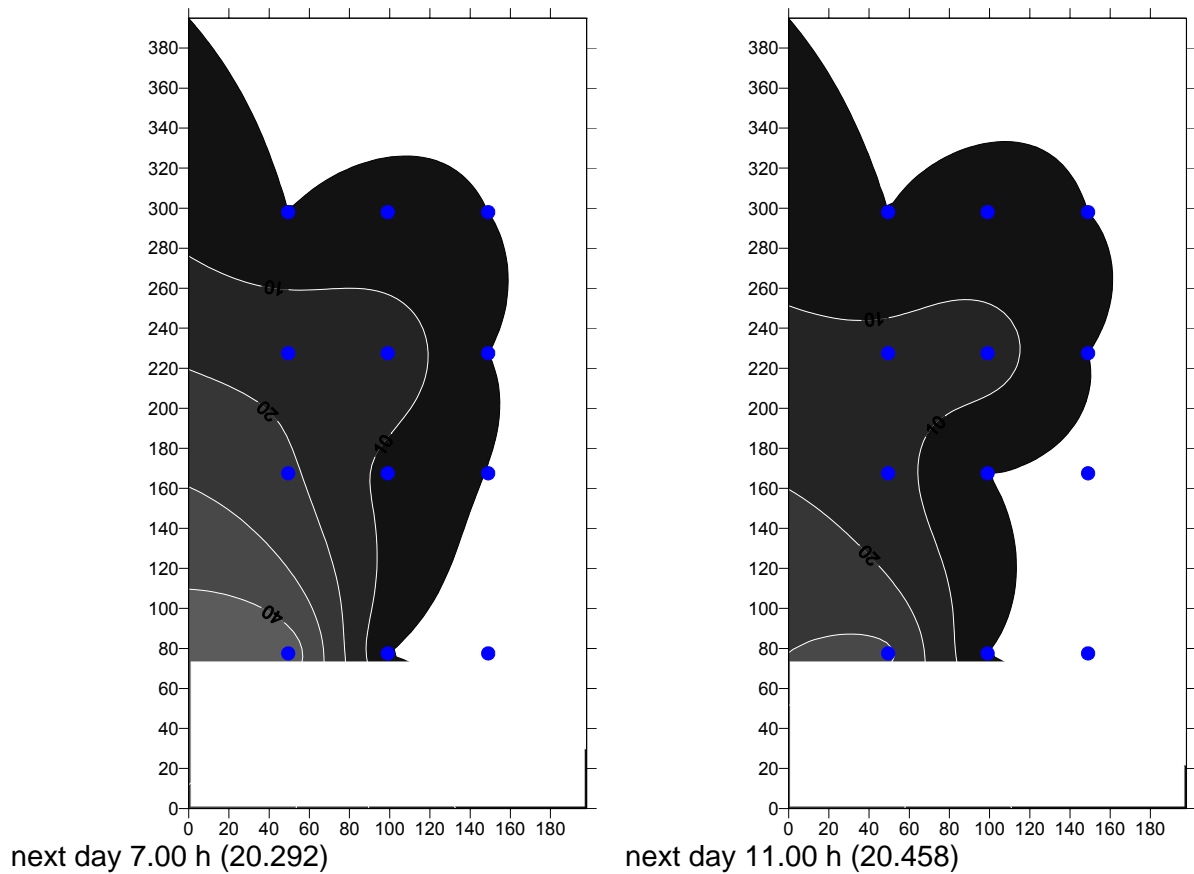


Fig. 6.6a: continued





**Fig. 6.6a:** *continued*

Out of these interpolated spatial water table data the total water volume in the table was calculated based on the measurements of absolute water content under saturated conditions. The data of sonde B was extrapolated to the overall soil. However, this offered an estimation of water volume in the system and is provided in Fig. 6.6b for a initial run of experiments. During saturation conditions the maximal water volume remaining in the system was about 400 l. The recession at the end was slow and went down to an amount of 50 l.

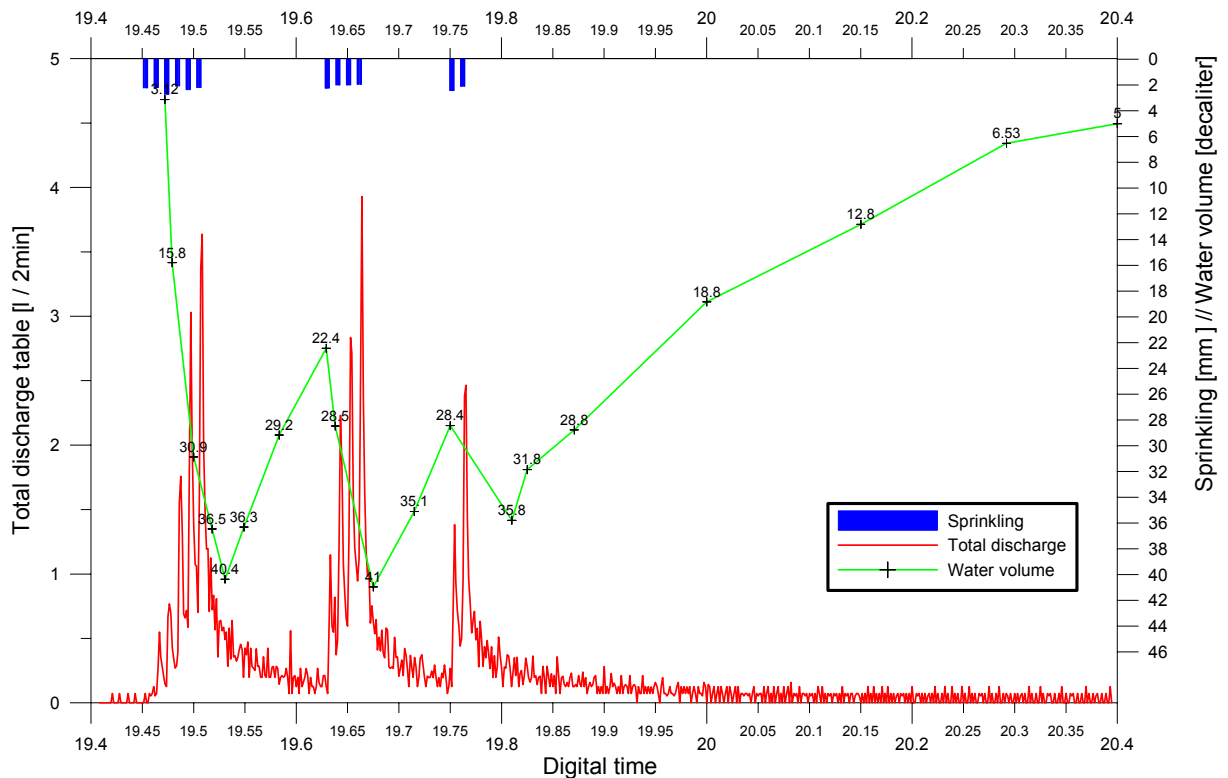


Fig. 6.6b: Sprinkling, runoff and water volume for the first interval of the experiments.

The time shift between precipitation and peak of water volume (refer section 4.5) was calculated to 74, 42, and 76 min (in chronological order).

### Discussion of water table and water volume

The symmetry of the water table movement is relevant for an assessment of the soil filling. The shown data with a left dominated table recession is contrary to the runoff distribution at the TBs. No explanation was found for this pattern. A remark highlights the assumptions of the interpolation method, which blur the pattern. Finally it is concluded that once again the properties of the artificial filling trigger this pattern and are a major factor.

For the discussion of water balance calculation (section 6.4) additional data can be included. A comparison of the gap in the measured water balance (25.2 l) and the estimated water volume in the system (50 l) provides somehow an explanation. Bridging the gap in the balance is not possible with the inexactness contained by the interpolation method. However, the results showed that the estimated numbers fit roughly.

## 6.7 Tracer

For the interpretation of the Amino G Acid line source application and the Brilliant Blue line source the amount of sprinkling upslope the line was of major interest, rather than the total

amount of sprinkling for the table. This input resulted in lateral flow which was able to mobilize the tracer, plus of course the little amount of sprinkling which fell directly on the line. The line source of Amino G Acid was set at  $y = 285$  cm and Brilliant Blue FF was set at  $y = 290$  cm. The distribution of sprinkling was already shown in Fig. 3.2.5b and pointed out the decrease of precipitation in this area. A calculation based on an interpolated Kriging approach got an integrated total sprinkling amount above  $y = 280$  cm of 7.7 mm/hr. This is valid until digital time 21.3722, when a nozzle modification extended the area of intense sprinkling by about 15 cm towards upslope. The increased sprinkling input above the line source, which was able to carry the dye, was then interpolated to 13 mm/hr.

Generally tracer mobilisation is controlled by the non steady state conditions. For the 5-minutes sprinkling events no overlapping of flow paths due to occurring HORTONIAN overland flow was assumed.

### 6.7.1 Amino G Acid line source

For the entire experimental run the line source remained in an unsaturated environment; this was shown in section 6.6.

#### Results

The results of the Amino G line source experiment need special treatment as they are not clear and are hard to interpret. In order to clarify the pattern, Amino G concentrations below 20 ppb were treated as high background concentrations (MCGUIRE, personal communications; SMART & LAIDLAW, 1977). This data of no tracer breakthrough record is caused by high dissolved organic carbon (DOC) concentrations.

Sampling at the mini piezometers in the middle of the table did not result in any positive tracer record! Values here ranged within the background level.

A detailed view of the results of the tracer breakthrough at the final TBs is described now. As the corresponding runoff differed strongly (s. above) tracer breakthrough also varied between the individual TBs. The first one described is TB 8, which is singled out because of its major portion within total discharge. Tracer concentrations showed a very unusual pattern which is not comparable with a typical tracer breakthrough curve. Despite background concentration a clear tracer breakthrough is not detectable in Fig. 6.7.1a.

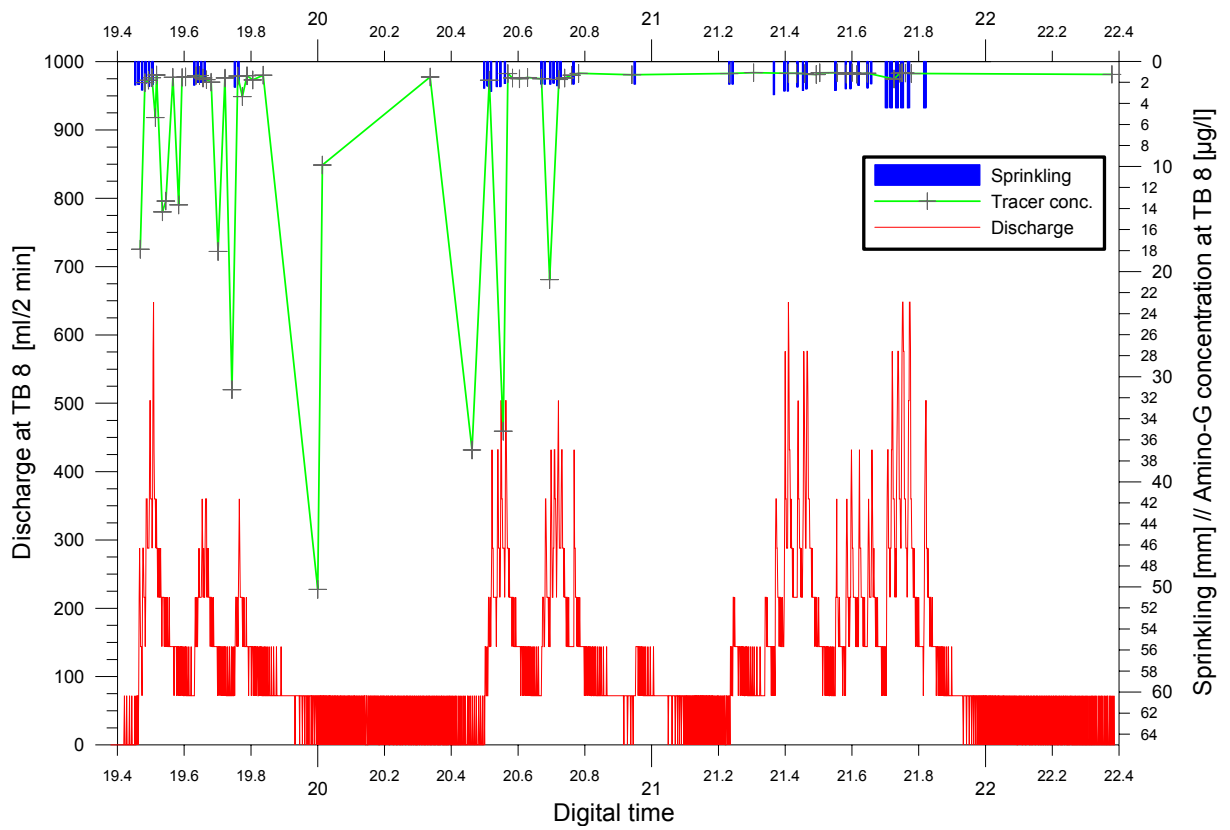


Fig. 6.7.1a: Amino G concentration and discharge at TB 8.

Fig 6.7.1b is a different presentation of the same data including accumulated discharge (Fig. 6.7.1b). A third version includes a flow-proportional illustration of the same data (Fig. 6.7.1c). The fact of high variations on Amino G concentrations is still obvious and this presents a difficult situation for the interpretation of the data.

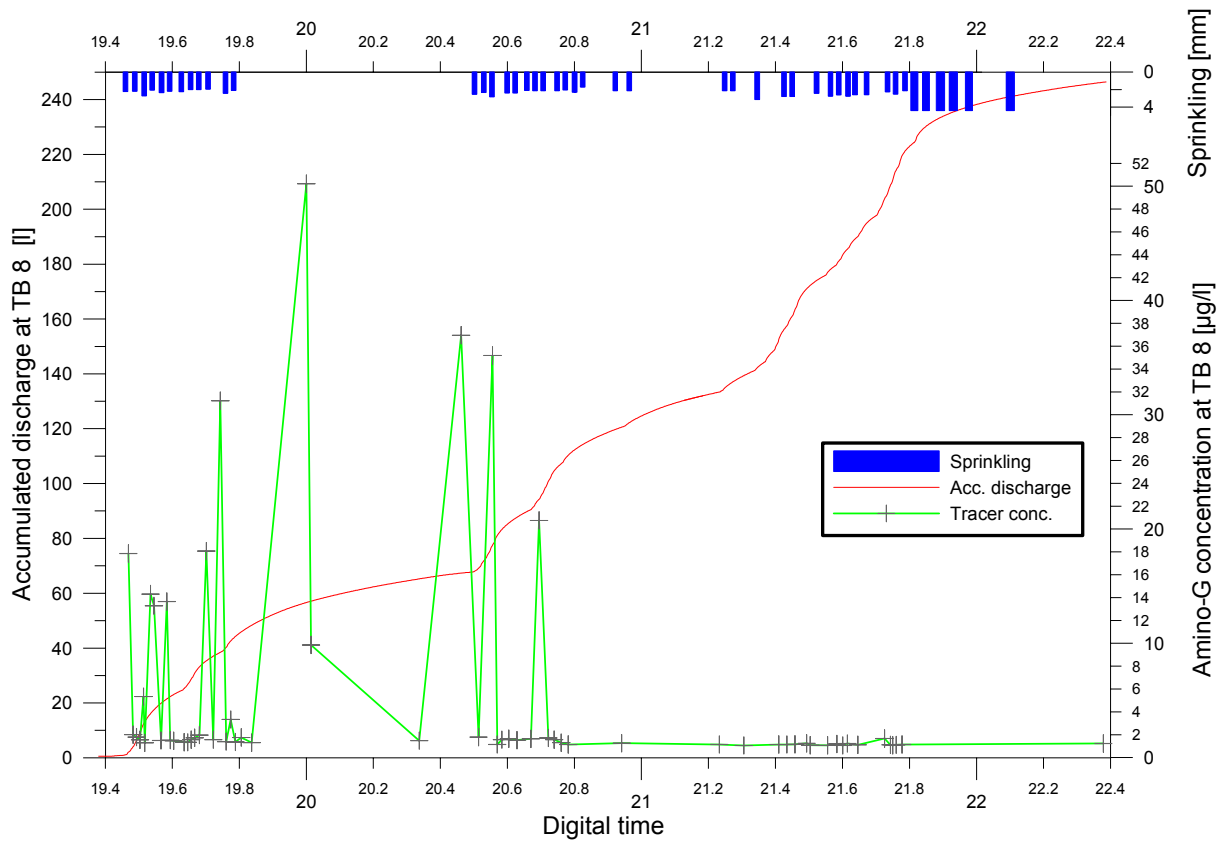


Fig. 6.7.1b: Amino G concentration, accumulated discharge and sprinkling for TB 8.

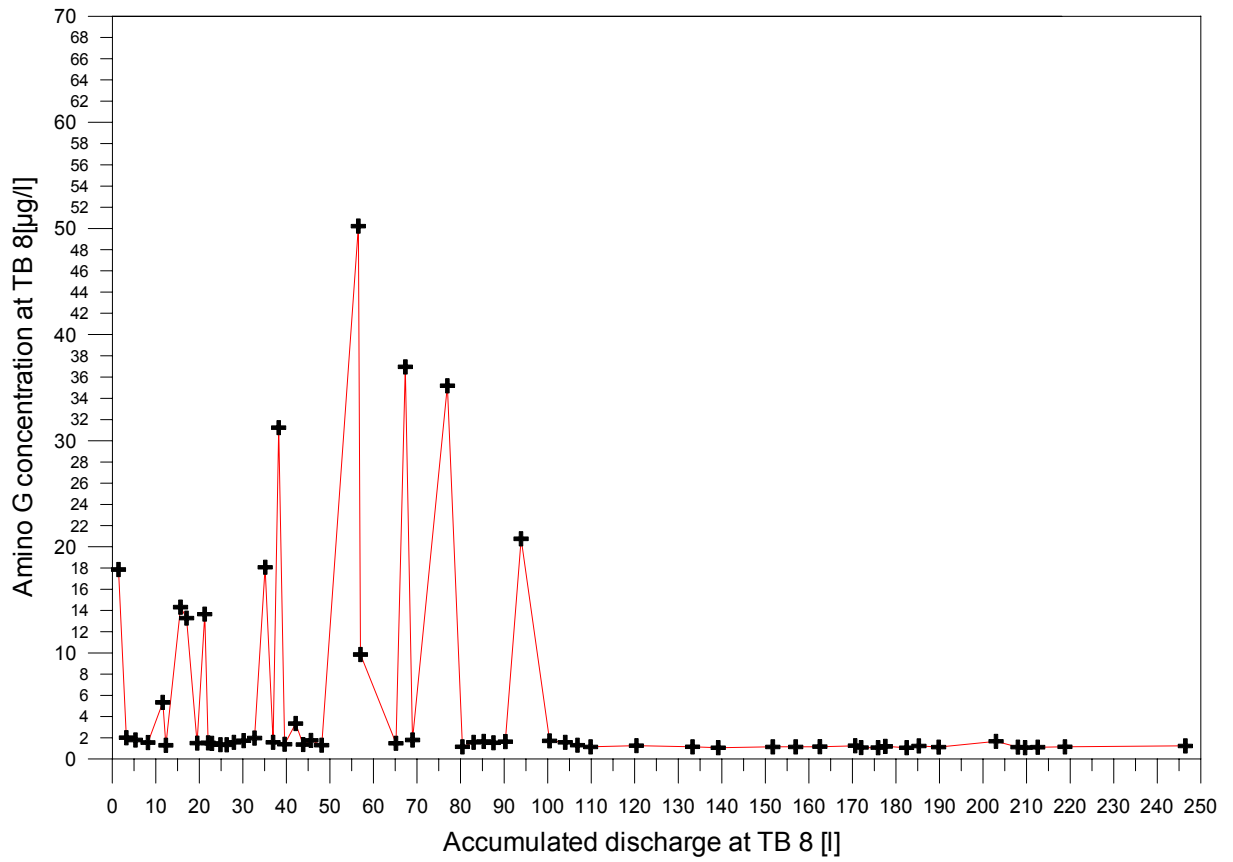


Fig. 6.7.1c: Accumulated discharge and Amino G concentration at TB 8.

So far, data presentation is of TB 8, where most of the discharge occurred. The results of the other TBs showed the same unclear pattern, and do not contain any significant information on tracer breakthrough either (Fig. B1- B7).

### **Recovery rate**

The calculation of a recovery rate is difficult to obtain as concentrations of point measurements did not show a typical breakthrough. Thus there was no way of interpolating a continuous graph which allowed the calculation of a tracer recovery rate.

## **6.7.2 Discussion of Amino G Acid line source**

Generally, these findings of minor, almost random peaks at the TBs instead of no or either a proper tracer breakthrough are suspicious, not satisfactory and thus open for discussion. Although the observed pulse of tracer fits with the idea of a water push caused by the sprinkling intervals and a final remobilisation of the remaining tracer. Thus the pulses could also be governed by the flow and its longitudinal dispersion. By the way a common result in unsaturated zone tracer experiments (SCHUDEL et al., 2003).

But the combination of these results at the outflow plus the samples of the mini piezometers support the theory of no tracer breakthrough during the run of experiment. Amino G Acid remained in the soil close below the line application. This trapping of tracer was caused by the minor hydrological conductivity of the soil.

A further possible error, photo decomposition of Amino G Acid is to be neglected, as the exposure to sunlight was zero during the subsurface flow in the table and very little towards the sampling. The samples themselves were stored in the dark until the determination.

## **6.7.3 Bromide**

### **General, preliminary remarks**

The system investigated by the extensive bromide applications contains two domains, the vertical flow through the soil and the lateral flow towards the tipping buckets. Viewing the upper and lower area of the slope with regard to section 6.6 both processes are a combination of saturated and unsaturated conditions.

In agreement with the Amino G acid analyses selected data of TB 1 + 8 are presented.

### **Results**

The surveillance on bromide was performed by a continuous monitoring of EC and discontinuous, flow proportional hand samples. The link between, and its regressions are presented in Fig. B8 + B10. However they show weak significances ( $R^2 = 0.12$  and  $R^2 = 0.49$ ). As the deviation between the series is also visible, the regression between EC and bromide concentrations was calculated again just for the first day. This increased confidences for TB 1 to  $R^2 = 0.73$  (Fig. B9). Concluding the data basis at TB 1 for the first day might be best, as

hand samples and EC-data fit best, whereas for TB 8 both series do not fit together well (see Fig. B11). Therefore, the analysis of breakthrough integrated selected data of TB 1. Further as series was restricted to the non-continuous hand samples, why it was refrained from calculating recovery.

Bromide breakthrough at the outflow of TB 1, relying on the samples, is characterised by a major peak at around digital time 19.503 with a few spiky peaks afterwards (Fig. 6.7.3a). This was also obtained by the continuous electrical conductivity, where the first, major breakthrough took place in accompany with the hand samples. However, peaks of electrical conductivity followed sprinkling events. The discrepancy increases towards the end, in particular from time 21.6 on, when sampling concentrations went to zero and sprinkling response still caused higher conductivities.

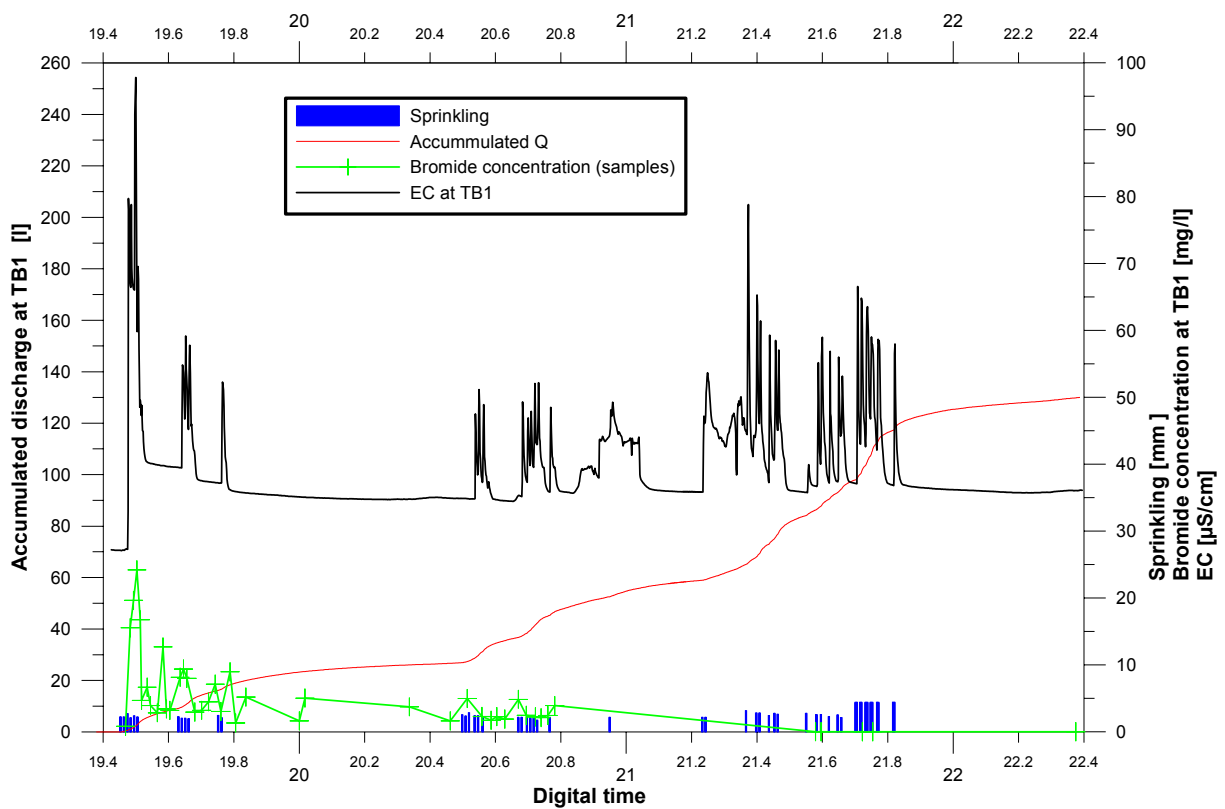


**Fig. 6.7.3a:** Bromide concentrations, electrical conductivity, sprinkling intervals and accumulated discharge at TB 1.

#### 6.7.4 Discussion of bromide

The presented tracer data of EC and samples at TB 1 includes both, reliable data and data where interpretation might be difficult. The first tracer breakthrough occurred when the dry table system got saturated. As the first sprinkling intervals avoided surface runoff, runoff at the TBs represents exclusively 'interflow' of the table. Further tracer peaks following indicate the remobilisation of water. This is particularly obvious at the time 20.4 past overnight drainage.

Interpretation of the peaks in EC after time 21 as well as in general should take the likely change in EC of the sprinkling water into account. The water came from the public water supply and was not monitored for the total period, but rare single data showed no significant change of EC.

Important to remark is the fact that bromide is treated as a conservative tracer. For these experiments no sorption processes are assumed. Further interpretations on this tracer input might be possible using different modelling approaches (e.g. MALOSCZEWSKI & ZUBER, 1996).

### 6.7.5 Dye tracing with Brilliant Blue

The additional information on the tracer movement from a dye tracing experiment was very helpful. The line source of Brilliant Blue FF was set at  $y = 290$  cm at the digital time 20.4. In the following sixteen of the 5-minute sprinkle events (sum of 10.2 mm above line) were applied. As so far no breakthrough occurred the area of sprinkling was extended (mentioned above). After another three 5-minute intervals the first tracer breakthrough at the mini piezometers occurred at P\_C3 which is at  $y = 240$  cm. This happened at digital time 21.42 almost 24 hours past the injection and what triggered it off was probably the extended spray area with higher input rates above the line source.

During the ongoing experiments no other mini piezometer (neither P\_C4 nor row B at  $y = 160$  cm) nor any tipping bucket recorded dye. Even the last more intense 10-minute sprinkling intervals did not result in any new dye occurrence. But still the colour of P\_C3 remained throughout indicating active flow paths from the line downwards.

The final excavation found dye along intersects from the injection down to  $y = 190$  cm, where only a tiny trace of indication was found. For photographic capture of the dye tracer and the soil Fig. 6.7.5b+c also provides colour scale (JOB0 lab equipment). The pictures show the decline in intensity towards  $y = 265$  cm. An overall mapping of the distance covered by the dye is shown in Fig. 6.7.5a. The maximum distance the dye travelled within preferential pathways was therefore 1 m.

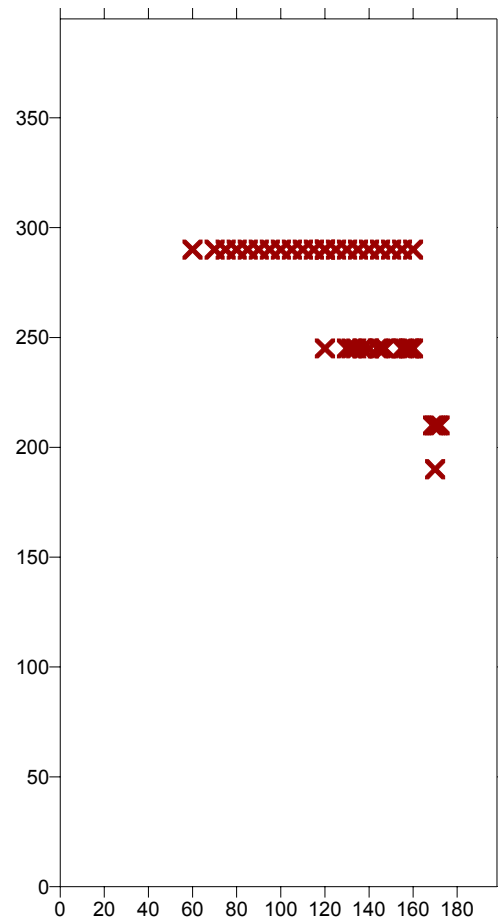


**Fig. 6.7.5a:** Line source of Magic blue at  $y=290$  cm and dye movement down slope. Illustrated are selected slices of soil profiles from excavation. Note the fading of dye tracer.



**Fig. 6.7.5b:** Documentation of Brilliant Blue pathways at  $y=265$  cm. The colour scale is made by JOBO lab equipment.



**Fig. 6.7.5c:** Documentation of Brilliant Blue pathways directly at the line application ( $y=290$  cm).

### **6.7.6 Discussion of dye tracing with Brilliant Blue**

In the interpretation of the very limited movement of the Brilliant Blue, two major factors may be emphasized. First, the amount of water input above the line was too little to initiate pronounced flow through the line source. Second, the low rate of little absorption of Brilliant Blue caused the dye also to bond to the soil matrix. Both factors caused the tracer to remain in the soil.

## **6.8 Conclusions of hillslope table**

The data of the sprinkling experiment on the table provided basic experience on the dealing with the physical modelling approach. Runoff irregularity within the array of TBs and the uneven water table decline during recession periods are no doubt indicators of non natural soil conditions. However they raise the question about the confidence of the experiments and the significance of the results of this artificial hillslope table. But still, the results provide doubtless information on the general pattern of runoff generation.

The experiments conducted represent conditions with a return period of about 100 years at the Low Pass site, based on the applied rainfall intensity (on 1 hour duration). Thus results available are linked to rare conditions of heavy rainfall, where the significance of preferential flow is much higher than during the more common low-intensity conditions. The observed processes at the hillslope table show similarities to the findings at the field site. In particular the line source tracer experiments showed no successful tracer breakthrough either. Reasons for the fail of the line source applications at the table are discussed with the less precipitation input falling above the lines. Additionally saturated conditions in the soil occurred at least 1.5 metre down slope, a further considerable reason for the limited movement.

## **6.9 Prospects for further experiments**

The limited tracer transport in the soil raised the question about the effect of soil pipes. This might be appropriate as conditions as well investigated by the experiments above. To follow up the idea on subsurface flowpaths the next step is the implementation of artificial soil pipes. Using cable tubing material which is bandaged with gauze, some artificial soil pipes were already prepared. The prospect would be an implementation of 100 artificial preferential pathways with a length of 20 cm in the soil of the table. A grid distribution (10 by 10) of installed soil pipes in the soil might be achieved. The horizontal alignment supposed to be parallel to table's bottom and the angle of installation should randomly differ between  $-90$  and  $+90^\circ$  (where zero indicates the normal down slope direction).

The hypothesis to be tested in the near future here would be whether the observed hydrograph shows a flash-type of runoff response, as described in my modelling experiments (WEILER, 2001). A further open question would be: What kinds of influence have soil pipes on the movement of tracer?

## 7 Concluding remarks and outlook

Previous chapters of this thesis presented the two main approaches focusing on the detection of subsurface flow mechanisms. Obtained data was separately shown in detail for the field site and the artificial hillslope. In the following the two distinct approaches are merged in order to get an overall view of the gained knowledge.

To obtain insight in the connection of flow paths at the Low pass field site various instrumentations provided data of water table (which may be called ground water levels) and pipe flow. Furthermore tracer experiments were applied. For statistical analysis on antecedent rainfall and runoff response of the system, the total number of events was often too small, which did not allow more detailed information. However, observations showed a fast response of pipe flow to rainfall events. This does indicate the dominance of preferential flow with lateral flow represented by macropore structures and transversal flow represented by soil pipes. Observations of water levels in the hillslope showed a temporal rise during rainfall events with maximum levels up to 80-100 cm below surface topography. Including event based variation as well as the seasonal variation, water table levels are seen as an important key to understand the pattern of pipe flow. From our point of view the drainage area of soil pipes changes by the variation of water table levels. This interpretation is supported by the conditions at the end of the investigation period during summer drought, when low water table levels restricted the drainage area and thus no pipe flow occurred. An estimation of the soil pipes drainage area was calculated by means of the dynamic contributing area (DCA), which ranged even bigger than 9500 m<sup>2</sup>. Further, the study showed that wetness of the trench face does not represent highly oscillating water tables respectively high moisture content in hillslope behind.

For the extensive and line-source tracer experiments results showed that tracer 'stranded' in the unsaturated zone. Probably none of the tracers reached the saturated zone. This hypothesis was also corroborated by no evidence for break through at the pipes outlet or at the first order stream (weir). It appears that the unsaturated conditions in the sandy loam limit the transport. These conditions were particularly dominant during the investigation period, because of abnormally little antecedent precipitation during winter term and little rainfall during the investigations itself. Further reasons for the unsuccessful outcome include little tracer input mass and in particular the unexpected dilution in the system! Concerning the objective of the connection of lateral and transversal pathways, tracer results did not bring up evaluable data.

Corresponding to field site similar experiments were performed at an experimental hillslope table. This physical modelling allowed the same tracer experiments as in the field under

triggered conditions. The data obtained got also insight in the problems arising with artificial soil filling (e.g. non uniform distribution of discharge along the width of outflow). Nevertheless, sprinkling experiments showed that runoff is quickly responding. Also water tables were established and backed up from the outlet towards upslope. The extensive bromide spraying generated tracer peaks following sprinkling intervals. This indicates the remobilisation of water. Tracer of the line source application (Amino G Acid) also stranded in the unsaturated zone in the upper slope of the experimental table, where sprinkling input was restricted. The excavation of the line application of Brilliant Blue showed a very limited movement of dye. Although for this tracer sorption processes are relevant. Generally, the experience made by this experimental study will be the base for further physical modelling including artificial soil pipes. Then, different drainage mechanisms of the table will be involved and finally another prominence of soil pipes might be investigated.

Closing, the combination of field site and experimental hillslope table - with both similar findings - helped to gain knowledge on subsurface flow paths at Low Pass field site. Despite the findings of this study various gaps in comprehension of the precesses are remaining. This is e.g. the initially mentioned question about the topographic convergence affecting subsurface flow and furthermore the impact of soil pipes at the experimental hillslope. Generally, field monitoring of natural pipeflow and artificial experiments provided information on the better understanding of hillslope drainage processes in relation to the relevance of subsurface flow. To provide a further outlook: The findings of this thesis may be included in the upcoming era of mathematical pipeflow modelling. Here, recent progress is driven by an attempt using a partially distributed physically based simulation algorithm (JONES & CONNELLY, 2002). Another outlook from a different point of view are concepts including the dynamically linkage of rapid vertical fluxes at the profile scale with their lateral counterparts in hillslopes may eventually replace soil hydrological approaches based on potential equilibrium and water saturation (GERMAN & WEINGARTNER, 2002). Finally, the improved 3D segmentation and representation of pore network extraction and hydrodynamic characterization will also help to model pipe flow and macropore processes in a more detailed way (DELERUE, 2001; WEILER et al., 2003).

## 8 References

- AG BODEN (1996<sup>4</sup>): Bodenkundliche Kartieranleitung. Nachdr., Hrsg. Bundesanstalt für Geowissenschaften und Rohstoffe und den Geologischen Landesämtern in der Bundesrepublik Deutschland, Hannover.
- AGRIMET (2003): Online Weather Data Corvallis. Website. URL: [http://www.ocs.orst.edu/crvo\\_dly.html](http://www.ocs.orst.edu/crvo_dly.html), 2003-07-11.
- ANDERSON, S.P., W.A. DIETRICH, D.R. MONTGOMERY, R. TORRES, M.E. CONRAD & K. LOAGUE (1997): Subsurface flow paths in a steep, unchanneled catchment. *Water Resources Research*, 33(12), 2637 – 2653.
- ANDERSON, M.G. & T.P. BURT (1990): Process Studies in Hillslope Hydrology. John Wiley & Sons Ltd. Chichester.
- BALDWIN, E.M. (1974): Eocene stratigraphy of southwestern Oregon. *Bull. Oreg. Dep. Geol. Miner. Ind.*, 83, 1-38.
- BEHRENS, H. (1986): Water tracer chemistry: A factor determining performance and analytics of tracers. 5<sup>th</sup> International Symposium on Underground Water Tracing: 121-133.
- BEIER, G.C. & K. HANSEN (1992): Evaluation of porous cup soil-water samplers under controlled field conditions: comparison of ceramic and PTFE cups. *J. of Soil Science*, 43: 261-271.
- BERGMANN, H., J. FRANK, T. HARUM, W. PAPESCH, D. RANK, G. RICHTIG & H. ZOJER (1996): Abflußkomponenten und Speichereigenschaften, Konzeptionen und Auswertemethoden. *Österreichische Wasser- und Abfallwirtschaft*. 48 (1/2): 27-45.
- BEVEN, K.J. & P. GERMANN (1982): Macropores and water flow in soils. *Water Resources Research*, 18 (5): 1311-1325.
- BONELL, M. (1993): Progress in the understanding of runoff generation dynamics in forest. *J. of Hydrology*, 150: 217-275.
- BOUMA, A.J., O. BOERSMA, A. JAGER & D. SCHOONDERBREEK (1977): The function of different types of macropores during saturated flow through four swelling soil horizons. Soil Science Society of America. *Journal*, 41: 945-950.
- BOWER, H. & R.C. RICE (1980): A Slug Test for Determining the Hydraulic Properties of Tight Formations. *Water Resources Research*, Vol. 16 (1): 233-238.
- BRONSTERT, A. (1999): Capabilities and limitations of detailed hillslope hydrology. *Hydrological Processes*, 13: 21-48.
- BURROUGH, P.A. & R.A. MCDONNELL (1998): Principles of Geographical Information Systems. Oxford University Press, New York.

- CHEN & WAGNER (1992): Simulation of water and chemicals in macropore soils. Part 1: representation of the equivalent macropore influence and its effect on soil water flow. *J. of Hydrology*, 130: 105-126.
- CHOQUETTE, P.W. & L.C. PRAY (1970): Geologic nomenclature and classification porosity in sedimentary carbonates. The American Association of Petroleum Geologists Bulletin, 54: 207-250.
- CROZIER, M.J., U. HARDENBICKER & A. POTT (2003): The influence of rainfall and soil hydrology on pipeflow in steep pasture-covered hill country. Geophysical Research Abstracts, Vol. 5, 07736. European Geophysical Society.
- DECAGON (2003): Soil moisture monitoring. Website. URL: <http://www.ech2o.com/probes.html>, 2003-07-11.
- DELERUE, J.F. (2001): Segmentation 3D, application à l'extraction de réseaux des pores et à la caractérisation hydrodynamique des sols. These. Université Paris XI Orsay.
- DINGMAN, S.L. (2002<sup>2</sup>): Physical Hydrology. Prentice-Hall. New Jersey.
- DYCK, S. & G. PESCHKE (1995): Grundlagen der Hydrologie. Verlag für Bauwesen, Berlin.
- EGGELSMANN, R. (1981<sup>2</sup>): Dränanleitung. Verlag Paul Parey. Hamburg.
- ELIAS, T.S. (1980): The complete trees of North America: Field guide and natural history. Van Nostrand. New York.
- FEYEN, H., H. WUNDERLI, H. WYDLER & A. PAPRITZ (1999): A tracer experiment to study flow paths of water in a forest soil. *J. of Hydrology*, 225: 155-167.
- FLURY, M. & H. FLÜHLER (1995): Tracer characteristics of Brilliant Blue FCF. *Soil Science of America Journal*, 59: 22-27.
- FLURY, M. & A. PAPRITZ (1993): Bromide in the natural environment: Occurrence and toxicity. *J. Environ. Qual.*, 22: 747-758.
- GERMÁN-HEINS, J. & M. FLURY (2000): Sorption of Brilliant Blue FCF in soils affected by pH and ionic strength. *Geoderma*, 97: 87-101.
- GERMAN, P. & R. WEINGARTNER (2002): Preferential Flow – the hydrological link between soil and catchment. *Hydrologie und Wasserbewirtschaftung* : 282-284.
- GLASS, R.J. & M.J. NICHOL (1996): Physics of gravity fingering of immiscible fluids with porous media: An overview of current understanding and selected complicating factors. *Geoderma*, 70: 133-163.
- GOARD, D.L. (in preparation): Characterizing the spatial distribution of short duration, high intensity precipitation in the central Oregon Coast Range. Thesis at Oregon State University, Corvallis, Oregon.
- GUTKNECHT, D. (1996): Abflußentstehung an Hängen – Beobachtungen und Konzeptionen. *Österreichische Wasser- und Abfallwirtschaft*. 48 (5/6): 134-144.

- HATFIELD MARINE SCIENCE CENTRE (2003): Weather data summaries Guin Library Weather Station. Website. URL: <http://hmsc.oregonstate.edu/weather/summaries/guinlib/2003/may2003.html>, 2003-07-11.
- HERSCHY, R.W. (1978): *Hydrometry, Principles and Practices*. Wiley and Sons, Chichester.
- HILLEL, D. (1987): Unstable flow in layered soils: A review. *Hydrological Processes*, 1: 143-147.
- HOLDEN, J., T.P. BURT & M. VILAS (2002): Application of ground-penetrating radar to the identification of subsurface piping in blanked peat. *Earth Surf. Process. Landforms*, 27: 235–249.
- HORNBERGER, G.M. & E. W. BOYER (1995): Recent advances in watershed modelling. U.S. Natl. Rep. Int. Union Geol. Geophys. 1991-1994, *Rev. Geophys.*, 33, 949-957.
- HURSH, C.R. (1936): Storm-water and adsorption. *Eos Trans. AGU*, 17, 301-302.
- HVORSLEV, T. (1951): Time Lag and Soil Permeability in Ground Water Observations. Bulletin No. 36, U.S. Army Corps of Engineers: 50-75.
- INW (2003): INSTRUMENTATION NORTHWEST. Water monitoring. Website. URL: <http://www.inwusa.com>, 2003-07-11.
- ISTOK, J.D.L. & L. BOERSMA (1986): Effect of Antecedent Rainfall on Runoff during low-intensity Rainfall. *J. of Hydrology*, 88: 329-342.
- JOERIN, C., A. MUSY & D. TALAMBA (2002): Study of hydrological processes for better models and flood estimations. Proceedings International Conference on Flood Estimation, CHR report: 123-132.
- JONES, J.A.A. (1997): Pipeflow contributing areas and runoff response. *Hydrological Processes*, 11: 34-41.
- JONES, J.A.A. (1971): Soil piping and stream channel initiation. *Water Resources Research*, 7, 602-610.
- JONES, J.A.A. & L.J. CONNELLY (2002): A semi-distributed model for natural pipeflow. *J. of Hydrology*, 262: 28-49.
- JONES, J.A.A. & F.G. CRANE (1984): Pipeflow and pipe erosion in the Maesnant experimental catchment. In: *Catchment Experiments in Fluvial Geomorphology*, ed. T.P. Burt and D.E. Walling, 55-85. Exeter: Geo Books.
- JONES, D. R. & R.F. JUNG (1990): Analytical problems arising from the use of bromide and Rhodamine WT as co-tracers in streams. *Water Resources*, 24: 125-128.
- KITAHARA, H. (1994): A study on the characteristics of soil pipes influencing water movement in forested slopes, *Bulletin of the Forestry and Forest Products Research Institute*, 367: 63–115 (in Japanese with English summary).
- KLEMEŠ, V. (1986): Dilettantism in Hydrology: Transition or Destiny? *Water Resources Research*, 22(9): 177S-188S.

- LANGE, H., G. LISCHIED, R. HOCH & M. HAUHS (1996): Water flowpaths and residence times in a small headwater catchment at Gårdsjön (Sweden) during steady state stormflow conditions. *Water Resources Research*, 32: 1689-1698.
- LEIBUNDGUT, CH. (1984): Zur Erfassung hydrologischer Messwerte und deren Übertragung auf Einzugsgebiete verschiedener Dimensionen. Veröffentlichung des 9. Basler Geomethodischen Colloquiums. *Geomethodica*, 9: 141-170.
- LEIBUNDGUT, CH. & H.R. WERNLI (1984): Zur Frage der Einspeisemengenberechnung für Fluoreszenztracer. In: Beitr. zur Geologie der Schweiz – Hydrologie. Bd. 28. Bern: 119-130.
- LITAOR, M.I. (1988): Review of soil solution samplers. *Water Resources Research*, 24(5): 727-733.
- LOY, W.G. (Ed.) (2001<sup>2</sup>): Atlas of Oregon. University of Oregon. Eugene.
- LUCE, C.H. (2002): Hydrological processes and pathways affected by forest roads: what do we still need to learn? *Hydrological Processes*, 16: 2901-2904.
- LUXMOORE, R.J. (1981): Micro-, meso-, and macroporosity of soil. *Soil Sci. Soc. Am. J.*, 45: 671-672.
- LUXMOORE, R.J., P.M. JARDINE, G.V. WILSON, J.R. JONES & L.W. ZELANZNY (1990): Physical and Chemical Controls of Preferred Path Flow through a Forested Hillslope. *Geoderma*, 46: 139-154.
- MAGID, J., N. CHRISTENSEN & H. NIELSEN (1992): Measuring phosphorous fluxes through the root zone of a layered sandy soil. Comparisons between lysimeter and suction solution. *J. Soil Sci.*, 43: 739-747.
- MALOSZEWSKI, P. & A. ZUBER (1996): Lumped parameter models for the interpretation of environmental tracer data. Manual on Mathematical Models in Isotope Hydrology, IAEA-TECDOC-910, 9-58, IAEA, Wien.
- MANIAK, U. (1997<sup>4</sup>): Hydrologie und Wasserwirtschaft – eine Einführung für Ingenieure. Springer Verlag. Berlin.
- MCDONNELL, J.J. (1990): A rationale for old water discharge through macropores in a steep, humid catchment. *Water Resources Research*, 26: 2821-2832.
- MCDONNELL, J.J., D.D. BRAMMER, C. KENDALL, N. HJERDT, L.K. ROWE, M. STEWARD & R.A. WOODS (1998): Flow paths on steep forested hillslopes: The tracer, tensiometer, and trough approach. In: TANI (Ed.): Environmental Forest Science. Kluwer Academic Publishing, Boston: 463-472.
- MCGLYNN, B.L., J.J. MCDONNELL, D.D. BRAMMER (2002): A review of the evolving perceptual model of hillslope flowpaths at the Maimai catchments, New Zealand. *J. of Hydrology*, 257: 1-26.
- MCINTOSH, J., J. MCDONNELL & N.E. PETERS (1999): Tracer and hydrometric study of preferential flow in large undisturbed soil cores from the Georgia Piedmont, USA. *Hydrological Processes*, 13: 139-155.
- MCLAREN, R.G. & K.C. CAMERON (1994): Soil Science: An introduction to the properties and management of NZ soils. Oxford University Press.

- MIKOVARI, A., C. PETER & CH. LEIBUNDGUT (1995): Investigation of preferential flow using tracer techniques. In: LEIBUNDGUT, CH. (1995): Tracer technologies for hydrological systems. IAHS Publication No. 229, Proceedings of a Boulder Symposium, Wallingford.
- NYBERG, L., A. RODHE & K. BISHOP (1999): Water transit times and flow from two line injections of  $^3\text{H}$  and  $^{36}\text{Cl}$  in a microcatchment at Gårdsjön, Sweden. *Hydrological Processes*, 13: 1557-1575.
- MOSLEY, M.P. (1979): Subsurface flow velocities through selected forest soils, south island, New Zealand. *J. of Hydrology*, 55: 65-92.
- OREGON CLIMATE SERVICE (2003): Weather data summaries Eugene. Website. URL: <http://www.ocs.orst.edu/pub ftp/weather/eugene/eug0503.txt>, 2003-07-11.
- OLIVIERA, I.B., A.H. DEMOND & A. SALEHZADEH (1996): Packing of Sands for the Production of Homogeneous Porous Media. *Soil Sci. Soc. Am. J.*, 60 (1): 49-53.
- ONODERA, S. & M. KOBAYASHI (1995): Evaluation of seasonal variation in bypass flow and matrix flow in a forested soil layer. In: LEIBUNDGUT, CH. (Ed.): Tracer technologies for hydrological systems. IAHS Publication No. 229, Proceedings of a Boulder Symposium, Wallingford.
- PARIZEK, R.R. & B.E. LANE (1970): Soil water sampling using pan and deep pressure vacuum lysimeters. *J. of Hydrology*, 11: 1-21.
- PATCHING, W. R. (1987): Soil survey of Lane County Area, Oregon. United States Department of Agriculture, Soil Conservation Service report. Website. URL: [http://www.or.nrcs.usda.gov/pnw\\_soil/oregon/or601.html](http://www.or.nrcs.usda.gov/pnw_soil/oregon/or601.html), 2003-07-11.
- PHILIP, J.R. (1993): Constant-Rainfall Infiltration on Hillslopes and Slope Crests. In: RUSSO, D. & G. DAGAN (Ed.): Water Flow and Solute Transport in Soils. Springer-Verlag, Berlin.
- ROTHACHER, J. (1963): Net Precipitation under a Douglas-Fir Forest. *Forest Science*, 9 (4): 434-429.
- RÖSSERT, R. (1981<sup>5</sup>): Hydraulik im Wasserbau. Oldenbourg Verlag. München.
- SCHRÖDER, R. (1994): Technische Hydraulik, Kompendium für den Wasserbau. Springer Verlag, Berlin.
- SCHUDEL ET AL (2003): Einsatz künstlicher Tracer in der Hydrogeologie – Praxishilfe. Berichte des BWG, Serie Geologie Nr. 3, Bundesamt für Wasser und Geologie.
- SKLASH, M.G., K.J. BEVEN, K. GILMAN & W.C. DARLING (1996): Isotope studies of pipeflow at Plynlimon, Wales. *Hydrological Processes*, 10: 921-944.
- SMART, P.L. & I.M. LAIDLAW (1977): An evaluation of some fluorescent dyes for water tracing. *Water Resources Research*, 13(1): 15-33.
- STAUFFER, F. & T. DRACOS (1986): Experimental and numerical study of water and solute infiltration in layered porous media. *J. of Hydrology*, 84, 9-34.
- STEPHENS, D. B. (1996): Vadose zone hydrology. CRC Press, Lewis Publishers, Boca Raton.

- STRESKY, S.J. (1991): Morphology and Flow Characteristics of Pipes in a Forested New England Hillslope. Durham, NH: Thesis, M.Sc. in Hydrology, University of New Hampshire.
- TERAJIMA, T., T. SAKAMOTO & T. SHIRAI (2000): Morphology, structure and flow phases in soil pipes developing in forested hillslopes underlain by a Quaternary sand-gravel formation, Hokkaido, northern main island in Japan. *Hydrological Processes*, 14: 713-726.
- THOMAS, G.W. & R.E. PHILLIPS (1979): Consequences of water movement in macropores. *J. Environ. Qual.*, 8, 149.
- TORRES, R., W.A. DIETRICH, D.R. MONTGOMERY, S.P. ANDERSON & K. LOAGUE (1998): Unsaturated zone processes and the hydrologic response of a steep, unchanneled catchment. *Water Resources Research*, 34(8): 1865-1879.
- TRUDGILL, S. T. (1987): Soil water dye tracing, with special reference to the use of Rhodamine WT, Lissamine FF and Amino G Acid. *Hydrological Processes*, 1: 149-170.
- TRUTRACK (2003): Manufactures of Data Loggers and Weather Stations. Website. URL: <http://www.trutrack.com/wt-hr.html>, 2003-07-11.
- TSUBOYAMA, Y., R.C. SIDLE, S. NOGUCHI & I. HOSODA (1994): Flow and solute transport through the soil matrix and macropores of a hillslope segment, *Water Resources Research*, 30(4), 879-890.
- TSUKAMOTO, Y., T. OHTA & H. NOGUCHI (1982): Hydrological and geomorphological studies of debris slides on forested hillslopes in Japan. In: Recent Developments in the Explanation and Prediction of Erosion and Sediment Yield (Proceedings of the Exeter Symposium, July 1982). IAHS Publ. no. 182: 89-98.
- TURDON, D.J., C.T. HAAN & E.L. MILLER (1992): Subsurface flow responses of a small forested catchment in the Ouachita Mountains. *Hydrological Processes*, 6: 111-125.
- UCHIDA, T., K.I. KOSUGI & T. MIZUYAMA (2002): Effects of pipe flow and bedrock groundwater on runoff generation in a steep headwater catchment in Ashiu, central Japan. *Water Resources Research*, 38(7): 24.1-24.14.
- UCHIDA, T., K. KOSUGI & T. MIZUYAMA (1999): Runoff characteristics of pipeflow and effects of pipeflow on rainfall-runoff phenomena in a mountainous watershed. *J. of Hydrology*, 222: 18-36.
- UHLENBROOK, S. (1999): Untersuchungen und Modellierung der Abflussbildung in einem mesoskaligen Einzugsgebiet. Freiburger Schriften zur Hydrologie, Band 10, Inst. für Hydrologie Universität Freiburg i. Br., Freiburg i. Br.
- UHLENBROOK S. & CH. LEIBUNDGUT (1997): Abflussbildung bei Hochwasser. *Wasser und Boden*, 9: 13-22.
- UNITED STATES DEP. OF AGRICULTURE (2003): Natural resources conservation service. Webpage. URL: [http://soils.usda.gov/survey/online\\_surveys/](http://soils.usda.gov/survey/online_surveys/) , 2003-07-11.
- WALKER, G.W. & N.S. MACLEOD (1991): Geologic map of Oregon. U. S. Geological Survey, scale 1:500000. 2 sheets.

- WALTER, M.T., J.-S. KIM, T.S. STEENHUIS, J.Y. PARLANGE, A. HEILIG, R.D. BRADDOCK, J.S. SELKER & J. BOLL (2000): Funnel flow mechanisms in a sloping layered soil: Laboratory investigations. *Water Resources Research*, 36(5): 841-849.
- WANG, D., J.M. NORMAN, B. LOWERY & K. MCSWEENEY (1994): Nondestructive determination of hydrogeometrical characteristics of soil macropores. *Soil Science of America Journal*, 58(2): 294-303.
- WEBSTER, C.P., M.A. SHEPHERD, K.W.T. GOULDING & E. LORD (1993): Comparison of methods for measuring the leaching of mineral nitrogen from arable land. *J. Soil Sci.*, 44: 49-62.
- WEILER, M. (2001): Mechanisms controlling macropore flow during infiltration – dye tracer experiments and simulations. Diss. ETHZ. No. 14237, Zürich, Switzerland.
- WEILER, M., T. UCHIDA & J. MCDONNELL (2003): Connectivity due to preferential flow controls water flow and solute transport at the hillslope scale. Proceedings of MODSIM 2003, Townsville, Australia.
- WENNINGER, J., S. UHLENBROOK, N. TILCH & CH. LEIBUNDGUT (submitted): Experimental evidences of fast groundwater responses in a hillslope / floodplain area. Submitted paper to *Hydrological Processes*.
- WESTERN REGIONAL CLIMATE CENTRE (2003): Climate data. Website. URL: <http://www.wrcc.dri.edu/cgi-bin/cliMAIN.pl?ornoti> , 2003-07-11.
- WILSON, G.V. P.M. JARDIN, J.D. O'DELL & M. COLLINEU (1993): Field scale transport from a buried line source in variably saturated soil. *J. of Hydrology*, 145: 83-109.
- WILSON, C.M. & P.L. SMART (1984): Pipes and pipe flow process in an upland catchment, Wales. *Catena* 11: 145-158.
- WOODS, R.A. & L.K. ROWE (1996): The changing variability of subsurface flow across a hillside. *J. of Hydrology (NZ)*, 35(1): 51-86.
- WORLD METEOROLOGICAL ORGANISATION (1971): Use of weirs and flumes in stream gauging. Technical Note No. 117. Geneva.
- YARON, B., E. BRESLER & J. SHALHEVET (1966): A method for uniform packing of soil columns. *Soil Sci.*, 101: 205-209.
- ZIEMER, R.R. (1992): Effect of logging on subsurface pipeflow and erosion: coastal northern California, USA. In: *Erosion, Debris Flows and Environment in Mountain Regions* (Proceedings of the Chengdu Symposium, July 1992). IAHS Publ. no. 209: 187-197.
- ZIEMER, R.R. & J.S. ALBRIGHT (1987): Subsurface pipeflow dynamics of north-coastal California swale systems. In: *Erosion and Sedimentation in the Pacific Rim* (Proceedings of the Corvallis Symposium, August 1987). IAHS Publ. no. 187: 71-80.

# Appendix A

## Data from Low Pass field site

Tab. A1.1: Field sheets, soil profile at P\_A1.

Profile description piezometer			
ID:	<b>A1</b>	Location: 1233351/ 933426	
Date:	12 / 19 / 2002		
Depth (cm)	Horizon	Texture Structure	Color on Munsell 7,5 Y R
	0 <sub>H</sub>	litter, twigs	
10		common fine roots	
20	A	sandy loam	2,5 / 2
30		subangular blocky	
40			
50			
60			
70	B <sub>1</sub>	loam	5 / 6
80		blocky	
90	B <sub>2</sub>	loam	3 / 4
100			
110			
120			
130			
140			
150			
160			
170			
180			
190			
<b>Total depth:</b>			<b>134</b>

Tab. A1.2: Field sheets, soil profile at P\_A3.

Profile description piezometer			
ID:	<b>A3</b>	Location: 1233328/ 933440	
Date:	12 / 19 / 2002		
Depth (cm)	Horizon	Texture Structure	Color on Munsell 7,5 Y R
	0 <sub>H</sub>	litter, twigs	
10		high organic	
20	A	sandy loam	2,5 / 1
30		subangular blocky	
40			
50			
60			
70	B	u loam	3 / 3
80		blocky	
90			
100			
110			
120			
130			
140			
150			
160			
170			
180			
190			
<b>Total depth:</b>			<b>110</b>

Tab. A1.3: Field sheets, soil profile at P\_A5.

Profile description piezometer			
ID:	<b>A5</b>	Location: 1233309 / 933457	
Date:	12 / 19 / 2002		
Depth (cm)	Horizon	Texture Structure	Color on Munsell 7,5 Y R
	0 <sub>H</sub>	litter, twigs	
10			
20	A	sandy loam	3 / 2
30		subangular blocky	
40			
50			
60			
70			
80			
90			
100	B	loam subangular blocky	4 / 4
110			
120			
130			
140			
150			
160			
170			
180			
190			
200			
210			
220			
<b>Total depth:</b>			<b>124</b>

Tab. A1.4: Field sheets, soil profile at P\_A7.

Profile description piezometer			
ID:	<b>A7</b>	Location: 1233295 / 933478	
Date:	12 / 19 / 2002		
Depth (cm)	Horizon	Texture Structure	Color on Munsell 7,5 Y R
	0 <sub>H</sub>	litter, twigs	
10			
20		sandy loam	
30	B <sub>1</sub>	subangular blocky	3 / 4
40			
50			
60			
70			
80			
90	B <sub>2</sub>	sandy loam subangular blocky	4 / 6
100			
110			
120			
130			
140			
150			
160			
170			
180			
190			
200			
210			
220			
<b>Total depth:</b>			<b>146</b>

Tab. A1.5: Field sheets, soil profile at P\_A9.

Profile description piezometer			
ID:	<b>A9</b>	Location: 1233284/ 933502	
Date:	12 / 12 / 2002		
Depth (cm)	Horizon	Texture Structure	Color on Munsell
			7,5 Y R
	0 <sub>H</sub>	litter, twigs	
10			
20			
30	B <sub>1</sub>	sandy loam silt content	5 / 3
40			
50			
60			
70			
80			
90	B <sub>2</sub>	silt loam subangular blocky	6 / 4
100			
110			
120			
130			
140			
150			
160			
170			
180			
190			
200			
210			
220			
<b>Total depth:</b>			<b>114</b>

Tab. A1.6: Field sheets, soil profile at P\_B1.

Profile description piezometer			
ID:	<b>B1</b>	Location: 1233362/ 933418	
Date:	03 / 20 / 2003		
Depth (cm)	Horizon	Texture Structure	Color on Munsell
			7,5 Y R
	0 <sub>H</sub>	litter, twigs	
10			
20			
30	AB	Root portion sandy loam subangular blocky	3 / 2
40			
50			
60		20 % concretions	
70	B <sub>1</sub>	loam pebbles	3 / 3
80			
90		organic portion ~ 5 % vol	
100			
110	B <sub>2</sub>	sandy loam blocky	
120			
130		concretions up to d=2 mm	4 / 6
140			
150			
160	B <sub>3</sub>	loam	5 / 8
170		condensed	6 / 8
180		concretions	
190			
200			
210	B <sub>4</sub>	sand bright yellow	on 2.5Y 6 / 6
220			
<b>Total depth:</b>			<b>240</b>

Tab. A1.7: Field sheets, soil profile at P\_B2.

Profile description piezometer			
ID:	<b>B2</b>	Location: 1233332/ 933417	
Date:	03 / 20 / 2003		
Depth (cm)	Horizon	Texture Structure	Color on Munsell
			7,5 Y R
10	0 <sub>H</sub>	litter, twigs	
20	AB	Root portion decreasing	3 / 2
30		sandy loam	
40		subangular blocky	
50	B <sub>1</sub>	concretions	3 / 4
60		loam	
70		organic portion (roots etc.) ~ 5 % vol	
80			
90	B <sub>2</sub>	sandy loam	4 / 6
100		blocky	
110		concretions	
120			5 / 8
130	B <sub>3</sub>	condensed	6 / 8
140			
150		concretions	
160	B <sub>4</sub>		on 2,5 Y
170		sand	6 / 6
180		bright yellow	
190			
200			
210			
220			
<b>Total depth:</b>			<b>250</b>

Tab. A1.8: Field sheets, soil profile at P\_B4.

Profile description piezometer			
ID:	<b>B4</b>	Location: 1233302/ 933436	
Date:	03 / 20 / 2003		
Depth (cm)	Horizon	Texture Structure	Color on Munsell
			7,5 Y R
10	0 <sub>H</sub>	litter, twigs	
20	A	sandy loam	3 / 2
30		subangular	
40		blocky	
50	B		2,5 / 3
60		loam	3 / 4
70			
80			
90	B <sub>2</sub>	organic portion (roots etc.) ~ 5 % vol	4 / 4
100			
110			
120			
130	B <sub>2</sub>	loam	4 / 6
140		blocky	
150			
160			
170		condensed	5 / 8
180			
190			
200		plastic !!	
210			
220			
<b>Total depth:</b>			<b>250</b>

Tab. A1.9: Field sheets, soil profile at P\_C1.

Profile description piezometer			
ID:	<b>C1</b> Location: 1233342/ 933401		
Date:	12 / 19 / 2002		
Depth (cm)	Horizon	Texture Structure	Color on Munsell 7,5 Y R
10	0 <sub>H</sub>	litter, twigs	
20	A	sandy loam	3 / 4
30	AB	loam subangular blocky	3 / 3
40			
50			
60	B <sub>1</sub>		
70			
80			
90	B <sub>2</sub>	loam blocky	4 / 4
100			
110			
120		plastic	
130			
140			
150			
160			
170			
180			
190			
200			
210			
220			
<b>Total depth:</b>			<b>141</b>

Tab. A1.10: Field sheets, soil profile at P\_C3.

Profile description piezometer			
ID:	<b>C3</b> Location: 1233314/ 933413		
Date:	12 / 19 / 2002		
Depth (cm)	Horizon	Texture Structure	Color on Munsell 7,5 Y R
10	0 <sub>H</sub>	litter, sandy	
20	A	loam crumbly	2,5 / 2
30			
40	AB	sandy loam subang. blocky	3 / 2
50			
60			
70			
80			
90	B	loam blocky	3 / 3
100			
110			
120			
130			
140			
150			
160			
170			
180			
190			
200			
210			
220			
<b>Total depth:</b>			<b>114</b>

Tab. A1.11: Field sheets, soil profile at P\_C5.

Profile description piezometer			
ID:	<b>C5</b>	Location: 1233302/ 933435	
Date:	12 / 19 / 2002		
Depth (cm)	Horizon	Texture Structure	Color on Munsell 7,5 Y R
	0 <sub>H</sub>	litter, twigs	
10		sandy	
20	A	loam crumbly	3 / 1
30		sandy loam	
40			
50	AB		3 / 2
60		blocky	
70			
80			
90	B	loam subangular blocky	4 / 4
100			
110			
120			
130			
140			
150			
160			
170			
180			
190			
200			
210			
220			
<b>Total depth:</b>			
<b>114</b>			

Tab. A1.12: Field sheets, soil profile at P\_C7.

Profile description piezometer			
ID:	<b>C7</b>	Location: 1233269/933466	
Date:	12 / 19 / 2002		
Depth (cm)	Horizon	Texture Structure	Color on Munsell 7,5 Y R
	0 <sub>H</sub>	litter, twigs	
10			
20			
30	A	sandy loam	3 / 3
40		subangular blocky	
50			
60			
70	B	loam subangular blocky	3 / 4
80			
90			
100			
110			
120			
130			
140	B <sub>2</sub>	silt loam	4 / 6
150		compact	
160			
170			
180			
190			
200			
210			
220			
<b>Total depth:</b>			
<b>176</b>			

Tab. A1.13: Field sheets, soil profile at P\_C9.

Profile description piezometer			
ID:	<b>C9</b>	Location: 1233263/ 933493	
Date:	12 / 19 / 2002		
Depth (cm)	Horizon	Texture Structure	Color on Munsell
			7,5 Y R
	0 <sub>H</sub>	litter, twigs	
10		sandy loam	
20	A	Subangular blocky	3 / 1
30			
40		loam	
50	B		3 / 4
60		blocky friable	
70			
80			
90	B2	loam	4 / 6
100		blocky	
110			
120			
130			
140			
150			
160			
170			
180			
190			
200			
210			
220			
<b>Total depth:</b>			<b>112</b>

Tab. A1.14: Field sheets, soil profile at P\_D1.

Profile description piezometer			
ID:	<b>D1</b>	Location: 1233316/ 933389	
Date:	03 / 20 / 2003		
Depth (cm)	Horizon	Texture Structure	Color on Munsell
			7,5 Y R
	0 <sub>H</sub>	litter, twigs	
10			
20	A	sandy loam subangular blocky	3 / 1
30			
40			
50	B	sandy loam	3 / 4
60		blocky friable	
70			
80			
90			
100			
110			
120			
130			
140			
150			
160			
170			
180			
190			
200			
210	B/C		6 / 8
220			
<b>Total depth:</b>			<b>230</b>

Tab. A1.15: Field sheets, soil profile at P\_D3.

Profile description piezometer			
ID:	<b>D3</b>	Location: 1233290/ 933383	
Date:	03 / 20 / 2003		
Depth (cm)	Horizon	Texture Structure	Color n Munsell 7,5 Y R
	0 <sub>H</sub>	litter, twigs	
10			3 / 1
20		root portion decreasing	
30	AB	sandy loam subangular blocky	3 / 2
40			
50			
60		concretions	
70	B <sub>1</sub>	loam	3 / 3
80			
90		~ 5 % vol	
100			
110		sandy loam blocky	
120	B <sub>2</sub>		5 / 8
130		concretions (OD = 2mm)	
140			
150			
160			
170	B <sub>3</sub>	sandy loam	
180			
190		concretions	
200			
210			
220			
<b>Total depth:</b>			<b>230</b>

Tab. A1.16: Field sheets, soil profile at P\_D5.

Profile description piezometer			
ID:	<b>D5</b>	Location: 1233284/ 933437	
Date:	03 / 20 / 2003		
Depth (cm)	Horizon	Texture Structure	Color on Munsell 7,5 Y R
	0 <sub>H</sub>	litter, twigs	
10		sandy	
20	A	loam subangular blocky	3 / 1
30			
40	B	sandy loam	3 / 4
50		blocky	
60			
70			
80			
90			
100			
110			
120			
130			
140			
150			
160			
170			
180			
190			
200	B/C	friable	6 / 8
210			
220			
<b>Total depth:</b>			<b>230</b>



**Fig. A2a:** Sabre growth indicating the soil creeping. The reflecting, white area shows the roof covering the trench.

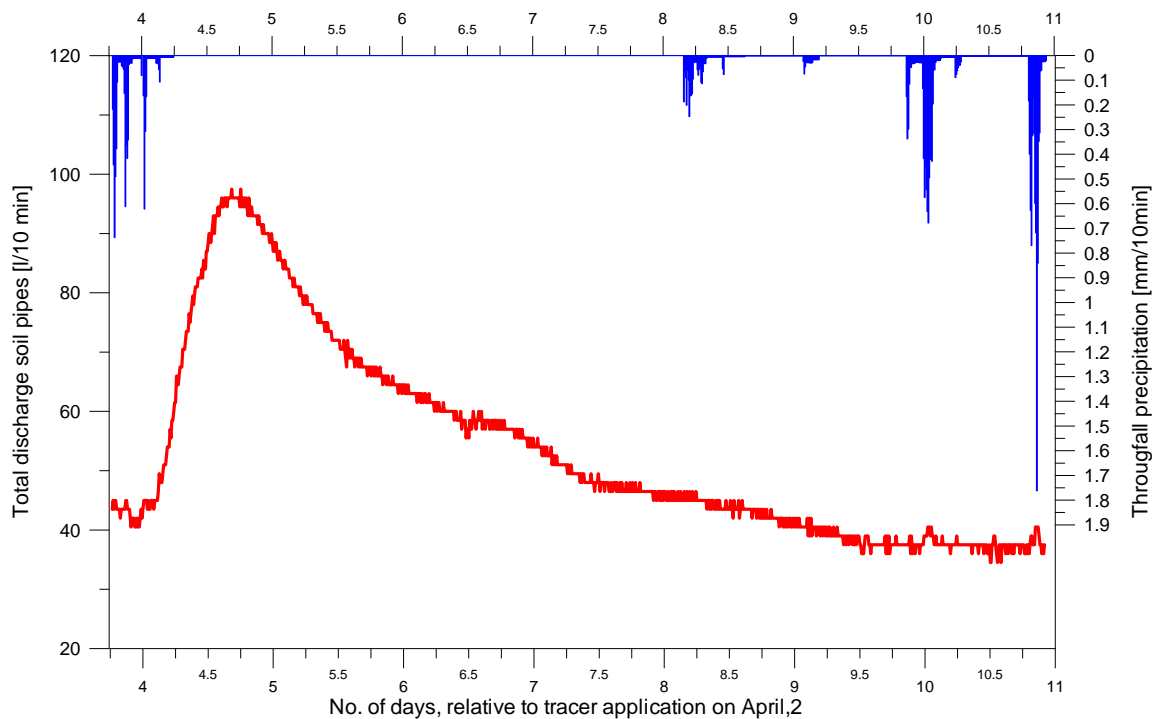


**Fig. A2b:** Sabre growth indicating the soil creeping. White pipe represents P\_A7.

**Tab. A3:** Exact data on hydrograph separation for selected runoff events.

Peak ID	Starting point	Time	Digitime	Ending point	Time	Digitime	Total flow [m <sup>3</sup> ]	Method	Event flow [m <sup>3</sup> ]
1	17-Feb-03	13:30	-43.4375	20-Feb-03	02:50	-40.8819	165	blip	74
2+3	6-Mar-03	19:50	-26.1736	12-Mar-03	14:20	-20.4028	807	blip	446
4	21-Mar-03	01:00	-11.9583	26-Mar-03	06:40	-6.72222	932	blip	535
4+5	21-Mar-03	01:00	-11.9583	29-Mar-03	13:40	-3.43056	1313	blip	760
6	5-Apr-03	15:40	3.65277	12-Apr-03	01:00	10.0417	523	horiz. Line; *	152
7	23-Apr-03	21:00	21.875	1-May-03	10:30	29.4375	315	horiz. line	87

\*) The hydrograph separation of peak ID 6 was done for the period up to digital time 10.0417 although little precipitation was recorded in between. This is visualised in Fig. A3. The included error might still be less dominant compared to the method of separation (e.g. hypothesis of vertical line).

**Fig. A3:** Discharge soil pipes and rain events for the period of hydrograph separation.

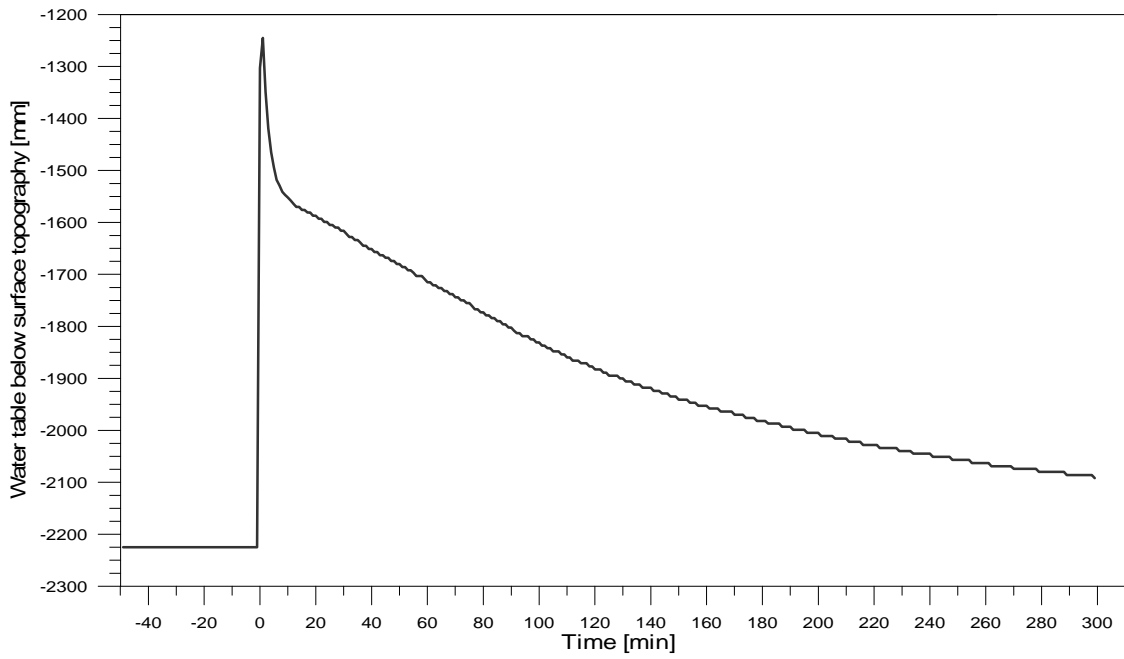


Fig. A4: Slug test at P\_D3 on March, 25 2003.

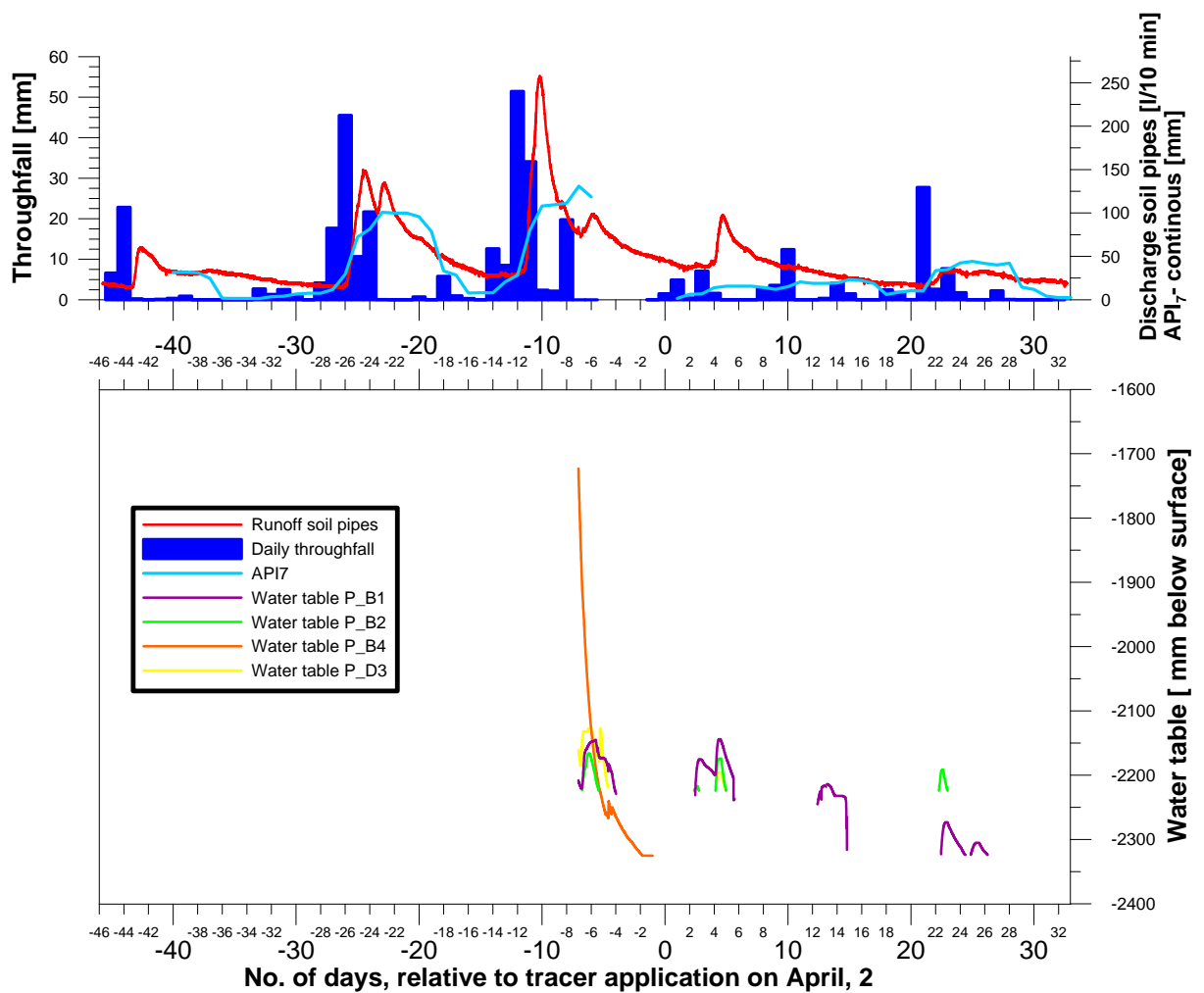


Fig. A5: Water table at P\_A3 and runoff soil pipes. Note that this piezometer is next to soil

pipes.

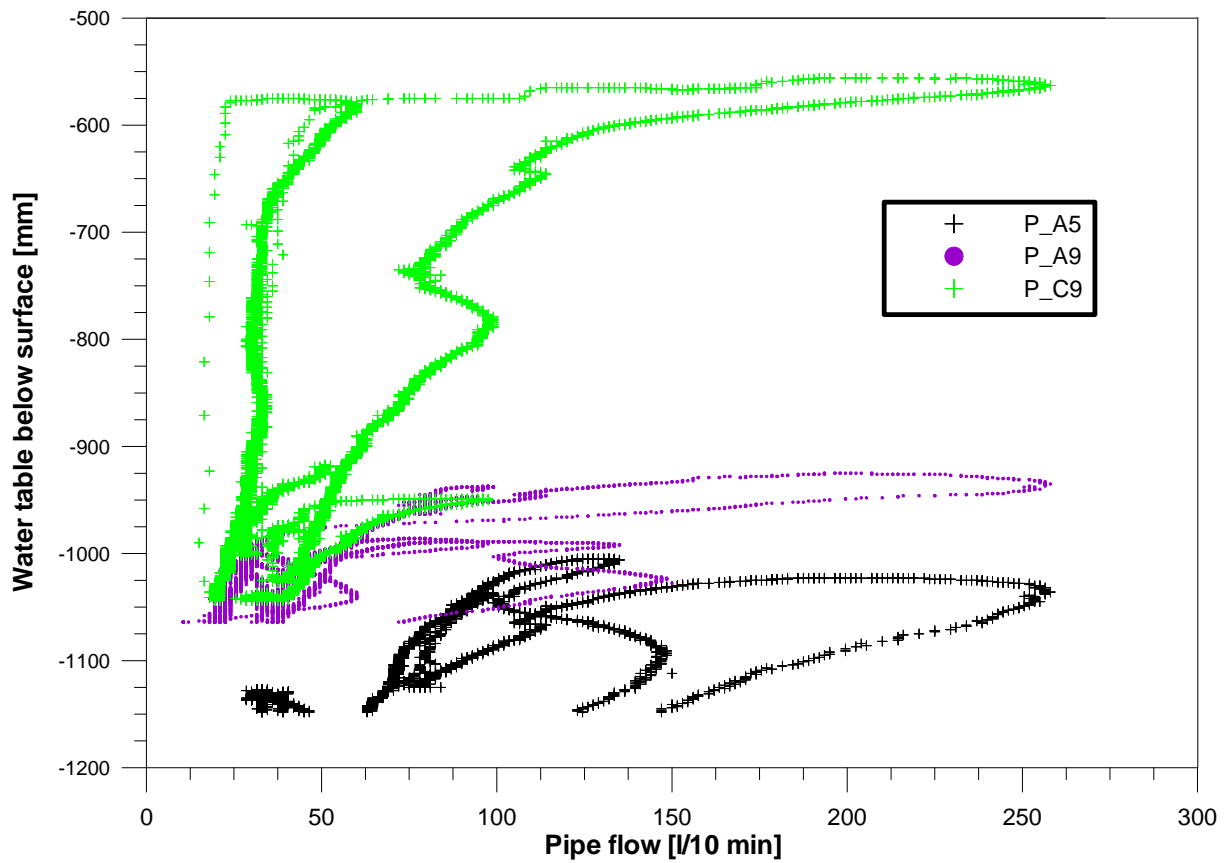


Fig. A6: Correlation between water table and pipe flow for selected piezometers.

Tab. A4: Determination of input mass for Low Pass experiment.

Tracer	Concentration, wanted [ppb]	Total flow volume* [m <sup>3</sup> ]	Tracer mass [g]	Portion of initial mobilisation [%]	Tracer mass [g]
Amino G Acid; line source	100	807	80.7	53	150
Bromide; areal application	10	807	8070	100	8000

\* For expected upcoming event similar ID 2+3, according to Tab. A3.

Tab. A5: Calculation on assumed drainage geometry of soil pipes.

Peak ID	Parameter description	Hydraulic conductivity, k [m/d] *	Water table rise, h [m]	Peak discharge [l/10 min]	DCA [dm <sup>2</sup> ]	Outflow to be drained by the system, s [m/d]	Distance between draining pipes, a [m] #
4 + 5	Max. DCA	0.015552	0.3	258	950000	0.03911	0.38
	Max. DCA, max. water table rise	0.015552	0.588	258	950000	0.03911	0.74
	DCA of peak ID 4+5	0.015552	0.3	258	580000	0.06406	0.30
	DCA of peak ID 4+5, max. water table rise	0.015552	0.588	258	580000	0.06406	0.58
	Max. DCA , proposed water table rise	0.015552	1	258	950000	0.03911	1.26
	DCA of peak ID 4+5, proposed water table rise	0.015552	1	258	580000	0.06406	0.99
	K times factor 10	0.15552	0.3	258	950000	0.03911	1.20
	K times factor 10	0.15552	0.588	258	950000	0.03911	2.35
	K divided by factor 10	0.0015552	0.3	258	950000	0.03911	0.12
	K divided by factor 10	0.0015552	0.588	258	950000	0.03911	0.23
6	Max. DCA	0,015552	0.13	98	950000	0.01485	0.27
	Max. DCA	0.015552	0.3	98	950000	0.01485	0.61
	DCA of peak ID 4+5	0.015552	0.13	98	580000	0.02433	0.21
	DCA of peak ID 4+6	0.015552	0.3	98	580000	0.02433	0.48
	K times factor 10	0.15552	0.13	98	950000	0.01485	0.84
	K times factor 10	0.15552	0.3	98	950000	0.01485	1.94

\* Basis was K value of 1.8 E-07 m/s according to section 5.5.

# According to E. 5.5.4; influences on pipes from below are neglected.

## Appendix B

**Data and information for the experimental hillslope table**

Tab. B1: Information on irrigation intervals during experiments at hillslope table.

Event ID	Status	Digitime	Date	Time	Sprinkling [mm]
1	on	19.45139	May, 19	1050	2.219
	off	19.45486	May, 19	1055	
2	on	19.46181	May, 19	1105	2.195
	off	19.46528	May, 19	1110	
3	on	19.47222	May, 19	1120	2.717
	off	19.47569	May, 19	1125	
4	on	19.48264	May, 19	1135	2.073
	off	19.48611	May, 19	1140	
5	on	19.49306	May, 19	1150	2.364
	off	19.49653	May, 19	1155	
6	on	19.50347	May, 19	1205	2.195
	off	19.50694	May, 19	1210	
7	on	19.62847	May, 19	1505	2.243
	off	19.63194	May, 19	1510	
8	on	19.63889	May, 19	1520	2.000
	off	19.64236	May, 19	1525	
9	on	19.64931	May, 19	1535	2.000
	off	19.65278	May, 19	1540	
10	on	19.65972	May, 19	1550	1.952
	off	19.66319	May, 19	1555	
11	on	19.75	May, 19	1800	2.437
	off	19.75347	May, 19	1805	
12	on	19.76042	May, 19	1815	2.098
	off	19.76389	May, 19	1820	
13	on	20.49653	May, 20	1155	2.534
	off	20.5	May, 20	1200	
14	on	20.50694	May, 20	1210	2.340
	off	20.51042	May, 20	1215	
15	on	20.51736	May, 20	1225	2.825
	off	20.52083	May, 20	1230	
16	on	20.53472	May, 20	1250	2.389
	off	20.53819	May, 20	1255	
17	on	20.54514	May, 20	1305	2.389
	off	20.54861	May, 20	1310	
18	on	20.55903	May, 20	1325	2.098
	off	20.5625	May, 20	1330	
19	on	20.66806	May, 20	1602	2.146
	off	20.67153	May, 20	1607	
20	on	20.67847	May, 20	1617	2.146
	off	20.68194	May, 20	1622	
21	on	20.69444	May, 20	1640	2.146
	off	20.69792	May, 20	1645	
22	on	20.70486	May, 20	1655	2.049
	off	20.70833	May, 20	1700	

Tab. B1: *continued*

Event ID	Status	Digitime	Date	Time	Sprinkling [mm]
23	on	20.71528	May, 20	1711	2.292
	off	20.71875	May, 20	1716	
24	on	20.72569	May, 20	1725	1.709
	off	20.72917	May, 20	1730	
25	on	20.76389	May, 20	1820	2.146
	off	20.76736	May, 20	1825	
26	on	20.94792	May, 20	2245	2.146
	off	20.95139	May, 20	2250	
27	on	21.23056	May, 21	532	2.146
	off	21.23403	May, 21	537	
28	on	21.24097	May, 21	547	2.146
	off	21.24444	May, 21	552	
29	on	21.36458	May, 21	850	3.146
	off	21.36806	May, 21	855	
30	on	21.39583	May, 21	930	2.806
	off	21.39931	May, 21	935	
31	on	21.40625	May, 21	945	2.806
	off	21.40972	May, 21	950	
32	on	21.43472	May, 21	1026	2.418
	off	21.43819	May, 21	1031	
33	on	21.45139	May, 21	1050	2.758
	off	21.45486	May, 21	1055	
34	on	21.46181	May, 21	1105	2.612
	off	21.46528	May, 21	1110	
35	on	21.54861	May, 21	1310	2.758
	off	21.55208	May, 21	1315	
36	on	21.57986	May, 21	1355	2.588
	off	21.58333	May, 21	1400	
37	on	21.59375	May, 21	1415	2.588
	off	21.59722	May, 21	1420	
38	on	21.61806	May, 21	1450	2.272
	off	21.62153	May, 21	1455	
39	on	21.64514	May, 21	1529	2.515
	off	21.64861	May, 21	1534	
40	on	21.65556	May, 21	1544	2.127
	off	21.65903	May, 21	1549	
40-I	on	21.7	May, 21	1648	4.408
	off	21.7064	May, 21	1658	
40-II	on	21.71389	May, 21	1708	4.408
	off	21.72083	May, 21	1718	
40-III	on	21.73056	May, 21	1732	4.408
	off	21.73889	May, 21	1744	
40-IV	on	21.74583	May, 21	1754	4.408
	off	21.75417	May, 21	1806	
40-V	on	21.76597	May, 21	1823	4.408
	off	21.77292	May, 21	1833	
40-VI	on	21.81458	May, 21	1933	4.408
	off	21.82153	May, 21	1943	

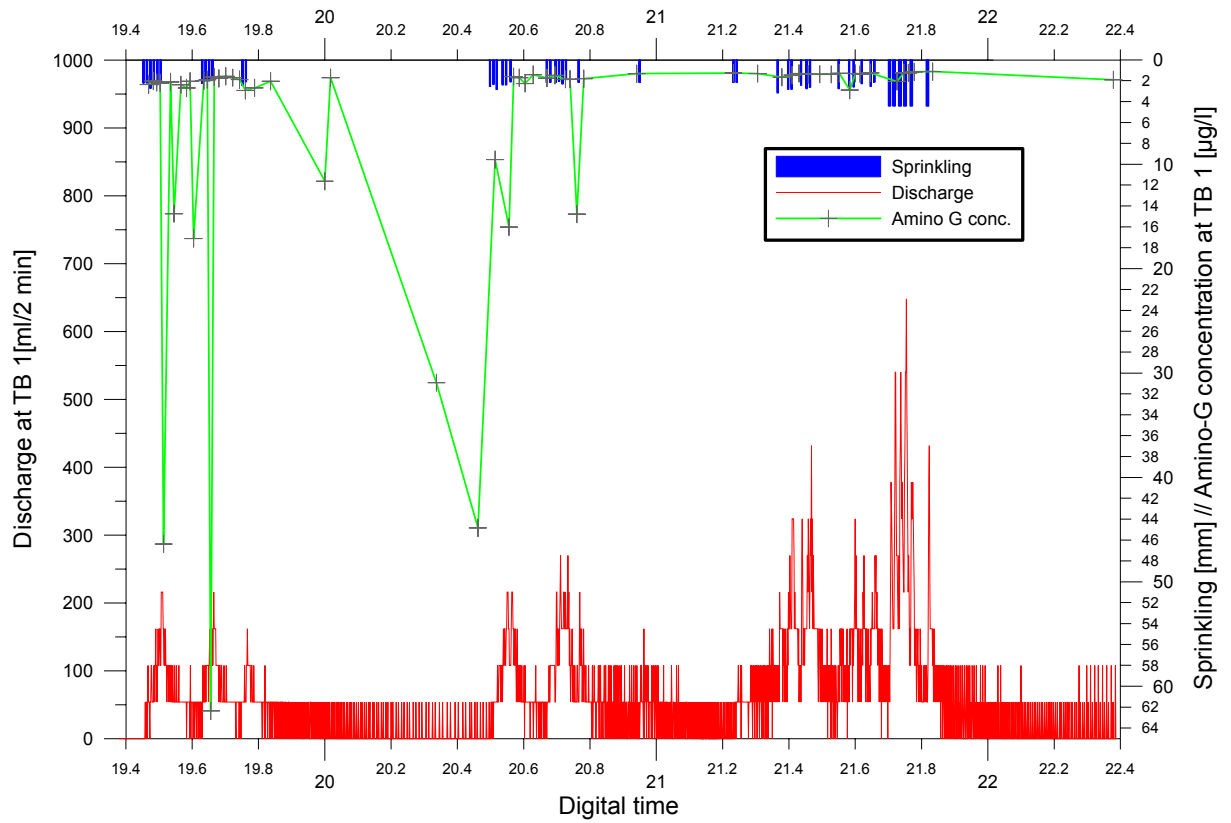


Fig. B1: Amino G breakthrough, accumulated discharge and sprinkling intervals at TB 1.

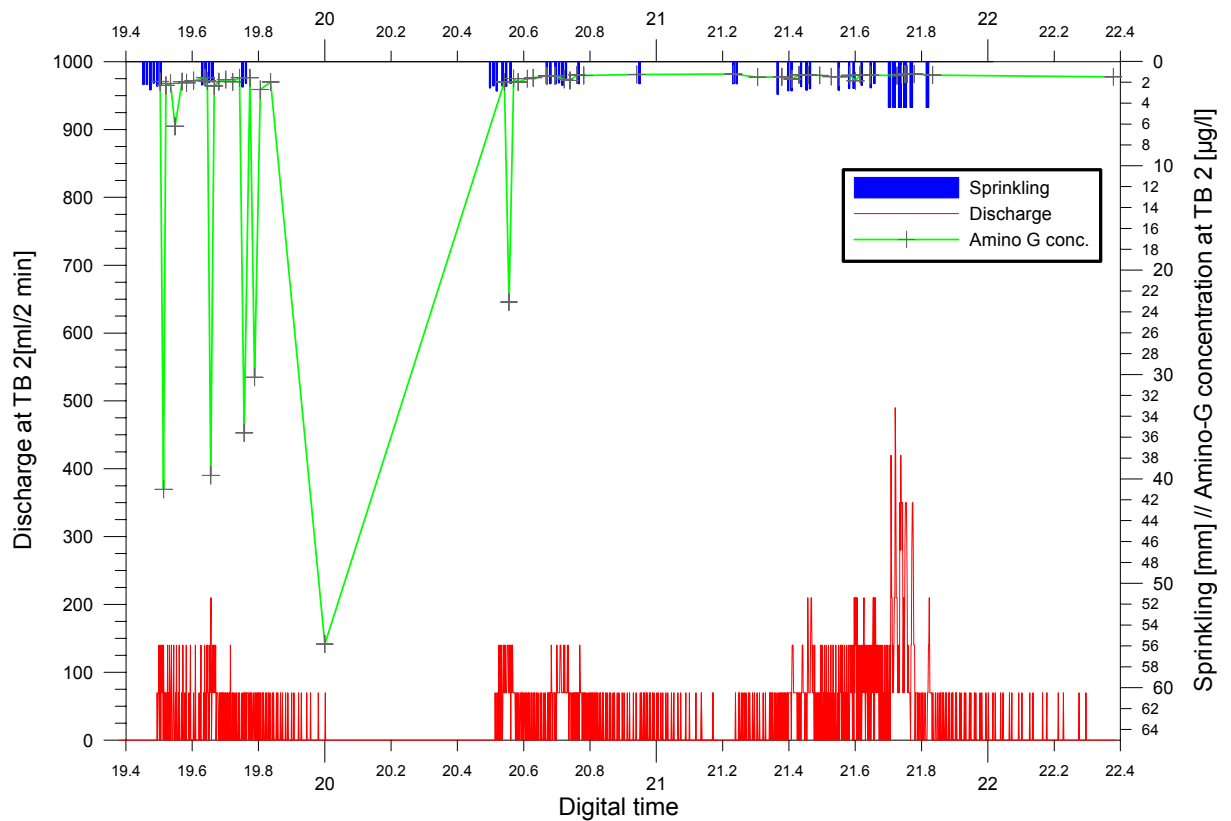


Fig. B2: Amino G breakthrough, accumulated discharge and sprinkling intervals at TB 2.

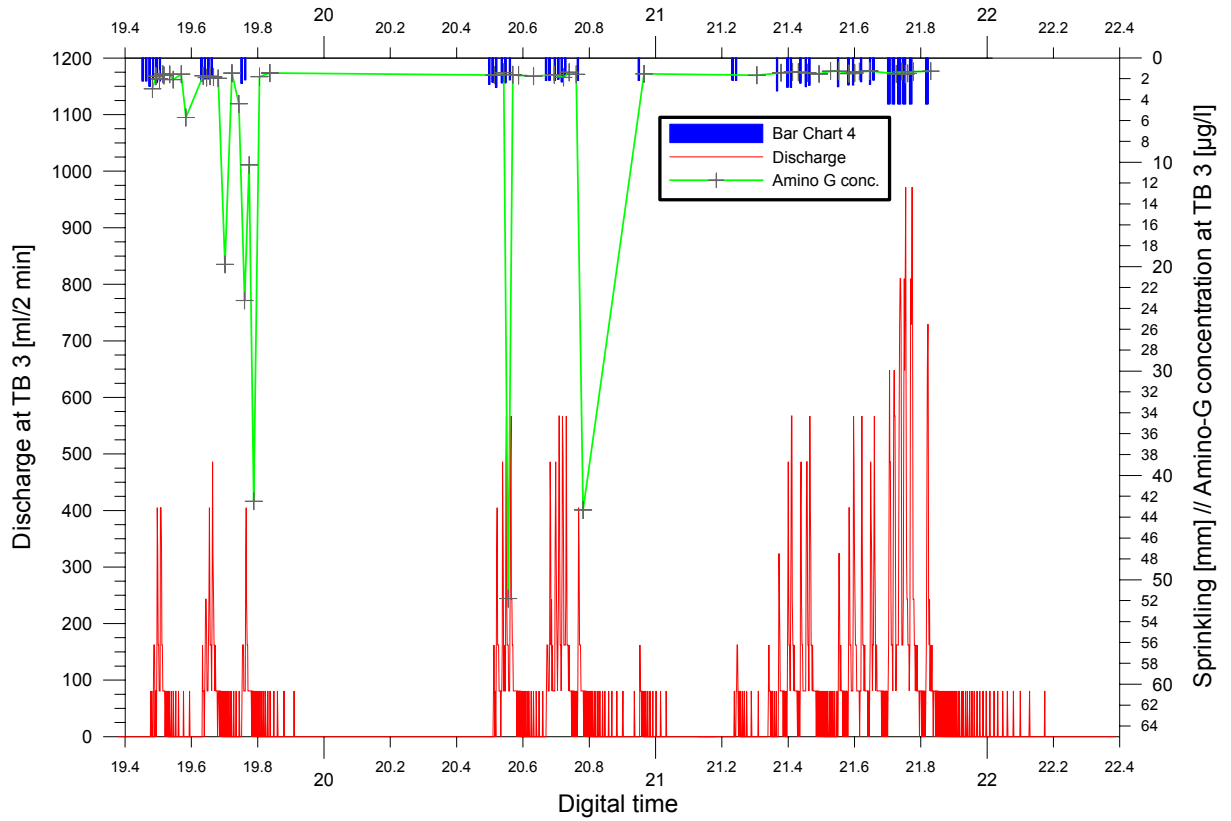


Fig. B3: Amino G breakthrough, accumulated discharge and sprinkling intervals at TB 3.

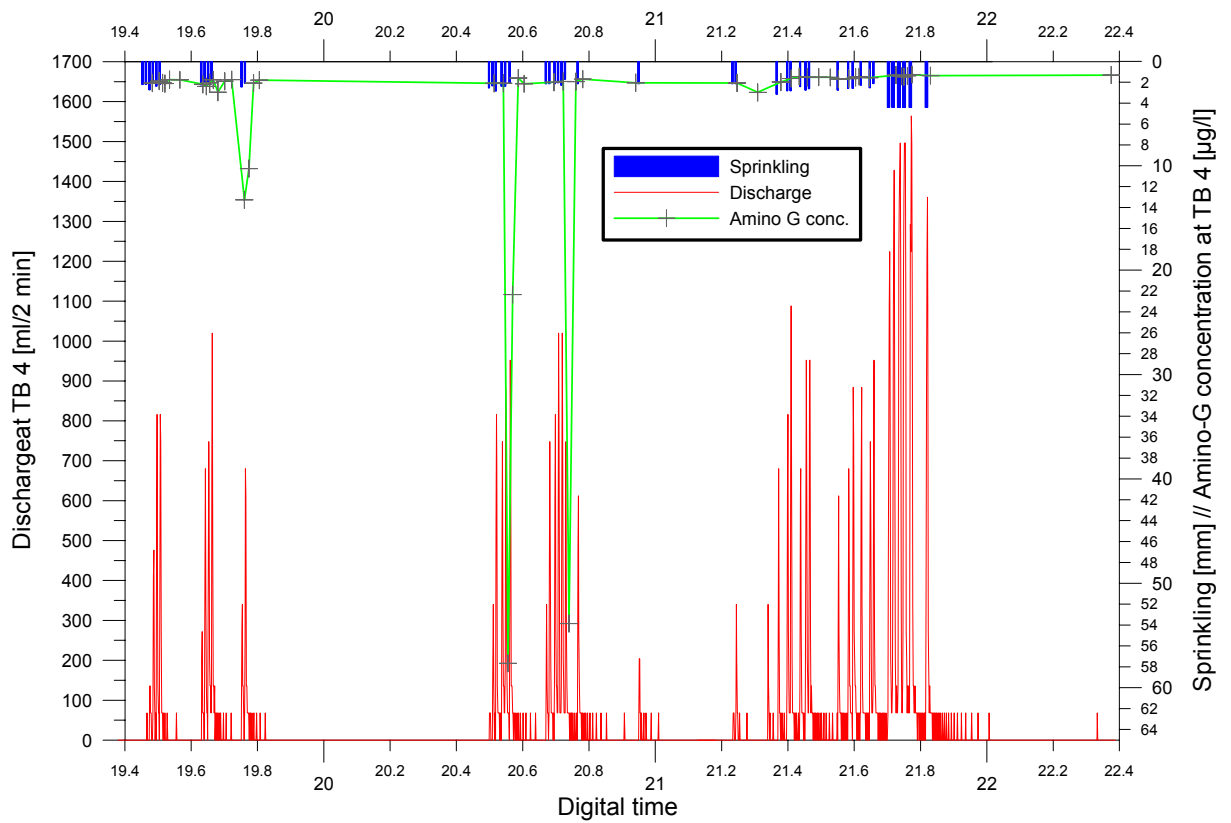


Fig. B4: Amino G breakthrough, accumulated discharge and sprinkling intervals at TB 4.

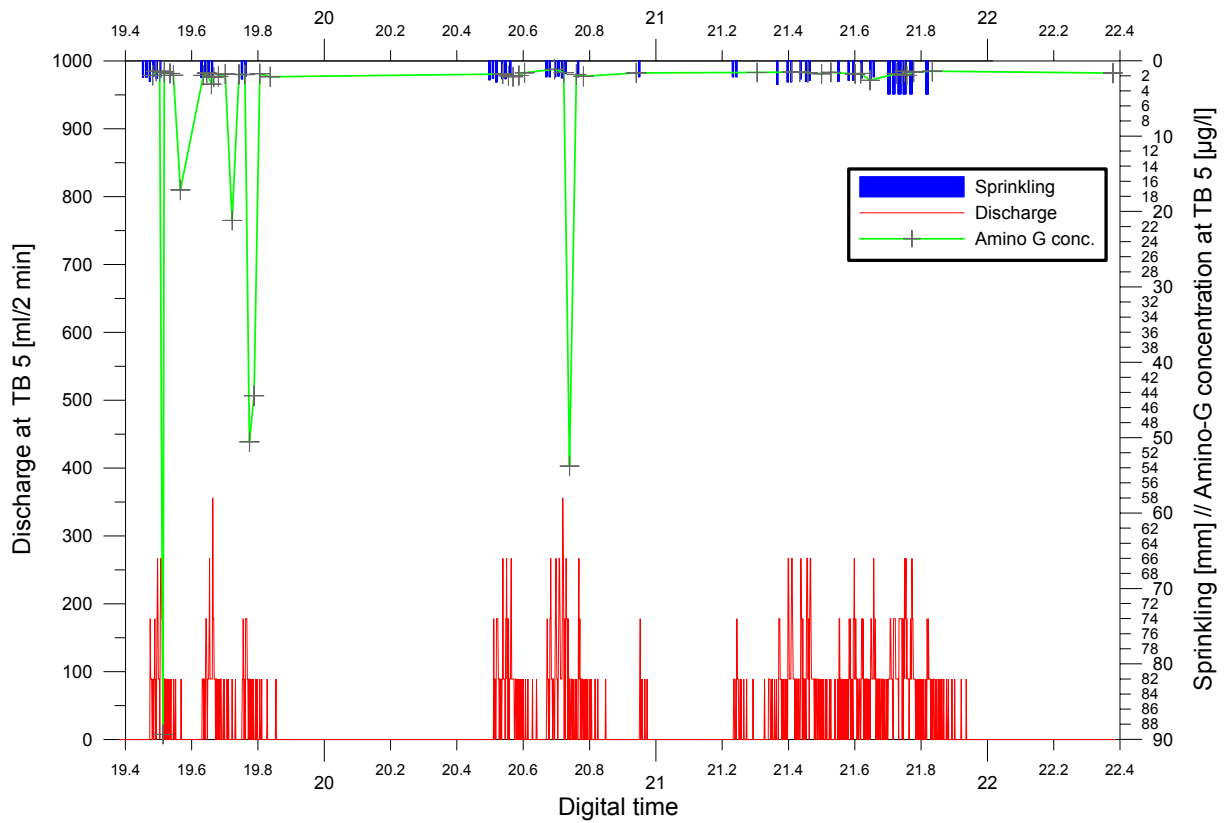


Fig. B5: Amino G breakthrough, accumulated discharge and sprinkling intervals at TB 5.

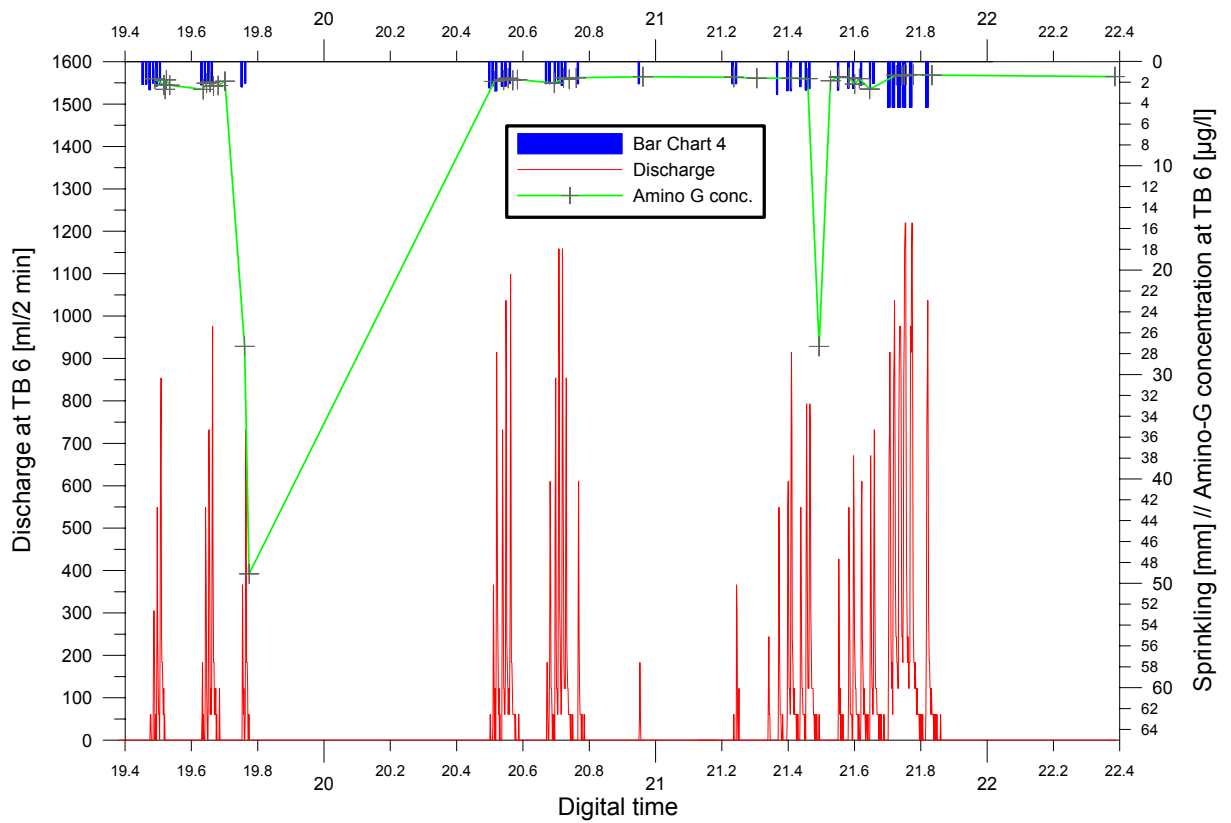


Fig. B6: Amino G breakthrough, accumulated discharge and sprinkling intervals at TB 6.

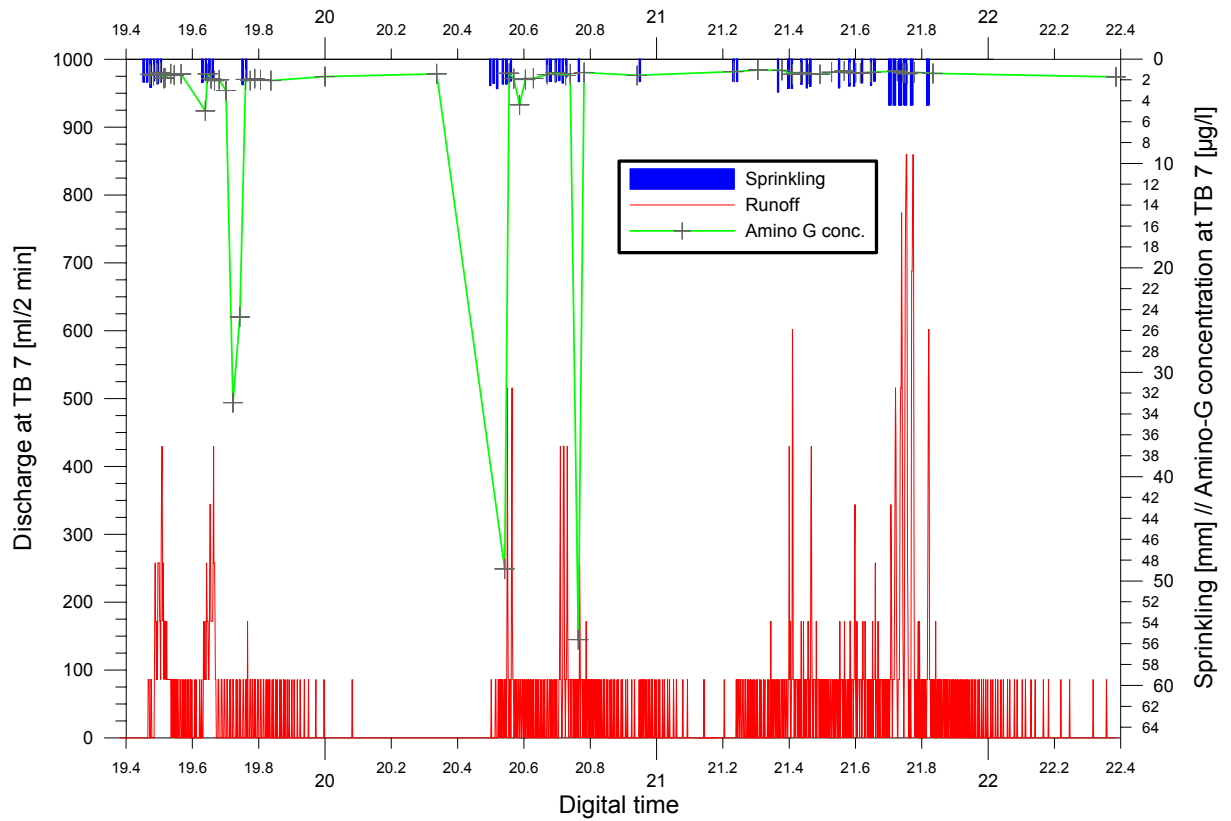


Fig. B7: Amino G breakthrough, accumulated discharge and sprinkling intervals at TB 7.

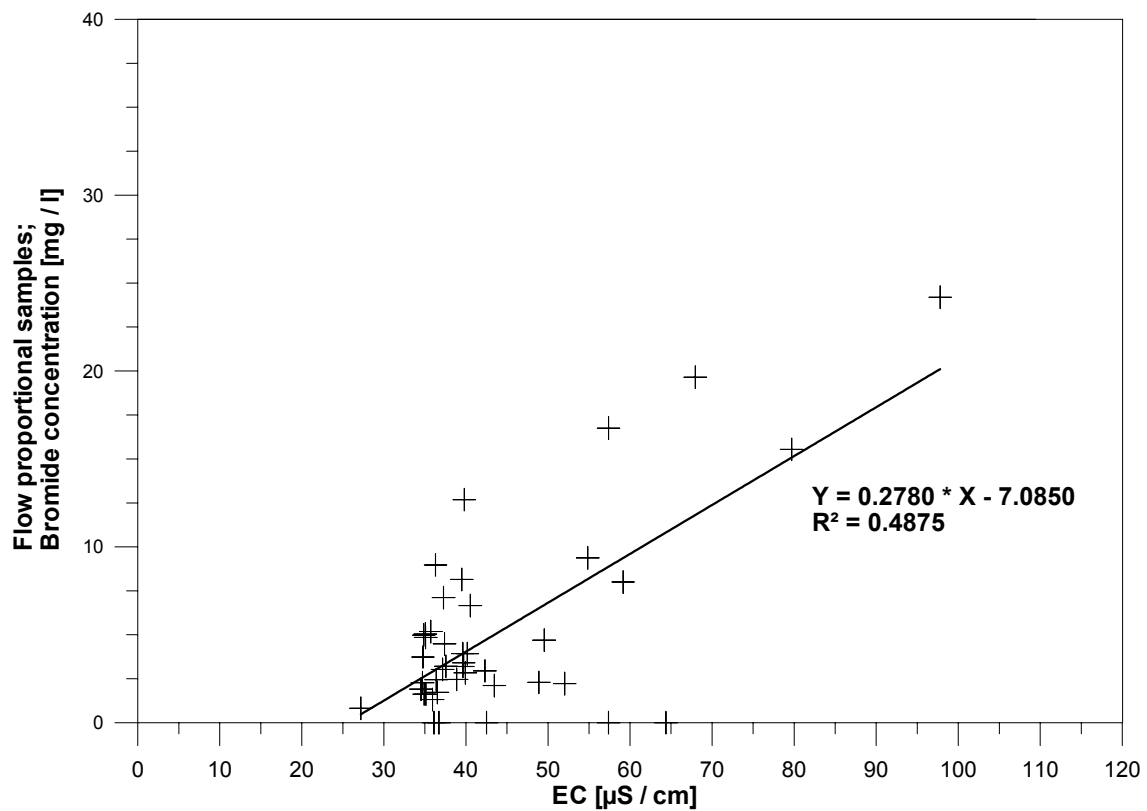
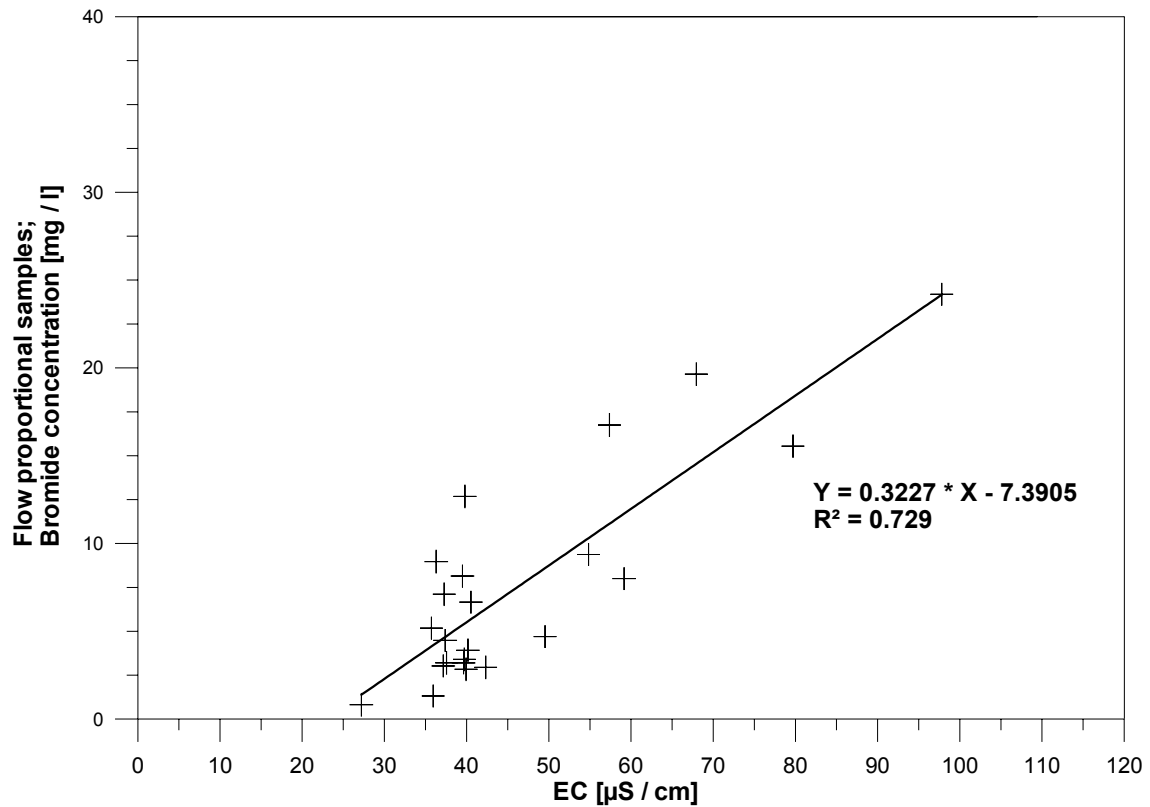
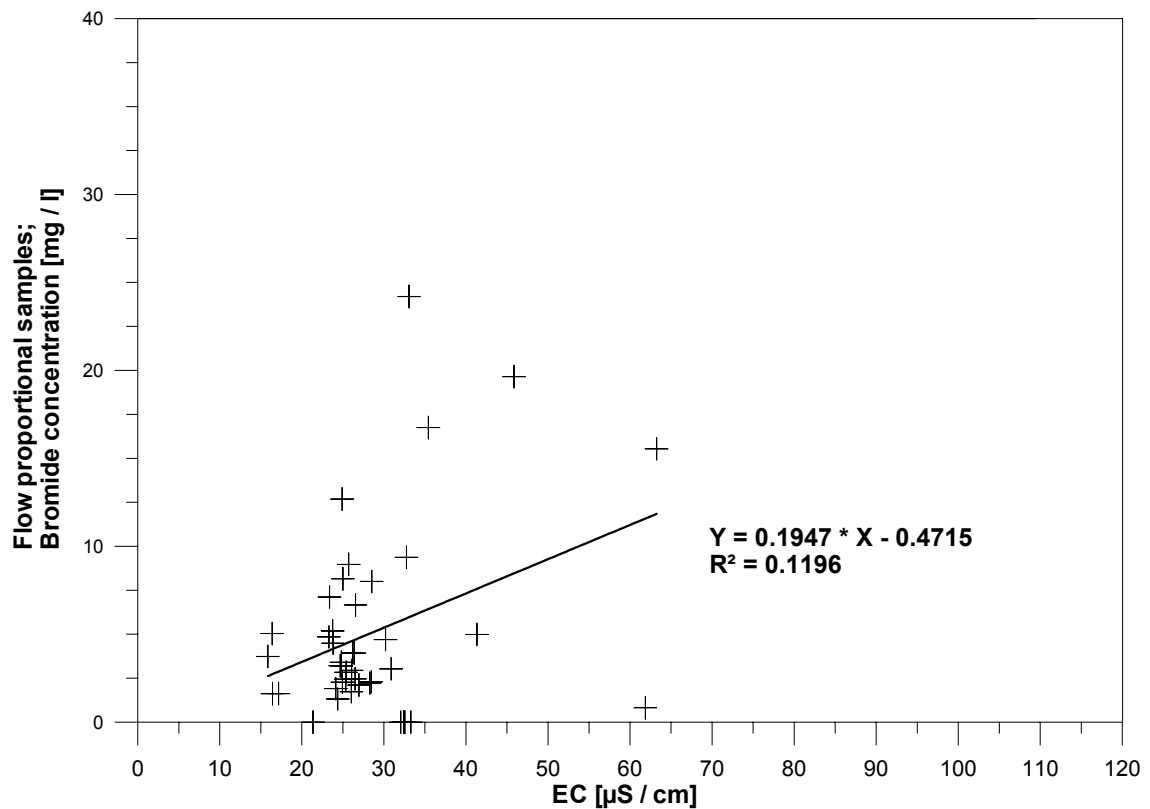


Fig. B8: Correlation between electrical conductivity and bromide concentration of flow proportional hand samples at TB 1.



**Fig. B9:** Correlation between electrical conductivity and bromide concentration of flow proportional hand samples at TB 1, for the times < 19.5.



**Fig. B10:** Correlation between electrical conductivity and bromide concentration of flow proportional hand samples at TB 8.

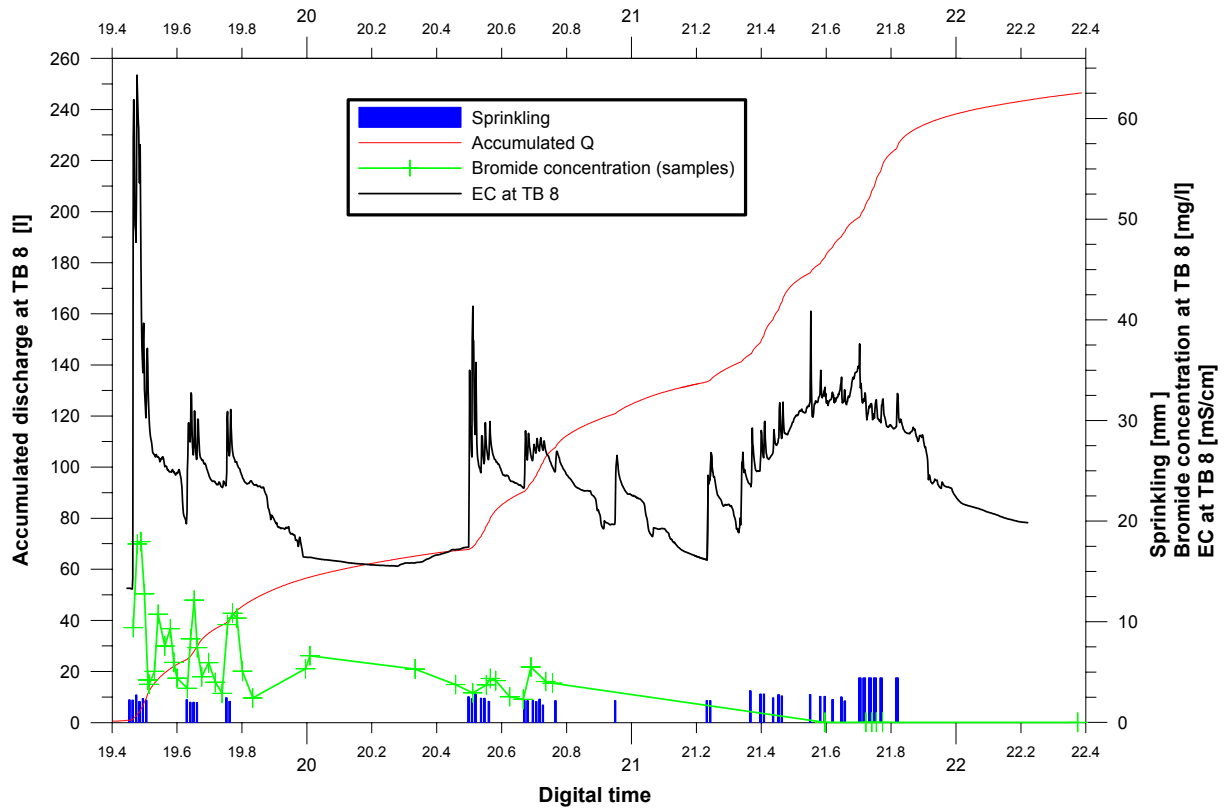


**Fig. B11:** Bromide concentrations, electrical conductivity, sprinkling intervals and accumulated discharge at TB 8.

# Appendix C

## Technical information

## C1 Tipping buckets

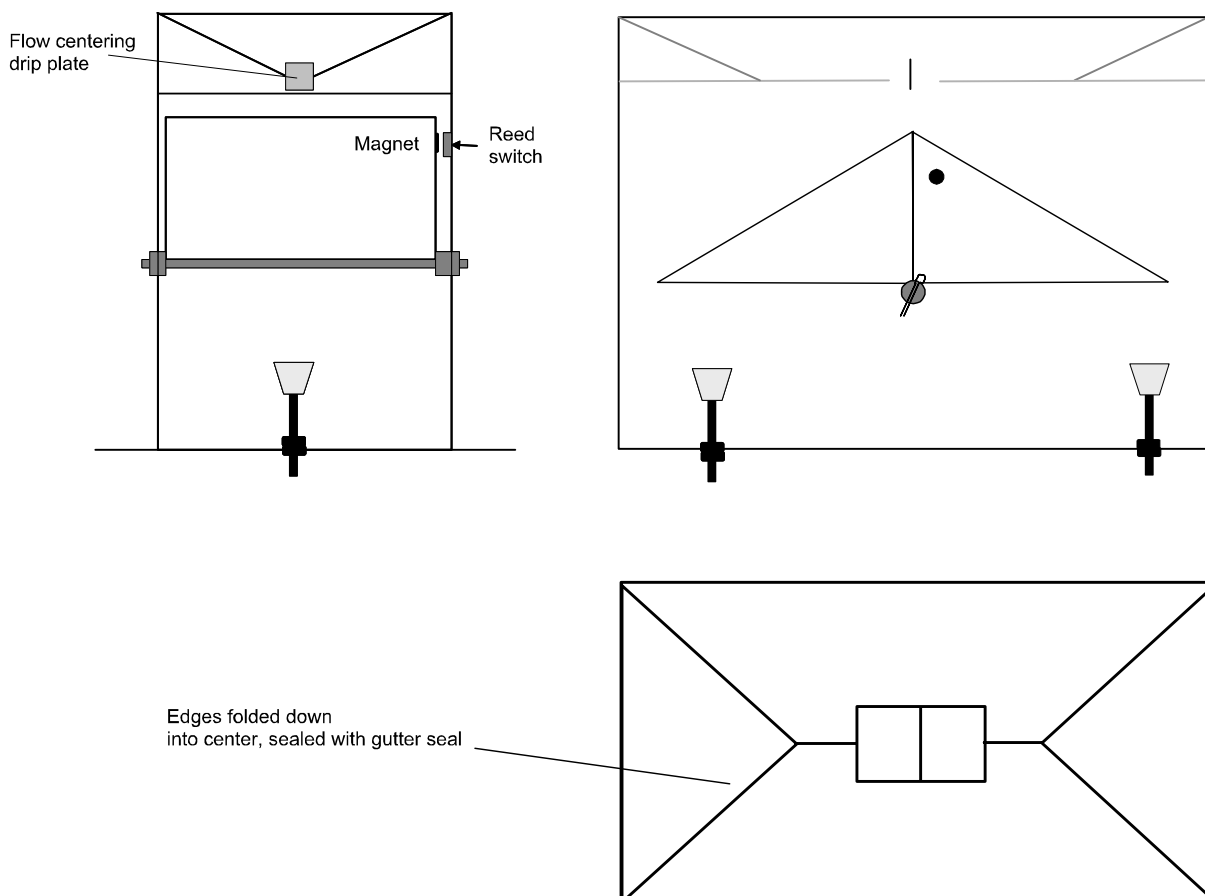


**Fig. C1:** Sketch of tipping buckets to provide a visual impression for information purposes. The drawing is intentionally simplified and includes only the most functional details.

## C2 Piezometer

This data logger offers high resolution data in either two channel (old models) or three channel modes. In this study (with two exceptions due to availability) the more recent ones were used. The channels of these relate to water height, water temperature and air temperature. The sensor type of the water table recorders is capacitive. Operation is effective within the temperature range of 0°C to +70°C (TRUTRACK, 2003). Within that, the accuracy equals  $\pm 1$  mm.

Piezometers of various lengths are available. In this study the WT-HR 500 (500 mm rod length measurable; total length: 820 mm) was used for the table experiment and the WT-HR 1000, WT-HR 1500 for the field experiments.

The data transfer by Omnilog software© offers automatic temperature correction, in case channel water temperature and air temperature are online. The dependent relationship of

water height for a water column of 1000 mm is a 0.65 mm decrease by increasing water temperature by 1 °C. Another error is connected with air temperature. According to the manufacture (TRUTRACK, 2003), the water height increases by 0.5 mm (starting at the offset / base level 0 mm) if the air temperature increases by 1 °C.

WT-HR data loggers are easy to handle, and they will even download reliably under rough weather conditions. The memory of the logger is large enough for intensive field campaigns. A three channel mode by 10 min intervals runs about two months. This implements for the 12 bit high resolution mode a memory capacity of 32000 samples (TRUTRACK, 2003).

The body of the logger is made out of solid stainless steel (Fig. C2a). Vibrations during transport (car driving) prior to installation were once the reason for a lost plugging connection between tub and middle rod. Therefore a compulsory check should be done before installing the capacity rods in the field.

Unfortunately there is no possibility of receiving raw data (simply voltage) from the logger. This may be an issue for self-adopted calibration on specific local conditions (particular water with its electrical conductivity, range in water and air temperature etc.). However, the data obtained in this study are all corrected for the temperature error automatically.



**Fig. C2a:** Water height recorder WT-HR. From: TRUTRACK (2003).

From the bottom end of the piezometers until the offset (reading zero) is a range of 74 mm. This means that the logger needs an established water table of at least that height in the pipe to provide results. Less than that the data were not reliable. Finally the result of the measurements shows water level in depth below surface.

The water table recorder is housed in a PVC-pipe, shown in Fig. C2b. For the purpose of sediment protection the slits are covered with gauze, as mentioned earlier. Early on the PVC-pipe was placed again in a drill hole. After positioning the pipe in the lower part of the left drill hole is refilled by sand. Afterwards soil follows, and after that, as a protection against passing water from the upper zones, the pipes are surrounded by a dense layer of bentonit. Finally, up to the surface there is some heavy dense soil again.

The data logger was lowered in the pipe connected by a rope to the lid of the pipe (see horizontal axis in Fig. C2b). The pipe is protected by a closed lid except during maintenance and during insertion.

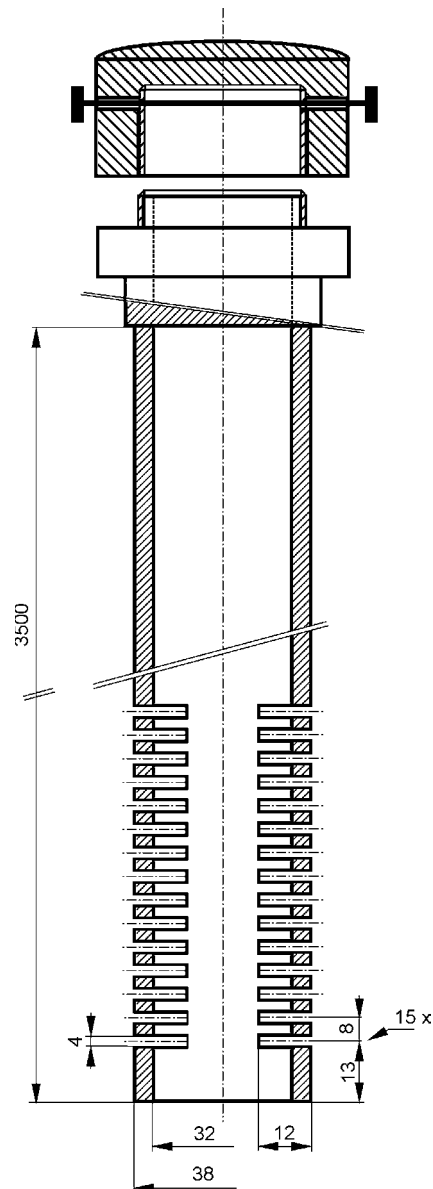


**Fig. C2b:** Sketch of PVC-pipe which encased the water table recorder, to be placed in a drill hole. Dimensions: mm. *Own compilation.*

### C3 Flume

So called THOMSON-flumes - or triangular notch weirs - are simple to construct. Flumes should be fully ventilated and not submerged. The construction plan (Fig. C3a) of the flume is based on the recommendations of WORLD METEOROLOGICAL ORGANISATION (1971). The material was stainless steel.

The thin plate is constructed perpendicular to the stream surface. Weir width is recommended to be the same as the stream width. The roughly estimated discharge at the side determined the flumes total angle of  $60^\circ (= 2\alpha)$ .



The discharge can be calculated for these kinds of weirs, using an integrating approach. The deviation necessary for determinations are shown in Fig. C3b.

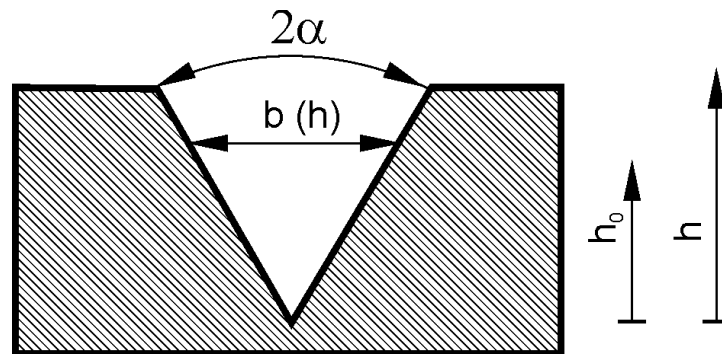


**Fig. C3b:** Details of notch. Modification of: RÖSSERT (1981).

According to that the general calculation for a “v”-shaped flume is (after RÖSSERT, 1981):

$$\begin{aligned}
 Q_{VFlume} &= \int_0^{h_0} \mu \sqrt{2gh} 2(h_0 - h) \tan(\alpha) dh \\
 &= 2\mu \sqrt{2g} \tan(\alpha) \int_0^{h_0} (h_0 \sqrt{h} - h^{3/2}) dh \\
 &= \mu \frac{8}{15} \sqrt{2g} \tan(\alpha) h_0^{5/2} \quad (E. C-1)
 \end{aligned}$$

where:  $Q_{VFlume}$  = discharge “v”-shaped flume [m<sup>3</sup>/s]  
 $\mu$  = coefficient [-]  
 $g$  = gravity [m/s<sup>2</sup>]  
 $h_0$  = water height above notch [m]  
 $\alpha$  = angle ½ notch [°]

In this study the flume is calibrated in a classical way by volumetric gauging of the discharge per time. This process needed a small barrel measuring at two minutes, which is later multiplied for a 10 minutes value. According to that the coefficient  $\mu$  is set to a constant 0.644. This is in agreement with the theoretical coefficient published by SCHRÖDER (1994), where  $\mu$  is about 0.64 for a fully ventilated, sharp-edged overfall. Based on this, discharge was calculated by the formula, which provides the rating curve in this case.

For an illustration of the rating curve of the flume see Fig. C3c. To understand this graphic, two facts are important: first the gauging on May, 23 is admittedly wrong, as it does not fit in the theoretical context (indicated by an error bar of 61 %, within which the regression would fit). This was certainly a procedural mistake. The minimal change of the coefficient  $\mu$  in lower heights of the “v”-shape, a circumstance mentioned by SCHRÖDER (1994), would not result in such a deviation. Second, the data processing is difficult. Very often the rating is wrong,

because of clogging up by branches. Therefore, the rating curve presented in Fig. C3c does not last for the total series but definitely for the first measured peak.

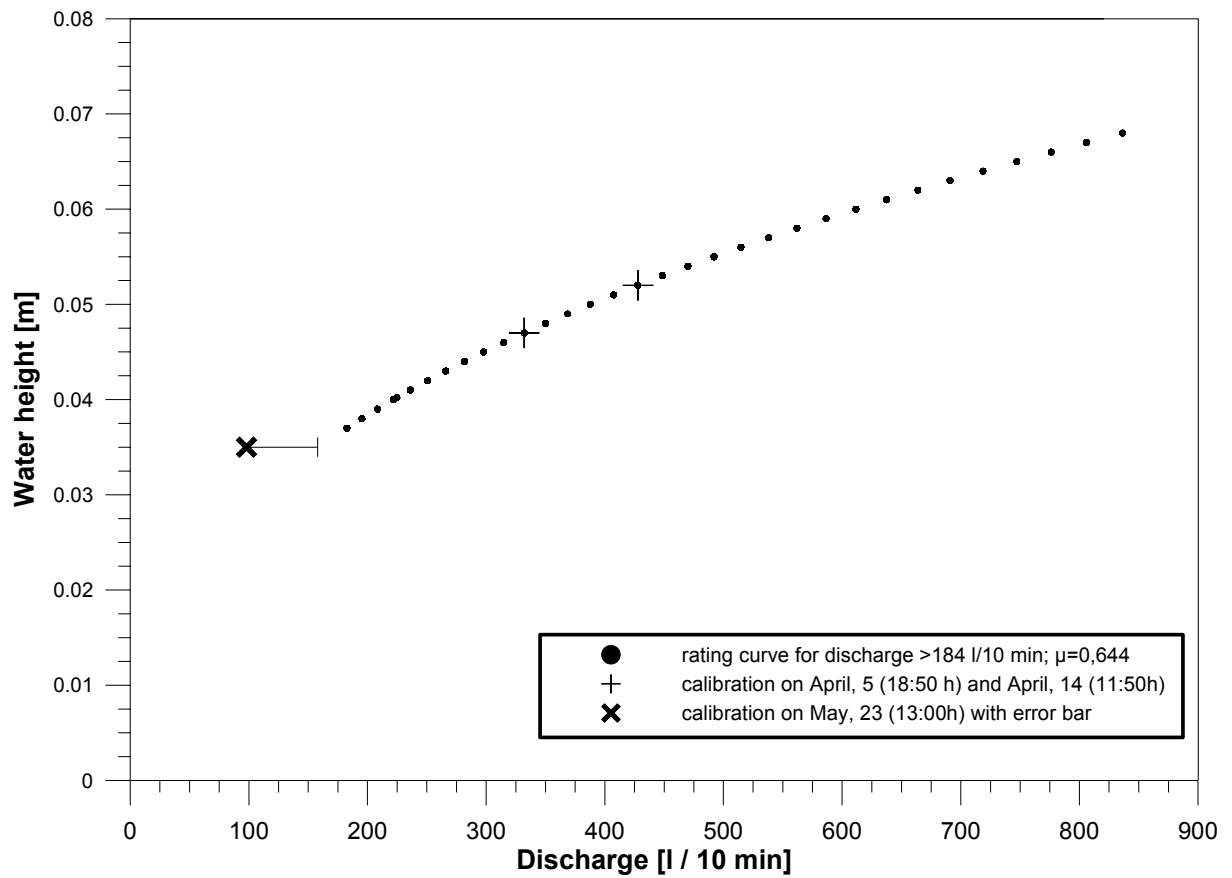
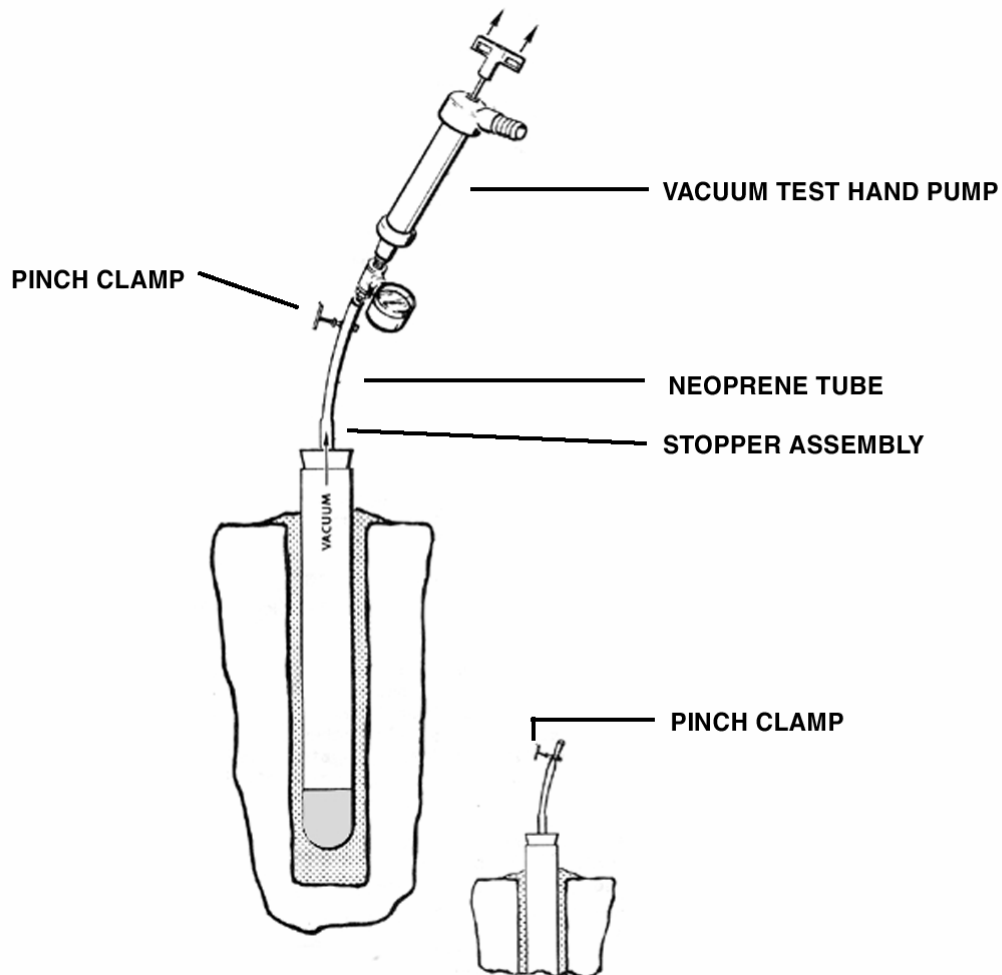


Fig. C3c: Rating curve of “v”-notched weir.

## C4 Lysimeter

The lysimeter instrument consisting of a tube, a head with a locking aperture, and a bottom, is described in Fig. C4. Most functional is the porous ceramic cup which allows the water to pass through in case of an inside vacuum.

The installation of suction lysimeters is essential for efficient water collection later on. This operation was based on PARIZEK & LANE (1970). Best results are obtained by pushing the bottom end of the lysimeter into a slurry remaining in the cored hole. The consistency of cement mortar provides the best soil contact with the porous ceramic cup. The remaining area around the sampler is later on backfilled with soil. As for the piezometers it is important to tamp soil firmly to prevent surface water from running down the cored hole.



**Fig. C4:** Sketch of soil water sampler. Adapted from: Soilmoisture Equipment Corporation.

## C5 Electrical conductivity probes

The body of the probe is a PVC-pipe, which serves as a reservoir at the upper side, where the water is measured. The lower part with the electrics was sealed completely by synthetic resin. This contained two circuits, one for electrical conductivity and another one for temperature levelling. Therefore all the conductivity values were temperature corrected. For circuit diagram and wiring instructions for the CAMPBELL data logger see Fig. C5. The shortcuts refer to corresponding input locations at the logger (excitation, high, and ground). A calibration with standard solutions set the conductivity reliably.

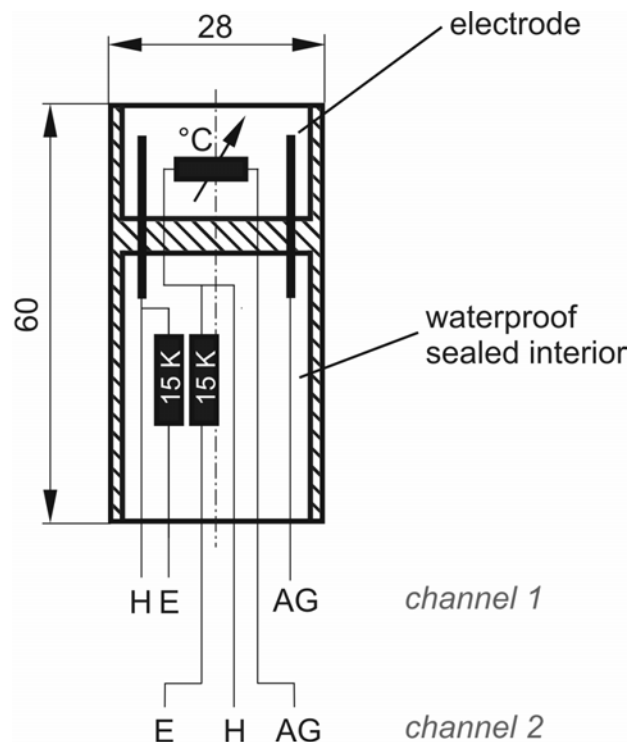


**Fig. C5:** Sketch and circuit diagram of electrical conductivity probe. Dimensions: mm. *Own compilation.*

## C6 Mini-wells for water sampling at table

Obvious similarities between the mini-wells and the piezometer in the field are shown in Fig. C6. The mini-wells are built out of PVC pipes, a rubber stopper, a tiny lid and a piece of elastic rubber hose. Not shown in the figure is the medical gauze around the slits for sediment protection. The foundation for the sampling tube is the ground of the table. This means there is a direct fit to the table. At the top of the mini well, the rubber hose runs up to a medical syringe (model: 20 ml content). Here the water samples are sucked into the syringe. Mini wells were included in the soil after levelling.

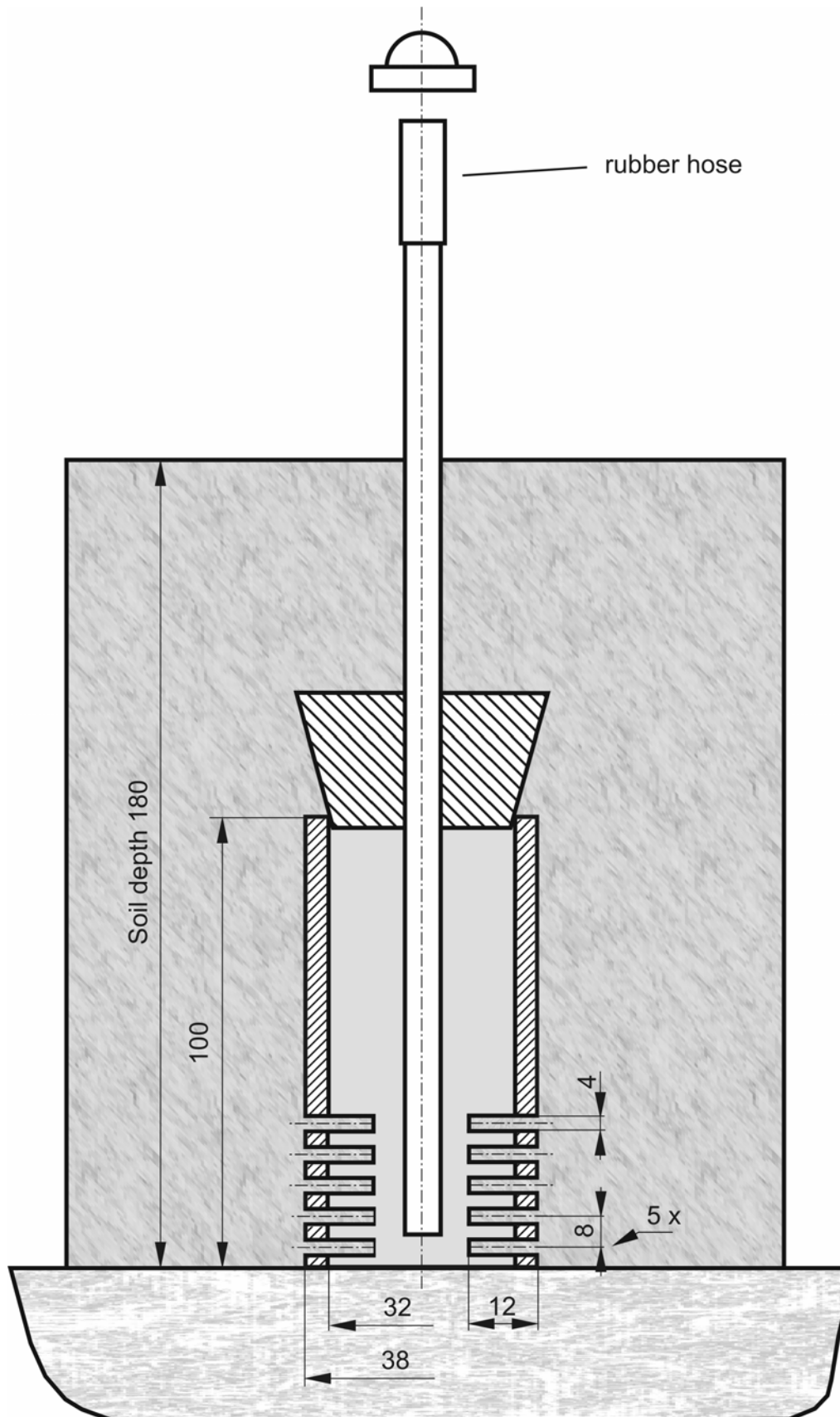


**Fig. C6:** Structure of a mini-well for water sampling. The bottom dyeing indicates the board of the basin (table). Dimensions: mm. *Own compilation.*

## C7 Program code for throughfall-data disaggregation

Macro program code, running in MS EXCEL®:

```

Dim start_time, end_time, timestep, tipval As Double 'days - max65536 steps
Dim counter
Dim data(0 To 65536) As Double 'Julian days - tip times
Dim bindata(1 To 65536, 1 To 2) As Double 'bin, start_time, volume
Sub main()
  Sheets("output_data").Range("a:b").Clear
  start_time = Sheets("program").Cells(4, 2)
  end_time = Sheets("program").Cells(5, 2)
  timestep = Sheets("program").Cells(7, 2)
  tipval = Sheets("program").Cells(9, 2)
  If (end_time - start_time) / timestep > 65536 Then
    Sheets("output_data").Cells(1, 1) = "OUTPUT ARRAY OVERFLOW"
    Exit Sub
  End If
  'create array of data
  counter = 1
  Do Until Sheets("input_data").Cells(counter, 1) = 0
    data(counter) = Sheets("input_data").Cells(counter, 1)
    counter = counter + 1
  Loop

  'choose algorithm and execute
  If Sheets("program").Cells(12, 2) = 1 Then binclick Else bincont
  'write out data
  counter = 1
  Do Until bindata(counter, 1) = 0
    For a = 1 To 2
      Sheets("output_data").Cells(counter, a) = bindata(counter, a)
    Next a
    If bindata(counter, 2) = 0 Then Sheets("output_data").Cells(counter, 2) = 0
    counter = counter + 1
  Loop
End
End Sub
Function binclick()
  countdata = 1
  countbin = 1
  'ignore data before start_time
  Do Until Sheets("input_data").Cells(countdata, 1) >= start_time
    countdata = countdata + 1
  Loop
  Do Until start_time >= end_time
    'add data to current bin
    bindata(countbin, 1) = start_time
    Do Until data(countdata) >= start_time + timestep
      bindata(countbin, 2) = bindata(countbin, 2) + tipval
      countdata = countdata + 1
      If countdata = counter Then Exit Do
      If countin = counter Then Exit Do
    Loop
  Loop

```

```

    If countdata = counter Then Exit Do
    countbin = countbin + 1
    start_time = start_time + timestep
Loop
End Function
Function bincont()
t1 = start_time
t2 = t1 + timestep

j = 1 'placeholder in the bindata array
a = 1 'placeholder in the data array

'ignore data before the time of interest; get to proper start in data array

'Do Until t1 >= data(a)
'  a = a + 1
'  If a > 65536 Then Exit Do
'Loop

Do Until j > ((end_time - start_time) / timestep)
  While t1 >= data(a)
    a = a + 1
    If a > counter Then Exit Do
  Wend
  If t2 <= data(a) Then
    binvol = (tipval / (data(a) - data(a - 1))) * (t2 - t1)
  ElseIf t2 <= data(a + 1) Then
    binvol = (tipval / (data(a + 1) - data(a))) * (t2 - data(a))
    binvol = binvol + (tipval / (data(a) - data(a - 1))) * (data(a) - t1)
  Else
    binvol = (tipval / (data(a) - data(a - 1))) * (data(a) - t1)
    Do While t2 > data(a + 1)
      If data(a + 1) = data(a) Then
        binvol = binvol + tipval
      Else: binvol = binvol + (tipval / (data(a + 1) - data(a))) * (data(a + 1) - data(a))
    End If
    a = a + 1
    If a > counter Then Exit Do
  Loop
  If data(a) = 0 Then
    binvol = 0
  Else: binvol = binvol + (tipval / (data(a + 1) - data(a))) * (t2 - data(a))
  End If
  End If
  bindata(j, 1) = t1
  bindata(j, 2) = binvol
  t1 = t2
  t2 = t1 + timestep
  j = j + 1
'  If j * timestep > end_time - start_time Then Exit Do
'Loop
End Function

```